CERKL, generació d'un model *knockout* de retinosi pigmentària i estudis funcionals

Alejandro Garanto Iglesias

CERKL, generació d'un model *knockout* de retinosi pigmentària i estudis funcionals

Memòria presentada per

Alejandro Garanto Iglesias

Per optar al grau de

Doctor

Tesi realitzada sota la direcció

de la Dra. Roser Gonzàlez Duarte i de la Dra. Gemma Marfany Nadal

al Departament de Genètica de la Facultat de Biologia

Universitat de Barcelona

Programa de Genètica (Bienni 2006-2008)

Roser Gonzàlez Gemma Marfany Alejandro Garanto

Barcelona, Juny de 2011

Resultats

INFORME DE LES DIRECTORES

La memòria de la Tesi Doctoral "*CERKL*, generació d'un model *knockout* de retinosi pigmentària i estudis funcionals" presentada per Alejandro Garanto Iglesias, es presenta com un compendi de 3 publicacions. La participació del doctorand és la que es detalla a continuació:

PUBLICACIÓ 1: *Overexpression of CERKL, a gene responsible for retinitis pigmentosa in humans, protects cells from apoptosis induced by oxidative stress*. Miquel Tuson, Alejandro Garanto, Roser Gonzàlez-Duarte i Gemma Marfany. **Molecular Vision, 15: 168-180, 2009**. Índex d'impacte (2009): 2.541 (Q1)

El doctorand, Alejandro Garanto, ha estat el responsable de part del treball experimental i comparteix co-autoria amb el primer signant. La seva contribució ha consistit en realitzar els assaigs de fosforilació *in vitro*, els estudis relacionats amb l'estrès oxidatiu, alguna de les localitzacions subcel·lulars i també el fraccionament subcel·lular. La seva aportació queda reflectida en les figures 3, 4F, 5, 6 i 7 de l'article.

PUBLICACIÓ 2: *High transcriptional complexity of the retinitis pigmentosa CERKL gene in human and mouse*. Alejandro Garanto, Marina Riera, Esther Pomares, Jon Permanyer, Marta de Castro-Miró, Florentina Sava, Josep F Abril, Gemma Marfany i Roser Gonzàlez-Duarte. **Investigative Ophthalmology and Visual Science, 52: 5202-5214, 2011**. Índex d'impacte (2009): 3.431 (Q1)

El doctorand ha contribuït en aquest treball realitzant tota la part experimental relacionada amb l'estudi de *Cerkl* en ratolins. El doctorand ha disseccionat els teixits, ha obtingut l'RNA, ha analitzat les seqüències, ha cercat els promotors, ha preparat les crioseccions i ha realitzat les immunohistoquímiques sobre aquestes. Aquest treball queda reflectit en les figures: 1B, 3B, 5B, 6 i 7.

PUBLICACIÓ 3: *The use of alternative promoters turns a targeted knockout of the Retinitis Pigmentosa gene Cerkl into a knockdown with mild affectation of the retinal ganglion cell layer*. Alejandro Garanto, Javier Vicente-Tejedor, Marina Riera, Pedro de la Villa, Roser Gonzàlez-Duarte, Roman Blanco i Gemma Marfany. **Investigative Ophthalmology and Visual Science** (Sotmès a publicació).

La contribució del doctorand en aquest treball ha consistit en la generació, manteniment i dissecció del ratolí *knockout*, l'anàlisi d'expressió i de promotors en diversos teixits, l'obtenció i la realització de crioseccions, per realitzar els experiments de tinció Hematoxilina-Eosina, d'immunohistoquímica i d'hibridació *in situ*, així com l'anàlisi de proteïnes a partir de lisats de retina WT i KO. L'aportació del doctorand queda reflectida en les Figures 1, 2, 3, 4, 5, 7 i S1.

Barcelona, 6 de Juny 2011

Roser Gonzàlez-Duarte Gemma Marfany

Capítol 1

Caracterització del gen *CERKL* i aproximació funcional

Publicació 1

Overexpression of CERKL, a gene responsible for retinitis pigmentosa in humans, protects cells from apoptosis induced by oxidative stress

PUBLICACIÓ 1

TÍTOL

"*Overexpression of CERKL, a gene responsible for retinitis pigmentosa in humans, protects cells from apoptosis induced by oxidative stress*"

AUTORS (ANY)

Miquel Tuson, Alejandro Garanto, Roser Gonzàlez-Duarte i Gemma Marfany (2009)

REFERÈNCIA

Molecular Vision 15: 168-180

RESUM

La retinosi pigmentària (RP) és una malaltia neurodegenerativa de la retina causada per diferents gens i que es caracteritza per la mort dels fotoreceptors per apoptosi. Un d'aquests gens és *CERKL* (*Ceramide Kinase-Like*). En aquest treball analitzem la seva funció i la seva possible contribució a la patogènesi. Primerament, es va realitzar un estudi transcripcional per poder identificar les isoformes que es produeixen a la retina. També, es va estudiar la localització subcel·lular d'aquestes, així com de la construcció que contenia la mutació descrita R257X. En quant als assaigs funcionals, es van realitzar experiments per trobar la funció quinàsica de la proteïna, així com diferents estudis d'estrès oxidatiu per tractar d'observar la susceptibilitat/protecció de CERKL davant d'aquesta agressió. Els resultats obtinguts van permetre concloure que *CERKL* produeix, com a mínim, 4 transcrits diferents en la retina, que codifiquen per proteïnes de 532, 558, 419 i 463 aminoàcids, que es localitzen majoritàriament al reticle endoplasmàtic i aparell de Golgi, fet que es va confirmar mitjançant un experiment de fraccionament cel·lular. A més a més, CERKL pot anar al nucli i al nuclèol, mentre que la forma mutada de CERKL que causa RP, R257X, queda retinguda a nucli gairebé en el 90% dels casos. La sobreexpressió d'algunes isoformes protegeix les cèl·lules en cultiu d'entrar en apoptosi sota condicions d'estrès oxidatiu, mentre que la proteïna CERKL-R257X no exerceix aquesta protecció, fet que podria explicar perquè mutacions en *CERKL* provoquen degeneració dels fotoreceptors. Per últim, no es va poder demostrar que CERKL sigui una quinasa de ceramides i per tant, aquesta proteïna continua essent una quinasa de lípids òrfena de substrat. La seva localització subcel·lular dinàmica suggereix múltiples llocs d'actuació. Tots aquests resultats ens ajuden a comprendre una mica més els mecanismes moleculars que causen degeneració retinal.

APORTACIÓ PERSONAL AL TREBALL

La part que he dut a terme en aquesta publicació d'autoria compartida ha consistit en: a) la generació de la construcció R257X, així com l'estudi de la seva localització subcel·lular (Figura 4F), b) fraccionament cel·lular mitjançant gradient de sucrosa per establir a quins compartiments membranosos està associada la proteïna CERKL (Figura 5), c) la cerca de la funció quinasa de lípids utilitzant diferents substrats i diferents isoformes (Figura 3) i d) estudi de la resposta de les cèl·lules quan sobreexpressen CERKL envers l'estrès oxidatiu (Figures 6 i 7).

Molecular Vision 2009; 15:168-180 <http://www.molvis.org/molvis/v15/a16>
Received 5 October 2008 | Accepted 8 January 2009 | Published 21 January 2009

Overexpression of *CERKL*, a gene responsible for retinitis pigmentosa in humans, protects cells from apoptosis induced by oxidative stress

Miquel Tuson,[1] Alejandro Garanto,[1,3] Roser Gonzàlez-Duarte,[1,3] Gemma Marfany[1,2]

(The first two authors contributed equally to this work.)

[1]Departament de Genètica, Facultat de Biologia, Universitat de Barcelona, Barcelona, Spain; [2]Institut de Biomedicina de la Universitat de Barcelona (IBUB), Barcelona, Spain; [3]Centre for Biomedical Research on Rare Diseases (CIBER-ER), Instituto de Salud Carlos III, Barcelona, Spain

Purpose: Retinitis pigmentosa (RP), a retinal neurodegenerative disorder characterized by apoptosis of photoreceptor cells, is caused by mutations in many different genes. We analyzed the RP gene ceramide kinase-like (*CERKL*) to determine CERKL function and contribution to pathogenesis.
Methods: RT–PCR was performed to characterize *CERKL* expression in many human adult and fetal tissues, including retina. We analyzed the protein subcellular localization by confocal microscopy and further verified it by sucrose gradients. We performed lipid kinase activity assays. And finally, we studied the effects on cell apoptosis after *CERKL* overexpression in transiently transfected cultured cells by propidium iodide staining and poly-(ADP-ribose)-polymerase (PARP) caspase-dependent cleavage.
Results: *CERKL* transcripts underwent alternative splicing. In the human retina, four different CERKL isoforms of 532, 558, 419, and 463 amino acids were expressed. CERKL proteins were mainly localized in the endoplasmic reticulum and Golgi compartments, but they also shifted localization to nuclei and nucleoli. We also found that CERKL prevented cells from entering apoptosis induced by oxidative-stress conditions.
Conclusions: CERKL remains a unique orphan lipid kinase in that no candidate substrate has been identified after intense research. The dynamic localization of CERKL suggests multiple sites of action. Remarkably, CERKL (but not the RP R257X mutant) exerts a protective role in cells against oxidative stress, consistent with RP mutations impairing the normal protein function in photoreceptors and thus tilting the balance toward apoptosis. These results provide valuable insights into the molecular mechanisms causing retinal degeneration.

Retinitis pigmentosa (RP) is an inherited retinal neurodegenerative disorder characterized by the progressive attrition of photoreceptor cells through apoptosis. Although mutations in many different genes have the same phenotypic outcome, there is not much information gathered on the biochemical processes linking the genotype to the eventual photoreceptor death. In the course of our search for new genes causing autosomal recessive RP in several Spanish families, we identified a previously unannotated gene, ceramide-kinase like (*CERKL*) [1,2]. Mutations in *CERKL* are responsible for a phenotypically distinct RP [2,3], with characteristic macular and peripheral lesions. The name of the gene stems from the diacylglycerol kinase domain–which shares homology to ceramide kinases–of the encoded protein.

Ceramide is a chore sphingolipid (SL), being the precursor of other bioactive and complex SLs and one of the initial key players in stress-induced apoptosis [4]. SLs are now considered lipid second messengers that behave as finely tuned sensors of cell status [4,5]. Accordingly, the enzymes involved in SL metabolism, and among them CERKL, are rheostats that integrate multiple stress stimuli [6]. Mutations in these genes cause multiple and complex phenotypic effects, including severe neurodegenerative disorders [7]. A variety of extracellular and intracellular stimuli, including cytokines, cytotoxic agents, and stress signals, cause the accumulation of ceramide via sphingomyelin hydrolysis or de novo synthesis. To avoid entering apoptosis, cells counteract this ceramide increase by activating enzymatic pathways involved in ceramide clearance. In this context, the phosphorylation of ceramide by ceramide kinase exerts a protective role against apoptosis. Ceramide can be produced in different subcellular membranous compartments, adding to the complexity and the homeostasis of the whole system [6,8]. Therefore, the

Correspondence to: Gemma Marfany, Departament de Genètica, Facultat de Biologia, Universitat de Barcelona, Institut de Biomedicina de la Universitat de Barcelona (IBUB), Avda. Diagonal 645, E-08028 Barcelona, Spain; Phone: +34 93 4021502; FAX: +34 93 4034420, email: gmarfany@ub.edu. Dr. Miquel Tuson is now at the Developmental Biology Program, Sloan-Kettering Institute, New York, NY.

TABLE 1. CERKL AMPLIFICATION PRIMERS FOR THE CONSTRUCTION OF EXPRESSION VECTORS AND THE RT–PCR ANALYSES.

	Forward primers (5′-3′)
CERKL_E2_F	CTGTTAAACAGCAGAGAAGTGGTAC
RT_CERKLab_F	GTAACAATAATGGAATATGAAGGG
RT_CERKLc_F	CAGTTCAAGAAAATATTGGCAGGATC
RT_CERKLd_F	GGAATAAAAACTGATGTAACAAGATC
mutCERKL_F[c]	TGGGATGGAAACAGAC**T**GAATCCTGACTCCTGTC
	Reverse primers (5′-3′)
CERKL_E13_R[a]	AT*GGATCC*TTACTTTGGAATCATTTCTTCCATG
RT_CERKLab_R	ATCCTGCTGGTATTAAGCCAAG
RT_CERKLcd_R	CCTTAACAACAGCAAAATCTCTCCG
CERKL_E13_HA_R[a,b]	CG*GATATC*AAGCGTAATCTGGAACATCGTATGGGTACTTTGGAATCATTTCTTCC
mutCERKL_R[c]	GACAGGAGTCAGGATTC**A**GTCTGTTTCCATCCCA

[a] CERKL_E13_R and CERKL_E13_HA_R introduce a restriction site (indicated in italics) for subsequent cloning. [b] CERKL_E13_HA_R contains the coding sequence of the HA epitope (underlined). [c] The truncated R257X CERKL proteins were obtained by site-directed mutagenesis using the primers mutCERKL_F and mutCERKL_R, which introduce the 847C>T change (in bold and underlined).

identification of *CERKL* as an RP gene provided a missing link between alterations in SL metabolism to inheritable retinal disorders and suggested a new avenue for elucidating the ethiopathological mechanisms.

Here we report that *CERKL* undergoes alternatively splicing events, which affect the exons encoding the lipid kinase domain. Four protein isoforms are generated, although only 2 of them contain the complete diacylglycerol (DAG) kinase domain. Here we present a detailed characterization of the expression of these 4 alternatively spliced isoforms in different human tissues, and demonstrate that these 4 variants are only present in the retina. The 4 proteins show a similar subcellular localization pattern, and are mainly located in the ER and Golgi compartments. Although *CERKL* substrates remains elusive under standard experimental conditions, we show that overexpression of CERKL isoforms protects cells from apoptosis induced by oxidative stress.

METHODS

Cloning of CERKL splicing variants in the human retina: Specific primers flanking exons 2 and 13 (Table 1) were used to clone *CERKL* alternative splicing variants by PCR from Marathon-Ready™ human retina cDNA (BD Biosciences, Franklin Lakes, NJ) under the following conditions: 94 °C for 30 s, 58 °C for 30 s, and 72 °C for 2 min for 35 cycles. The primer CERKL_E2_F annealed to exon 2 while the CERKL_E13_R primer annealed to exon 13 and introduced a BamHI site to facilitate subsequent subcloning. The 50 µl reaction mixture contained 10 µM of each primer, 2 µM of dNTPs, 1.5 mM $MgCl_2$ and 1 U of Pfu Turbo polymerase (Stratagene, La Jolla, CA). The PCR bands detected after electrophoresis on a 1.5% agarose gel were cloned into the EcoRV site of pBluescriptII KS and verified by sequencing. The full-length cDNAs of these *CERKL* isoforms were reconstituted by digesting the partial clones with EcoRI and BamHI and subcloning the corresponding fragments into a pBluescriptII KS vector that already contained the 5′ end of *CERKL* (the complete exon 1 and the stretch of exon 2 before the EcoRI site, obtained from the IMAGE clone 3870103).

RT–PCR analysis of the presence of CERKL splicing variants in human tissues: The splicing pattern of *CERKL* was analyzed in human retina cDNA and a panel of first-strand cDNAs from several human adult and fetal tissues, using specifically designed pairs of primers to amplify and distinguish each isoform (Table 1), as follows: 1) to detect splicing variants *CERKLa* and *CERKLb* (RT_CERKLab_F and RT_CERKLab_R); 2) to amplify splicing variant *CERKLc* (RT_CERKLc_F and RT_CERKLcd_R); 3) to detect splicing variant *CERKLd* (RT_CERKLd_F and RT_CERKLcd_R). Two-step PCR conditions were as follows: 35 cycles of 94 °C for 30 s and 58 °C for 30 s. The 25 µl reaction mixture contained 10 µM of each primer, 2 µM of dNTPs, 1.5 mM $MgCl_2$ and 1 U Taq polymerase (Promega, Madison, WI). The concentration of the Marathon-Ready™ human retina cDNA and first-strand cDNAs from the tissue panel (BD Biosciences) in the reactions were 0.01 ng/µl and 0.1 ng/µl, respectively.

Overexpression of CERKL isoforms in cultured cells and preparation of protein cell lysates: Expression vectors containing the full-length open reading frame of the four *CERKL* isoforms were assembled by PCR amplification of each variant using the CERKL_E2_F primer, which anneals upstream of the EcoRI site in exon 2 and the CERKL_E13_HA_R primer, which anneals in exon 13 (Table 1). Primer CERKL_E13_HA_R also encoded a C-terminal hemagglutinin (HA) epitope tag and included an EcoRV site for subsequent cloning. The PCR products were digested with EcoRI and EcoRV and cloned into a pcDNA3 (Invitrogen Life Technologies, Carlsbad, CA) that contained exons 1 and 2 of *CERKL* (previously cloned between HindIII and EcoRI sites). The integrity of all constructs was verified by sequencing. To generate the truncated RP mutant protein (R257X), site-directed mutagenesis was performed on the 2 constructs containing the isoforms CERKLa and CERKLb

(encompassing the lipid kinase domain). The 847C>T change was introduced with the mutCERKL_F and mutCERKL_R primers (Table 1). In these constructs, the HA epitope was added to the N-terminus of the protein for immunodetection.

Human embryonic kidney (HEK293T) or African green monkey kidney (COS-7) cells were seeded at 3×10^6 cells/dish in 10 cm cell culture dishes 1 day before transfection. Cells were tranfected with 24 µg/dish using either the pcDNA3 vector alone or each pcDNA3–CERKL construct and 60 µl/dish of Lipofectamine™2000 (Invitrogen Life Technologies), following the manufacturer's instructions. After 2 days, the cells were harvested and lysed by sonication in lysis buffer [20 mM MOPS pH 7.2, 2 mM EGTA, 1 mM dithiothreitol, 10% glycerol, and complete™ protease inhibitor (Roche Diagnostics, Indianapolis, IN)], as described elsewhere [9].

In vitro and in vivo kinase activity assays: DAG and ceramide kinase activities were assayed in vitro as described [10]. Briefly, the source of the enzymatic activity were protein lysates from either HEK293T or COS-7 cells transfected with each CERKL isoform (250 µg total protein), the empty vector or a CERK-expressing construct (negative and positive control, respectively) obtained by sonication in 20 mM MOPS pH 7.0, 2 mM EGTA, 1 mM DTT, 10% glycerol plus protease inhibitors. The source of lipids were either: a) micelles obtained from commercial sphingolipids, which contained 880 µM lipids (ceramide and sphingosine, both from bovine brain sphingomyelin, or 1,2-dioleoyl-sn-glycerol, Sigma-Aldrich, St. Louis, MO), 1 mM cardiolipin, 1.5% β-octylglucoside, 0.2 mM diethylenetriamine-pentaacetic acid (DETAPAC); b) lipid micelles, obtained by sonication of 50 µg of lipids extracted from cultured 661W murine photoreceptor-derived cells in 1 mM DETAPAC, 7.5% β-octylglucoside; or c) total 661W cell lysates that were heat-inactivated at 65 °C for 20 min to abrogate endogenous enzymatic activities. Reactions were performed at 100 µl final volume containing 20 mM MOPS pH 7.2, 50 mM NaCl, 1 mM dithiothreitol, 2 mM EGTA, and 3 mM $CaCl_2$, with the corresponding lipid and protein sources. Reactions were started by adding $MgCl_2$ at 0.5 mM final concentration plus γ-^{32}P-ATP (2–5 µCi/reaction), incubated at 30 °C for 30 min, 60 min, or overnight, and stopped with 250 µl of chloroform, 250 µl of methanol and 125 µl HCl 2.4 M. After vortexing, the phases were separated by centrifugation, and the organic phase removed and vacuum-dried. Lipids were resuspended in 25 µl chloroform:methanol (95:5, v/v), spotted onto silica gel plates and separated by thin-layer chromatography (TLC). For the enzymatic assays in vivo, we seeded 1.5×10^6 661W cells on 10 cm diameter plates and transfected using either the two pEGP-CERKL long isoforms (a and b) or the pEGFP empty-vector (negative control). Transfected cells were enriched by using Fluorescence Activated Cell Sorting (FACS) to select green fluorescent protein (GFP) positive cells. These cells were reseeded on smaller plates, and 4 µl of radioactive ^{32}P-orthophosphate was added to the medium. Cells were collected after 4 h, and lysed directly in a solution of chloroform:methanol:chlorhydric acid (100:100:1). After vigorous vortexing, cellular debris was sedimented by centrifugation in a microfuge (100x g) and the liquid phase was vacuum-dried on completion. The lipid pellet was resuspended in a solution of 1:1 chloroform:methanol and loaded onto silica gel 60 TLC plates (Merck, Whitehouse Station, NJ). All TLCs (assays in vivo and in vitro) were run in chloroform:acetone:methanol:acetic acid:water (10:4:3:2:1, v/v). Radiolabeled lipids were visualized by autoradiography.

Purification of recombinant proteins: To express the four CERKL isoforms as glutathione-S-transferase (GST) fusion proteins, we subcloned each variant in-frame into pGEX-4T-1 (Amersham Biosciences, Chalfont St. Giles, UK), between the XhoI and NotI sites. The constructs were transformed into BL21 Codon Plus *E.coli* cells (Stratagene) to avoid premature protein truncation due to the strongly biased codon usage of the *CERKL* human gene. Recombinant proteins were produced in 500 ml cultures induced by the addition of 0.5 mM Isopropyl-β-D-thiogalactopyranoside (IPTG). Purified GST-recombinant proteins were obtained after elution with reduced glutathione of the protein bound to the glutathione-sepharose bead batch, following the manufacturer's instructions (Amersham Biosciences).

Lipid-protein overlay assay: Binding of CERKL isoforms to sphingolipids was assessed using SphingoStrips™ and PIP Strips™ (Echelon Biosciences, Salt Lake City, UT), which consist of several nitrocellulose-immobilized sphingolipids and phosphoinositides (100 pmol/spot) respectively. The membranes were equilibrated for 5 min in 10 mM Tris-HCl pH 8.0, 150 mM NaCl, and 0.1% v/v Tween-20 (TBST). They were then blocked with 3% BSA in TBST (blocking solution) for 1 h at room temperature. Subsequently, the membrane was then incubated overnight at 4 °C in blocking solution containing 0.5 µg/ml of the GST-fusion protein on a rocking platform. The membranes were washed twice for 15 min in TBST with gentle agitation, and then incubated for 1 h with 1:1,000 anti-GST monoclonal antibody (Santa Cruz Biotechnology, Santa Cruz, CA). After washing as before, membranes were incubated for 1 h with 1:3,000 horseradish peroxidase-conjugated anti-mouse IgG antibody (Sigma). Finally, the membranes were washed 6 times in an hour in TBST, and developed with the ECL western blotting detection system (Amersham Biosciences).

Transfection, immunolocalization and confocal laser microscopy: COS-7 cells were grown in Dubecco's Modified Eagle Medium (DMEM) containing 10% fetal bovine serum, 4 mM L-glutamine, 100 U/ml of penicillin, and 100 µg/ml streptomycin (Invitrogen Life Technologies). Cells were grown on coverslips in 12 well plates. Transient transfections were performed using Lipofectamine™2000 (Invitrogen Life Technologies) according to the manufacturer's protocol.

Next, 24 h or 48 h post-transfection cells were rinsed with PBS 1X (137 mM NaCl, 2.7 mM KCl, 1.5 mM KH_2PO_4, 8 mM Na_2HPO_4, pH 7.4) and fixed in 3% paraformaldehyde and 2% sucrose in 0.1 M phosphate buffer at 4 °C for 30 min. Cells were then washed and permeabilized for 10 min with a solution that contained 0.1% Triton X-100, 20 mM glycine, and 10 mM PBS. After permeabilization, cells were rinsed and blocked in a solution composed of 1% BSA, 20 mM glycine, and 10 mM PBS. Then, cells were incubated with 1:250 anti-HA polyclonal antibody and either specific 1:25 anti-calnexin, 1:250 anti-GM130, or 1:1,000 anti-EEA1 monoclonal primary antibodies (all from BD Biosciences) at 37 °C for 1 h. Mitochondria were labeled by adding reduced MitoTracker Orange (Molecular Probes, Invitrogen Life Technologies, Carlsbad, CA) to the cell culture medium at a final concentration of 500 nM for 45 min before the fixation procedure and subsequent immunocytochemistry. Upon washing, cells were incubated with 1:300 AlexaFluor 488-conjugated anti-rabbit and 1:300 AlexaFluor 546-conjugated anti-mouse (Molecular Probes) secondary antibodies. When required, slides were counter-stained with 1:200 DAPI (Sigma) nuclear blue dye in PBS for 15 min. All preparations were mounted in Vectashield medium for fluorescence (Vector Laboratories, Burlingame, CA) and analyzed by confocal laser scanning microscopy with Olympus Fluoview 500 (Olympus, Tokyo, Japan) and Leica TSC NT and TSC SPII (Leica, Wetzlar, Germany) laser scanning microscopes. In silico predictions for CERKL subcellular localization were performed using PSORT, ProSLP v2.0, ESLPred, and SubLoc v1.0.

Subcellular fractionation by sucrose gradient: HeLa cells (human cervical cancer derived cell line ATCC CCL-2) were seeded (1.5×10^6 cells/dish) in 10 cm plates and transfected with the CERKLa isoform tagged with the HA epitope. At 48 h post-transfection, cells were washed twice with 1X PBS, and then incubated 20 min at 4 °C in a solution that contained 10 mM Tris HCl, pH 7.4, 3% sucrose w/v, and 1% protease inhibitors (Roche). After this incubation, the concentration of sucrose was increased up to 0.25 M, and cells were broken by 15 strokes in an iced-chilled Dounce homogenizer. Cellular debris, nuclei, and unbroken cells were separated by centrifugation at 1,300x g for 5 min at 4 °C, and the supernatant was further centrifuged overnight at 100,000x g at 4 °C. The pellet containing cell organelles was resuspended in 1.5 M sucrose and laid at the bottom of a 1.8 ml swing-out (Beckman, Fullerton, CA) centrifuge tube. Subsequent layers of equal volumes of 1.15, 0.9, 0.6, and 0.25 M sucrose were added, and the final sucrose gradient was centrifuged for 2 h at 100,000x g at 4 °C. Next, 11 fractions of approximately 150 µl were collected from bottom to top. Samples were loaded onto 10% polyacrylamide SDS–PAGE gels, transferred to 0.45 µm polyvinylidene fluoride PDVP membranes (Immobilon-P, Millipore, Billerica, MA) and underwent immunodetection with the corresponding antibodies.

Immunodetection: After blocking membranes for 1 h in 10% nonfat milk in phosphate buffered saline, 0.1% Tween-20 (MTP), membranes were incubated overnight at 4 °C or 1 h at room temperature, separately, with any of the following primary antibodies, all diluted at 1:1000, anti-GM130 (BD Biosciences), anti-PDI (BD Biosciences), anti human TGN38 (Santa Cruz Biotechnology, Inc.) or anti-HA (Covance, Princetown, NJ). After extensive washes in MTP, membranes were incubated for 1 h with 1:3,000 of the corresponding peroxidase-conjugated secondary antibody (Sigma), and the bands were visualized using the ECL western blotting detection system (Amersham Biosciences).

Propidium iodide staining assay: COS-7 cells were grown on coverslips in 24 well plates. Transient transfections were performed on the following: the constructs encoding each of the four isoforms (pcDNA3-CERKL), the truncated variant (pcDNA3-R257X), empty pcDNA3.1 (negative control), or pcDNA6.2-DEST-CERK (provided by F. Bornancin, Novartis). At 44 h post-transfection, cells were treated with 200 µM H_2O_2 (Fluka, Sigma-Aldrich, St. Louis, MO) and 3 h later propidium iodide was added at a final concentration of 7 µg/ml. After 1 h, cells were rinsed twice with PBS and fixed in 3% paraformaldehyde and 2% sucrose in 0.1 M phosphate buffer at 4 °C for 30 min. They were then washed 2 times in 0.1 M PBS and mounted in Vectashield medium (Vector Laboratories). Several fields were analyzed under the visible and green light channels in a fluorescence microscope (Leica DM IL) coupled to a Leica DFC camera (Leica, Wetzlar, Germmany). A minimum of 500 cells were counted and compared to detect pignotic nuclei in the total cell count. Three independent replicates were performed for each construct.

Analysis of PARP cleavage-dependent apoptosis: HeLa cells were seeded in 24 well plates and transfected with either empty pcDNA3.1 (negative control) or pcDNA3-CERKLa (containing the lipid kinase domain). At 40 h post-transfection, the medium was replaced by fresh solution containing one of the following: 300 µM H_2O_2, 400 µM H_2O_2, or 0.3 M sodium nitroprusside (Fluka), or serum-deprived medium. After 24 h, cells were rinsed with PBS, harvested, and lysed directly in protein electrophoresis loading buffer. Samples were then boiled for 5 min and centrifuged to sediment cellular debris. Protein preparations were loaded onto 7.5% SDS–PAGE gels. Either 1:1,000 monoclonal anti-PARP (Invitrogen Life Technologies) or 1:8,000 monoclonal anti-tubulin (Sigma) were used as primary antibodies. Anti-mouse secondary antibody was conjugated to 1:3,000 horseradish peroxidase. Immunodetection was performed using chemiluminescent ECL reagents (GE Healthcare, Waukesha, WI), and the

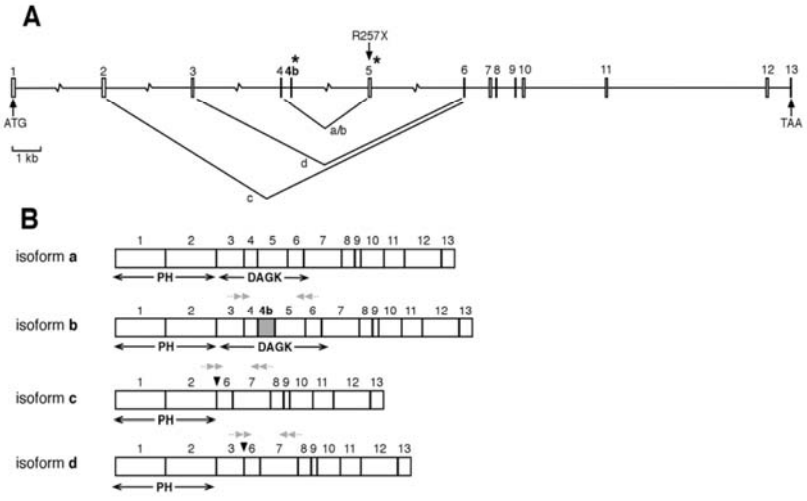

Figure 1. *CERKL* isoform structure. **A:** The diagram shows the genomic exon-intron structure of the *CERKL* gene with the initiation and stop codons. The position of the nonsense mutation (R257X) identified in RP families as well as the splicing junctions resulting in isoforms a, b, c, and d are indicated. Asterisks indicate the position of the rare GC-splicing donor sites. **B:** The mature *CERKL* mRNA isoforms, indicating the relative position of the encoded DAG kinase and putative PH domains, are depicted. Note that exon 4b (isoform b, in gray) is located well within the DAG kinase domain, while isoforms c and d lack this domain. Grey small double arrows indicate the position of the primers used for specific isoform RT–PCR analyses (see Methods). The figure is drawn to scale except for the introns depicted with a broken line.

intensity of each band was quantified using the Quantity-One 1-D Analysis Software (Bio-Rad, Hercules, CA).

RESULTS

CERKL transcripts are alternatively spliced in the human retina: The initially characterized *CERKL* gene spanned 13 exons in chromosome 2q31.2–31.3 (Figure 1A). While attempting to clone the full-length *CERKL* on retina cDNA using primers spanning the ATG (forward) and the STOP (reverse) codons, we observed several faint bands, which were indicative of alternatively spliced variants. Therefore, we devised a two-step strategy of RT–PCR and cloning (see Methods) to characterize the full-length isoforms based on the structure of the gene. The RT–PCR analysis of human retina mRNA using primers from exons 2 and 13 allowed us to identify several spliced transcripts (Figure 1A) that would result in several protein isoforms (Figure 1 B): 1) CERKLa, which corresponded to the already reported variant [2], spanning 13 exons and encoding a 532 amino acid protein (GenBank accession number AY357073); 2) CERKLb, a 14 exon isoform, which includes an additional exon (4b) between exons 4 and 5 and encodes a 558 amino acid protein (accession number AY690329); 3) CERKLc, a splicing variant devoid of exons 3-4-4b-5, which encodes a 419 amino acid protein (accession number AY690330); and 4) CERKLd, a splicing variant that skips exons 4-4b-5 and encodes a 463 amino acid protein (accession number AY690331). Two very faint bands corresponded to not in-frame splicing variants (accession numbers AY690332 and AY690333) that would generate prematurely truncated proteins. These were considered aberrant transcripts, and given the mRNA quality control regulation, if they were produced in cells, they would be most probably cleared by the nonsense mediated decay mechanism.

The longest isoforms (CERKLa and CERKLb) contained the complete DAG domain and a putative N-terminal pleckstrin homology (PH) region. In contrast, the short forms (CERKLc and CERKLd) skipped most of the DAG kinase domain, although the putative PH domain (encoded in exons 1 and 2) was preserved (Figure 1B).

Noticeably, exons 4b and 5, which are alternatively spliced, show the rare GC donor splice site instead of the more common GT (marked by asterisks in Figure 1A). Both exons and the GC donor site sequences are conserved in the chimpanzee genome. The mouse *Cerkl* gene, which shows overall strong conservation in exon and intron structure, has no equivalent for exon 4b, thus suggesting that there are only 3 CERKL isoforms in the mouse. Again, the donor site of exon 5 in rodents is GC.

CERKL shows a complex alternative splicing pattern in human tissues: As we had previously found that *CERKL* was expressed in a variety of human adult and fetal tissues [2], we searched for *CERKL* isoforms in tissues other than retina. To this end, we used a panel of first strand cDNAs from several human tissues. In accordance with our previous data, no *CERKL* isoform was found in adult skeletal or heart muscle. However, some of the four in-frame splicing variants were detected in other adult and fetal tissues (Figure 2). cDNAs encoding protein isoforms CERKLa and CERKLb (with an intact DAG kinase domain) were present in adult liver and pancreas, as well as in fetal brain, lung, and kidney. One or both short isoforms (c and d) were detected in adult lung, adult kidney, adult pancreas, fetal lung, and fetal liver. Notably,

retina was the only tissue in which all 4 isoforms were expressed under the conditions tested. However, basal levels of most isoforms were observed in most tissues after a saturating number of PCR cycles (data not shown).

CERKL does not phosphorylate ceramide under standard conditions: Given the structural similarities of CERKL to the reported ceramide kinases, a series of experiments were conducted to assess ceramide kinase activity. The protocol from [10] with minor modifications was used for in vitro ceramide kinase assays. We changed either of the following: 1) the source of the ceramides, namely a commercial mixture of brain ceramides (Sigma) or lipid micelles prepared from 661W cells (mouse photoreceptor precursor cell line, kindly provided by M.R. Al-Ubaidi) [11]; or 2) the source of the enzymatic activity to be tested, namely protein lysates from transiently transfected HEK293T and COS-7 cells overexpressing each CERKL isoform, or affinity-purified recombinant GST-CERKL variants (after expression in *E. coli* cells and only used in assays in vitro). No kinase activity was detected for any isoform at any combination of the lipid and protein lysate sources (Figure 3A). Additionally, lysates from co-transfections with constructs expressing 2 different isoforms, or the 4 of them together, were assayed for kinase activity. However, no significant difference with respect cells transfected with the empty vector or single CERKL isoforms could be detected (data not shown). We then attempted to detect CERKL kinase activity in vivo using photoreceptor-derived 661W cells. As 661W are neuronal, they transfect poorly; therefore, we used CERKL-GFP fusion constructs to enrich by FACS the population of transfected cells. Unfortunately, no differences were detected between cells transfected with CERKL and the empty vector (Figure 3B).

The absence of kinase activity prompted us to test the ability of CERKL isoforms to bind sphingolipids by protein-lipid overlay. As PH domains have been reported to have an affinity for phosphoinositides, these substrates were also included. We used the CERKLa isoform (532 aa, containing the complete DAG kinase domain) either as a pure preparation of recombinant GST-CERKL fusion protein (in *E.coli*) or as total fresh protein lysate from HEK293T cultured cells transiently transfected with the CERKLa HA-tagged construct. Again, no positive binding signals were produced (data not shown).

Subcellular CERKL localization is highly dynamic: Ceramide and other sphingoid lipids are highly dynamic membrane components. Proteins involved in sphingolipid metabolism appear to be specifically localized in subcellular compartments of the secretory pathway, from the ER-Golgi network to the plasma membrane. In this context, we aimed to determine CERKL subcellular localization by transient expression of each alternative splicing variant in cultured COS-7 cells, as the 4 isoforms display a specific domain architecture, which might account for slight differences in

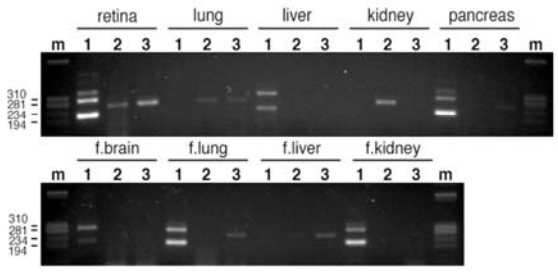

Figure 2. RT–PCR analysis of specific *CERKL* isoforms in several human tissues. For each tissue, lane 1 shows amplification of isoforms a (fast migrating band) and b (slow migrating band), whereas lanes 2 and 3 show the amplified product of isoform c and d, respectively. In the second gel, "f" represents fetal tissue. Marker band sizes are indicated in base pairs (bp). The additional faint bands in lane number 1 correspond to heteroduplexes of the PCR products.

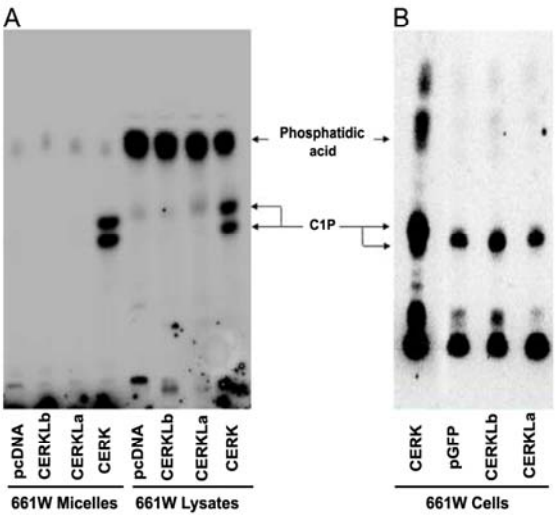

Figure 3. CERKL kinase activity assays. A: The autoradiography of one out of many thin layer chromatographies (TLC) from in vitro assays is shown. Lipid micelles and heat-inactivated cell lysates from 661W (murine photoreceptor-derived cell line) cells were used as substrates, whereas protein lysates from COS-7 cells transfected with either empty vector (pcDNA), CERKL isoform a (532 aa), CERKL isoform b (558 aa) or ceramide kinase CERK (positive control) expressing constructs were the source of the enzymatic activity. **B:** Autoradiography of a TLC from in vivo assays is shown. Cultured 661W cells were transfected with either pGFP (empty vector), or CERKLa-GFP, CERKLb-GFP, or CERK-GFP (positive control), selected by FACS and grown in a medium supplemented with ^{32}P-orthophosphate (see Material and Methods for details on the protocols). C1P represents Ceramide-1-phosphate. The images are representative of many different assays, with several experimental parameters, such as the type of cell line and the CERKL isoforms overexpressed, changed. The results of the assays were negative under all the conditions tested.

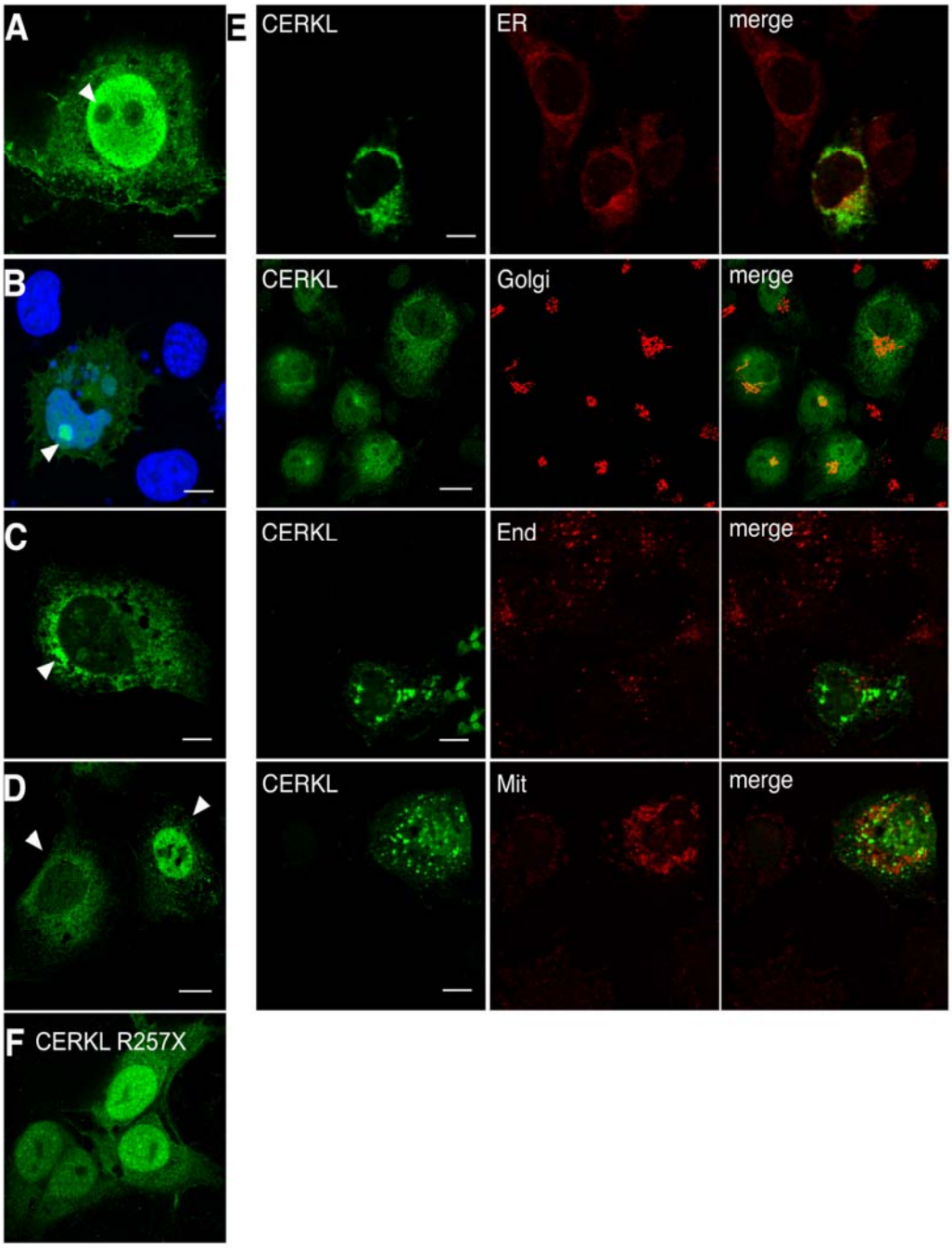

Figure 4. CERKL-HA (isoform a, 532 amino acids) shows a dynamic subcellular localization in COS-7 transfected cells. **A:** Several cells per field showed uniform distribution of CERKL in the cytosol and the nucleus, with clear exclusion from the nucleoli. **B:** A similar pattern but with strong accumulation in the nucleoli (nuclei, counter-stained with DAPI, appear in blue). **C** and **D:** In most cells, CERKL was absent from the nucleus and instead accumulated in clusters, preferentially in the perinuclear region (**A**). These two patterns were cell-specific and could be observed in the same field **(D)**. **E:** CERKL localized to several membranous subcellular compartments, mainly ER and Golgi. The markers used were calnexin for ER, GM130 for Golgi, EEA1 for endosomes and MitoTracker for mitochondria. **F:** R257X truncated CERKL localized preferentially in the nuclei, although it was also detected in the ER. Arrows highlight the relevant CERKL localizations, as immunodetected with an anti-HA monoclonal antibody. Scale bar corresponds to 10 µm. The same results were obtained for all the CERKL isoforms, irrespective of the epitope used, HA or GFP (data not shown). Abbreviations: endoplasmic reticulum (ER), endosomes (End), mitochondria (Mit).

function or compartment localization. We used C-terminal HA-tagged CERKL isoforms (CERKL-HA), as well as the fusion CERKL-GFP constructs, in these transient transfections.

Interestingly, neither a unique localization pattern nor a restricted subcellular localization could be ascribed to any CERKL isoform, as all variants showed similar patterns that appeared to be cell-specific. Two main protein localizations emerged consistently in all preparations, as seen for the isoform CERKLa (532 amino acids; Figure 4A–D). Most cells showed CERKL in a strong perinuclear distribution, while the nucleus was practically devoid of signal (Figure 4C,D). Additionally, few cells in each field presented CERKL within the nucleus, where it was either localized to, or clearly excluded from, the nucleoli (Figure 4A,B,D). No exclusive colocalization with reference markers of subcellular compartments was observed, as CERKL colocalized both with the ER (calnexin) and Golgi matrix (GM130) markers (Figure 4E). To further assess association of CERKL with other membranous compartments, we assayed colocalization to endosomes (EEA1) or mitochondria (labeled by MitoTracker staining). However, no precise colocalization was observed (Figure 4E). Instead, the mutant RP truncated protein CERKLa R257X (the localization of CERKLb 257X was identical; data not shown) showed a more stable localization pattern in the ER and nuclei (Figure 4F), in agreement with other reports [12,13]. Similar CERKL subcellular localization results were obtained at 24 h or 48 h post-transfection, although a shift toward perinuclear accumulation was clearly observed. The same pattern was obtained when analyzing the localization of all 4 CERKL-GFP isoform constructs (data not shown). Overall, these results point to a highly dynamic localization of CERKL, which may relocate according to the stimuli acting upon a cell.

To further confirm that CERKL was localized at the membranous organelles, we performed subcellular organelle fractionation in a sucrose gradient. Cells transfected with the wild-type CERKLa isoform were homogenized, and nuclei and cellular debris were discarded. Membranes were pelleted by centrifugation, resuspended in 1.5 M sucrose, and further centrifuged in a 5-step sucrose gradient, ranging from 1.5 M to 0.25 M. Fractions were collected from bottom to top, run in an SDS–PAGE and immunodetected against HA (for CERKL detection) or distinctive organelle markers. The results (Figure 5) clearly showed that CERKL distributed to the same fractions where the Trans-Golgi (TGN38), Golgi (GM130), and ER (PDI) markers localized, although CERKL was more abundant in the Trans-Golgi and Golgi fractions.

CERKL protects cells from apoptosis in oxidative stress conditions: One of the working hypotheses to explain why mutations in *CERKL* cause RP is based on its cellular protective role through the regulation of the ceramide/ceramide-1-phosphate ratio [14]. Photoreceptors are under constant oxidative challenge. Environmental stress as well as genetic mutations (e.g., on *CERKL*) would make them more susceptible to damage, tilting the survival/death balance and triggering apoptosis. To test whether CERKL has a protective role, we assayed the effect of CERKL overexpression in transiently transfected cells under normal or oxidative stress conditions. As most neuronal cell lines, retina derived cells are very poorly transfected, so we had to resort to transfections on COS-7 and HeLa cell lines to obtain statistically significant results.

COS-7 cells were transfected with each of the CERKL isoforms as well as the mutant RP protein, and cell death was assayed by propidium iodide staining after treatment with 200 μM H_2O_2 for 4 h. The results were compared to those obtained with cells transfected with either empty vector or a construct expressing the known ceramide kinase, CERK (this construct was a gift from F. Bornancin). Dead cells were stained with propidium iodide and quantified (as a percentage) against total cell number (Figure 6A). Expression of the CERKL or CERK constructs caused a slight increase in mortality in basal conditions. Under oxidative stress, there was a 3.4-fold increase in mortality in the empty-vector transfected cells, whereas cells overexpressing any of the 4 CERKL isoforms maintained a similar mortality rate (no increase in mortality) with a high statistical significance (Mann–Whitney, $p<0.05$; Figure 6B). Remarkably, the CERKL R257X (the RP mutant) failed to protect cells; the mortality rate increased under oxidative stress (Figure 6B),

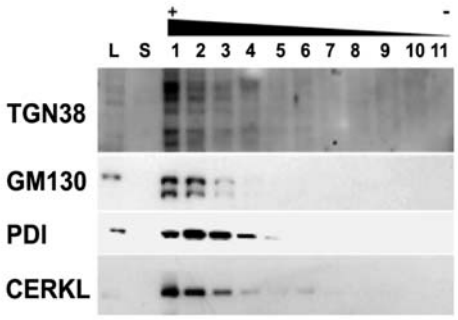

Figure 5. CERKL colocalizes with Trans-Golgi, Golgi and ER markers. HeLa cells transfected with CERKLa-HA were submitted to subcellular fractionation by sucrose gradient. The strongest signal of CERKLa coincides with the Trans-Golgi TGN38 marker, but it is also localized in the same fractions as the Golgi GM130 marker and extends to the ER PDI marker fractions. The multiple banded pattern observed in the TGN38 immunodetection has been previously reported as this protein undergoes complex post-translational modification events. CERKLa-HA was immunodetected with a monoclonal anti-HA antibody. The lanes are numbered according to the sucrose fractions as collected from 1 (bottom, with higher sucrose concentration) to 10 (top, lower sucrose concentration). Abbreviations: total protein lysate (L); supernatant after pelleting the membranes by centrifugation at 100,000x g (S).

although to a lesser level than the empty-vector cells (1.8 fold increase in mortality; statistical significance, $p<0.05$ in comparison to either CERKL isoforms or the empty vector). As propididum iodide staining was performed on coverslips, the transfection efficiency of each construct was assessed by western detection on protein lysates of replicate transfections.

Propidium iodide labels both apoptotic and necrotic cell nuclei. We attempted then to determine whether this protective effect of CERKL overexpression was on preventing cells from entering apoptosis. Activation of caspases is a well established event in apoptosis, and detection of caspase-cleaved substrates, such as PARP-1 (poly-ADP-ribose-polymerase)-1, is one of the most widespread hallmarks to quantify cell apoptosis [15,16]. PARP caspase-dependent cleavage was immunodetected in HeLa cells that were transiently transfected with either the empty vector or the CERKLa isoform (532 amino acids, encompassing the DAG kinase domain) in normal or under oxidative stress conditions, and using several reagents and concentrations: 300 µM and 400 µM H_2O_2, fetal bovine serum (FBS) deprivation and 0.3 mM sodium nitroprusside (SNP). The analysis was performed at different window times to determine the best range of conditions for quantification of any potential protective effect. CERKL did protect against apoptosis induced by oxidative stress (Figure 7A) in cells treated with 300 µM H_2O_2. This effect was dependent on the degree of oxidative insult, as it was much more effective at 300 µM (no apoptosis increase), than at 400 µM H_2O_2 (no significant protection). It was also dependent on the type of inducer, as cells overexpressing CERKLa did not behave differently from empty-vector transfected cells after FBS deprivation or SNP addition.

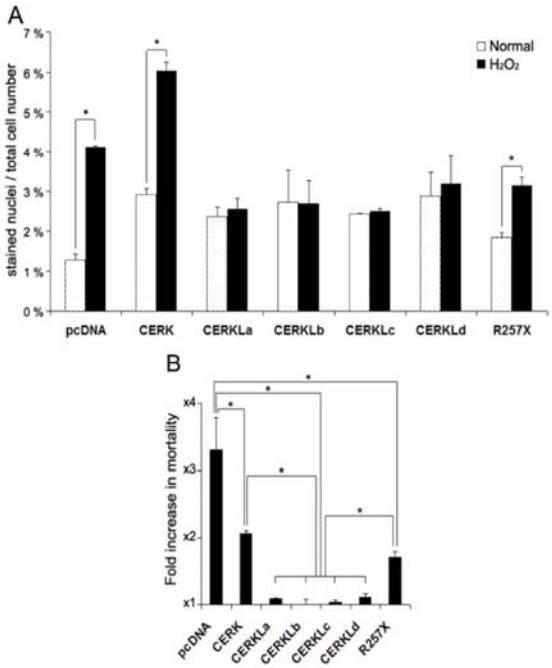

Figure 6. Cells overexpressing CERKL showed no mortality increase in a comparison of normal and oxidative stress conditions. **A:** The histogram shows the mortality (depicted as percentage) of pyknotic nuclei of COS-7 cells. Cells were transfected with either the wild-type CERKL isoforms (named CERKLa to CERKLd), the truncated RP form (R257X), CERK or the empty vector (negative control) and grown in either normal conditions (dotted bars) or treated for 4 h with 200 µM H_2O_2 (solid bars). There was no increase in mortality when the cells were transfected with any of the wt CERKL isoforms. In contrast, there was an increase in mortality in cells transfected with, either the empty vector, a CERK (ceramide kinase) construct or the R257X CERKL mutant. Statistical significance is shown by an asterisk (Mann–Whitney test, $p<0.05$). **B:** The histogram shows the mortality fold-increase of H_2O_2-treated versus untreated cells for each construct. Statistically significant differences are shown by asterisks (Mann–Whitney test, $p<0.05$). More than 500 cells were counted for each construct and condition, in 3 independent replicates.

This protective effect was also dependent on time, and presented an effective window frame. It was already detectable at 12 h (Figure 7B) with an average of 20% protection (statistical significance $p<0.05$, Mann–Whitney test). In addition, this effect appeared to be much more prominent at 24 h (Figure 7C), where the protection appeared to be maximal, around 50% protection ($p<0.05$, Mann–Whitney test). However, the effect was no longer observed at 48 h (data not shown), where PARP cleavage was high and comparable between empty-vector and CERKLa transfected cells. The expression of CERKLa was comparable in all transfections (65%–68%), as assayed by western blot (data not shown), thus the observed differences were solely attributable to the overexpression of this isoform. Interestingly, this protective effect at 24 h-treatment was only found for the full-length CERKLa but not the truncated R257X mutant (neither in the a nor the b isoform constructs; Figure 7D), in accordance to the pathogenicity of this mutation.

DISCUSSION

There is mounting evidence that most human genes show alternatively spliced isoforms, many of them regulated by tissue-specific factors. Indeed, alteration of alternative splicing is frequently linked to severe genetic diseases [17]. We report the characterization of 4 in-frame alternatively spliced isoforms of *CERKL*, which is responsible for an autosomal recessive form of retinitis pigmentosa (RP26). In our case, the isoform multiplicity increased the complexity of the functional analysis of a yet to be characterized lipid kinase. For instance, comparison of isoforms CERKLa and CERKLb revealed an additional exon (E4b), which introduces 26 additional amino acids in-frame within the DAG kinase catalytic domain and immediately upstream of the phosphate-

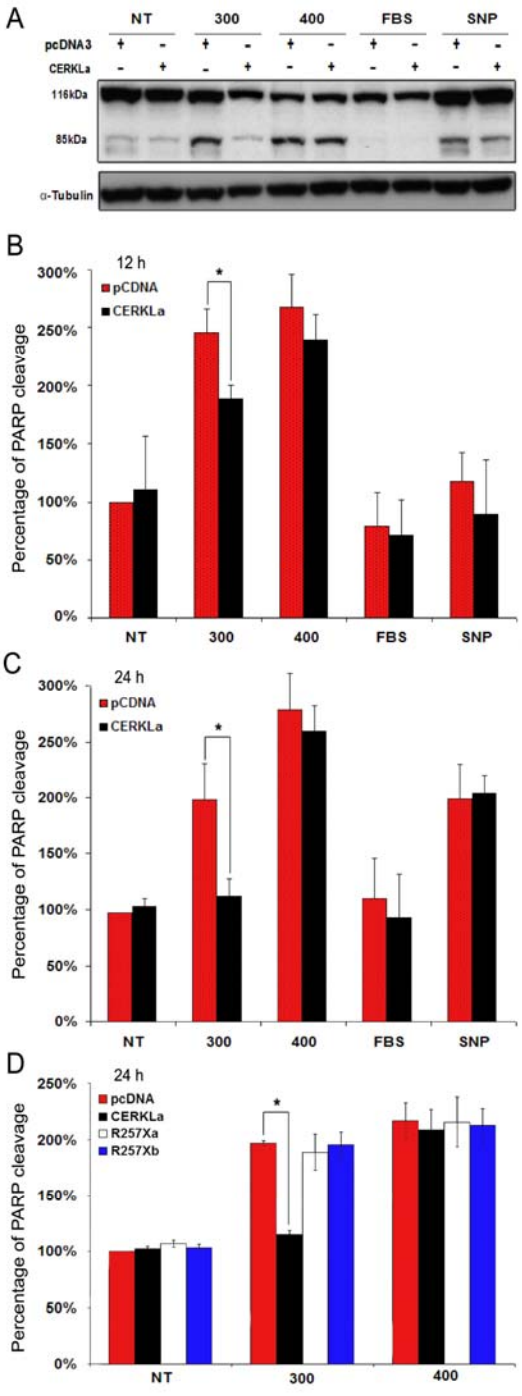

Figure 7. Overexpression of CERKL protects HeLa cells from apoptosis caused by oxidative stress. **A**: The western blot of the PARP apoptosis-dependent cleavage was obtained and immunodetected 24 h after treatment with several oxidative reagents, as indicated. The PARP precursor protein size is 116 kDa, whereas the proteolytic product after caspase-3 cleavage is 85 kDa. Cells were transfected with either the CERKLa (532aa, encompassing the kinasic domain) or the empty vector pcDNA3. Immunodetection of tubulin was used for normalization. This is one image of several similar replicates. The transfection efficiency was comparable as assessed by western immunodetection (data not shown). **B** and **C**: Quantification of the PARP-cleaved peptide with respect to total PARP immunodetected protein (both precursor plus peptide) in empty vector (red bars) versus CERKLa transfected cells (solid bars) under the different treatments. Basal apoptosis in empty vector untreated cells was arbitrarily considered 100%. CERKL protection against apoptosis was clearly detected after 12 h treatment with 300 µM H_2O_2 compared with the empty-vector transfected cells, whereas in the other oxidative conditions this protective effect was not significant (**B**). This protective effect of CERKL against apoptosis induced by 300 µM H_2O_2 was much more pronounced after 24 h treatment (**C**). **D**: The histogram shows the quantification of the PARP-cleaved peptide with respect to total PARP immunodetected protein (both precursor plus peptide) in empty vector-transfected cells (red bars) versus cells transfected with either CERKLa (solid bars), the R257X CERKLa mutant (white bars) or the R257X CERKLb mutant (blue bars). Cells were grown under normal conditions or treated with different concentrations of H_2O_2. Basal apoptosis in empty vector untreated cells was arbitrarily considered 100%. The protective effect is clearly detected for the full-length protein but not for the truncated mutants. NT-untreated cells; 300-cells treated with 300 µM H_2O_2; 400-cells treated with 400 µM H_2O_2 ; FBS-cells grown in medium deprived of fetal bovine serum; SNP-cells grown in medium supplemented with 0.3 mM sodium nitroprusside; R257Xa-cells transfected with the construct bearing the R257X mutation in the CERKLa sequence background; R257Xb-cells transfected with the construct bearing the R257X mutation in the CERKLb sequence background. At least 3 independent experiments were used for replication. Statistical significance is indicated by an asterisk (Mann–Whitney test, $p<0.05$).

donor binding site (GGDGS). The position of this exon in the presumptive catalytic domain makes it a good candidate for modulating the catalytic, substrate- or partner-binding abilities of the protein, as has been postulated for alternatively-spliced exons within encoded functional domains after an in silico genomic survey [18]. Interestingly, the other two in-frame isoforms, CERKLc and CERKLd, lack the exons encoding the DAG kinase (mainly encoded in exons 4 and 5) domain, which may severely compromise the catalytic activity while preserving other functions, among them substrate recognition. That exons 4b and 5 share a rare splice donor site (GC) strongly suggests that the production of these alternatively spliced isoforms is regulated. Genome-wide analyses on the usage of splice sites showed that only 0.69% of exon/intron donor sites are GC [19], making it highly improbable that 2 such sites flanking exons tandemly arrayed occurred in the same gene unless there was some kind of regulation behind. Given that GC- splice donor sites are intrinsically weak, explaining why 60% of the GC-flanked exons are alternatively processed [20], and that this site is evolutionarily conserved, *CERKL* splicing is probably highly regulated.

From sequence comparisons and phylogenetic analysis, CERKL unambiguously clusters within the ceramide kinase subfamily of lipid kinases [2]. However, at present, there is no experimental evidence to support CERKL kinase activity on ceramides. Therefore, it still stands as an orphan lipid kinase, in agreement with other reports [12,13]. It may well be that, although not yet identified for other lipid kinases, a partner is required for substrate recognition or catalysis. Alternatively, the substrate may be a ceramide-derived lipid undetectable under standard ceramide separation conditions. In any case, the presence of 4 different isoforms, of which 2 are devoid of the kinase domain, suggests that CERKL is involved in cellular roles other than lipid phosphorylation. Remarkably, in contrast to other lipid enzyme genes that are spread throughout all the eukaryotes, *CERKL* may be exclusive to the vertebrate lineage. Highly homologous sequences can be found in chick and fish, but no evidence of *CERKL* is found in the lancelet, the closest chordate ancestor to the vertebrates, which instead shows an unambiguous hit to *CERK* (data not shown). Further support to its vertebrate confinement comes from the fact that other invertebrate genomes, such as *Drosophila* and *C. elegans*, are also devoid of any *CERKL* homologs. In this evolutionary context, the more complex vertebrate retina may have required genes with novel enzymatic functions to protect cells against stress, adding further refinement to the metabolism of bioactive lipids as second messengers.

The versatile subcellular localization of CERKL in the COS-7 and HEK293T cell lines is common to all isoforms. This complex and highly dynamic pattern may reflect changes in the intracellular sphingolipid pools, as it occurs with other proteins in the ceramide metabolism [21–24]. CERKL has been reported to contain one bona fide nuclear localization signal (amino acids 102–106) [13], which would account for its import into the nuclei. In our studies and for all wild-type CERKL isoforms, nuclear localization is not a general event. Thus, the evident retention of the truncated R257X protein mutant seemed relevant to pathogenesis [13,14]. Further investigation is needed to determine how and why CERKL is imported into the nuclei and the nucleoli as well as what is the function of the protein in these organelles. Indeed, transient nuclear localization of CERKL may be related to the regulation of the chromatin-associated ceramide and sphingomyelin pools, in accordance with the intranuclear distribution of other key enzymes of the ceramide metabolism, as happens for SMase [25], ceramidase [26], and SPHK2 [27]. In addition, the consistent localization in the ER and Golgi compartments is compatible with the membrane-associated roles—such as non-vesicular trafficking—reported for lipid kinases and other lipid-related proteins. It has been claimed that compartmentalization of ceramide function requires transfer between different membranous organelles [8,21,23], although ceramide kinase activity has also been detected in the cytosol, where it is not associated with membranes [10], This indicates, overall, that these enzymes translocate between different compartments. In this scenario, the observed variable CERKL intracellular distribution is not so surprising, particularly when considering that similar protein localization dynamics—which shift depending on the cellular state or stimuli—are now being reported for other proteins involved in lipid metabolism [5, 24,28]. Under our conditions, the 4 isoforms showed a similar localization pattern, irrespectively of the epitope used (HA or GFP), suggesting that the functional differences among them are not dependent on subcellular localization. Besides lipid phosphorylation, CERKL isoforms may be involved in the regulation of its own enzymatic activity, lipid trafficking and storage, as well as in binding to distinct substrates or protein partners. In this context, the multiplicity of isoforms in the same tissue (or even in the same cell) and the fact that two of the four isoforms lack the lipid kinase domain, gives support to the rationale of multiplicity of functions.

RP is characterized by progressive depletion of photoreceptor cells through apoptosis. Many different genetic defects converge in retinal cell malfunction and trigger programmed cell death. The retina consists of several ordered layers of differentiated neuronal cells that are under constant oxidative stress conditions due to light exposure and a high metabolic rate. Therefore, photoreceptor survival depends on the action of anti-apoptotic mechanisms to prevent premature death. Our data support that CERKL plays a crucial protective role as its overexpression protects cells from entering apoptosis. This protective effect is dependent on time and the severity of the insult suggesting that CERKL overexpression is effective only under a range of stress conditions, but probably not after massive cell damage. Remarkably, the

R257X protein causing RP cannot protect cells after sustained injury. The weak protective effect observed at 4 h treatment with H_2O_2 was no longer detectable after 24 h treatment. This RP mutation lies within the *CERKL* exon 5, which is skipped in the variants that do not contain the DAG kinase domain (isoforms CERKLc and CERKLd). Thus, these two variants probably are not compromised in the RP26 patients. In this context, the physiologic relevance of each CERKL isoform and their particular contribution to retinal disorders is yet to be determined. Conceivably, the RP pathology could be caused by the absence of the longer isoforms or alternatively, the toxicity of the 2 truncated proteins. Our results, and the fact that most transcripts with premature STOP codons are degraded by nonsense mediated decay, support the first scenario.

To our knowledge this is the first time CERKL has been shown to be directly involved in protection against apoptosis. Thus, we link RP-causative mutations to a regulatory mechanism for cell survival, which highlights the feasibility of an RP-gene therapy approach based on protection factors to prevent photoreceptor neurodegeneration and promote cell survival.

ACKNOWLEDGMENTS

We thank Y. León and I. Varela-Nieto for their help in the first in vitro ceramide kinase activity assays. We also thank J. Garcia-Fernàndez for his help in the comparison of CERKL and CERK sequences to the amphioxus genome. We are deeply indebted to Gemma Fabriás and Josefina Casas for constant support, helpful discussions, and technical advice and help on lipid-handling and TLC techniques. We thank the Serveis Científico-Tècnics de la Universitat de Barcelona for the Sequencing and Confocal microscopy facilities. We thank Robin Rycroft and the Servei d'Assessorament Lingüístic for revising the English. This study was funded by Fundaluce (2004), Bidons-Egara, and grant BFU2006–04562 (Ministerio de Educación y Ciencia) to R.G.-D. A.G. is in receipt of an FPI grant (Ministerio de Educación y Ciencia).

REFERENCES

1. Bayés M, Goldaracena B, Martínez-Mir A, Iragui-Madoz MI, Solans T, Chivelet P, Bussaglia E, Ramos-Arroyo MA, Baiget M, Vilageliu L, Balcells S, Gonzàlez-Duarte R, Grinberg D. A new autosomal recessive retinitis pigmentosa locus maps on chromosome 2q31-q33. J Med Genet 1998; 35:141-5. [PMID: 9507394]
2. Tuson M, Marfany G, Gonzalez-Duarte R. Mutation of *CERKL*, a novel human ceramide kinase gene, causes autosomal recessive retinitis pigmentosa (RP26). Am J Hum Genet 2004; 74:128-38. [PMID: 14681825]
3. Auslender N, Sharon D, Abbasi AH, Garzozi HJ, Banin E, Ben-Yosef T. A common founder mutation of CERKL underlies autosomal recessive retinal degeneration with early macular involvement among Yemenite Jews. Invest Ophthalmol Vis Sci 2007; 48:5431-8. [PMID: 18055789]
4. Hannun YA, Obeid LM. The ceramide-centric universe of lipid-mediated cell regulation: stress encounters of the lipid kind. J Biol Chem 2002; 277:25847-50. [PMID: 12011103]
5. Hannun YA, Obeid LM. Principles of bioactive lipid signalling: lessons from sphingolipids. Nat Rev Mol Cell Biol 2008; 9:139-50. [PMID: 18216770]
6. Spiegel S, Milstien S. Sphingosine-1-phosphate: an enigmatic signalling lipid. Nat Rev Mol Cell Biol 2003; 4:397-407. [PMID: 12728273]
7. Wymann MP, Schneiter R. Lipid signalling in disease. Nat Rev Mol Cell Biol 2008; 9:162-76. [PMID: 18216772]
8. Hannun YA, Luberto C. Lipid metabolism: ceramide transfer protein adds a new dimension. Curr Biol 2004; 14:R163-5. [PMID: 15027471]
9. Sugiura M, Kono K, Liu H, Shimizugawa T, Minekura H, Spiegel S, Kohama T. Ceramide kinase, a novel lipid kinase. molecular cloning and functional characterization. J Biol Chem 2002; 277:23294-300. [PMID: 11956206]
10. Bajjalieh S, Batchelor R. Ceramide kinase. Methods Enzymol 2000; 311:207-15. [PMID: 10563327]
11. Tan E, Ding XQ, Saadi A, Agarwal N, Naash MI, Al-Ubaidi MR. Expression of cone-photoreceptor-specific antigens in a cell line derived from retinal tumors in transgenic mice. Invest Ophthalmol Vis Sci 2004; 45:764-8. [PMID: 14985288]
12. Bornancin F, Mechtcheriakova D, Stora S, Graf C, Wlachos A, Dévay P, Urtz N, Baumruker T, Billich A. Characterization of a ceramide kinase-like protein. Biochim Biophys Acta 2005; 1687:31-43. [PMID: 15708351]
13. Inagaki Y, Mitsutake S, Igarashi Y. Identification of a nuclear localization signal in the retinitis pigmentosa-mutated PR26 protein, ceramide kinase-like protein. Biochem Biophys Res Commun 2006; 343:982-7. [PMID: 16581028]
14. Gonzalez-Duarte R, Tuson M, Marfany G. Ceramide, ceramide kinase and vision defects: a BLIND spot for LIPIDS. In Hirabayashi Y, Igarashi, Y, Merrill Jr AH, editors. Sphingolipid Biology. Tokyo: Springer-Verlag; 2006. p. 337–344.
15. Duriez PJ, Shah GM. Cleavage of poly(ADP-ribose) polymerase: a sensitive parameter to study cell death. Biochem Cell Biol 1997; 75:337-49. [PMID: 9493956]
16. Affar EB, Germain M, Winstall E, Vodenicharov M, Shah RG, Salvesen GS, Poirier GG. Caspase-3-mediated processing of poly(ADP-ribose) glycohydrolase during apoptosis. J Biol Chem 2001; 276:2935-42. [PMID: 11053413]
17. Garcia-Blanco MA, Baraniak AP, Lasda EL. Alternative spliding in disease and therapy. Nat Biotechnol 2004; 22:535-46. [PMID: 15122293]
18. Wen F, Li F, Xia H, Lu X, Zhang X, Li Y. The impact of very short alternative splicing on protein structures and functions in the human genome. Trends Genet 2004; 20:232-6. [PMID: 15109776]
19. Thanaraj TA, Clark F. Human GC-AG alternative intron isoforms with weak donor sites show enhanced consensus at acceptor exon positions. Nucleic Acids Res 2001; 29:2581-93. [PMID: 11410667]
20. Clark F, Thanaraj TA. Categorization and characterization of transcript-confirmed constitutively and alternatively spliced introns and exons from human. Hum Mol Genet 2002; 11:451-64. [PMID: 11854178]

21. Hanada K, Kumagai K, Yasuda S, Miura Y, Kawano M, Fukasawa M, Nishijima M. Molecular machinery for non-vesicular trafficking of ceramide. Nature 2003; 426:803-9. [PMID: 14685229]
22. Munro S. Cell biology: earthworms and lipid couriers. Nature 2003; 426:775-6. [PMID: 14685214]
23. Hanada K, Kumagai K, Tomishige N, Kawano M. CERT and intracellular trafficking of ceramide. Biochim Biophys Acta 2007; 1771:644-53. [PMID: 17314061]
24. Yamaji T, Kumagai K, Tomishige N, Hanada K. Two sphingolipid transfer proteins, CERT and FAPP2: their roles in sphingolipid metabolism. IUBMB Life 2008; 60:511-8. [PMID: 18459163]
25. Albi E, Lazzarini R, Magni MV. Reverse sphingomyelin-synthase in rat liver chromatin. FEBS Lett 2003; 549:152-6. [PMID: 12914942]
26. Tsugane K, Tamiya-Koizumi K, Nagino M, Nimura Y, Yoshida S. A possible role of nuclear ceramide and sphingosine in hepatocyte apoptosis in rat liver. J Hepatol 1999; 31:8-17. [PMID: 10424278]
27. Igarashi N, Okada T, Hayashi S, Fujita T, Jahangeer S, Nakamura S. Sphingosine kinase 2 is a nuclear protein and inhibits DNA synthesis. J Biol Chem 2003; 278:46832-9. [PMID: 12954646]
28. Irvine R. Inositol lipids: to PHix or not to PHix? Curr Biol 2004; 14:R308-10. [PMID: 15084300]

The print version of this article was created on 16 January 2009. This reflects all typographical corrections and errata to the article through that date. Details of any changes may be found in the online version of the article.

Publicació 2

High transcriptional complexity of the retinitis pigmentosa CERKL gene in human and mouse

PUBLICACIÓ 2

TÍTOL

"*High transcriptional complexity of the retinitis pigmentosa CERKL gene in human and mouse*"

AUTORS (ANY)

Alejandro Garanto, Marina Riera, Esther Pomares, Jon Permanyer, Marta de Castro-Miró, Florentina Sava, Josep F Abril, Gemma Marfany i Roser Gonzàlez-Duarte (2011)

REFERÈNCIA

Investigative Ophtalmology and Visual Science, 52: 5202-5214

RESUM

S'han descrit diverses mutacions en *CERKL*, que causen retinosi pigmentària (RP). Ens vàrem proposar realitzar un estudi transcripcional exhaustiu, tant en teixits humans com murins, enfocat a identificar el repertori de possibles formes d'*splicing*, determinar la utilització de promotors alternatius i, l'efecte de les mutacions descrites fins el moment. Per caracteritzar l'espectre transcripcional de *CERKL* vàrem emprar dues estratègies diferents, *in silico* i *in vitro*. L'anàlisi *in silico*, va consistir en la cerca d'inicis de transcripció i predicció de metionines iniciadores, així com en la generació d'una matriu a partir de tots els gens causants d'RP no sindròmica, per cercar motius estructurals, comuns a tots ells i possibles dianes de factors de transcripció específics de retina. Mitjançant RT.PCRs, es van caracteritzar els transcrits aïllats de diferents teixits, especialment a la retina. El resultat d'aquesta caracterització va ser una elevada multiplicitat de transcrits, on es van aïllar més de 20 en cadascuna de les espècies i la gran majoria d'ells, no descrits fins el moment. Endemés, es van identificar tres promotors nous en cada espècie, fet que encara augmenta més la complexitat transcripcional d'aquest gen. Per últim, es va estudiar la localització de CERKL en la retina de ratolí mitjançant tècniques immunohistoquímiques. Aquests experiments van mostrar que CERKL és majoritàriament citosòlica, i que localitza sobretot en el segment extern dels cons i regions perinuclears. Tant els estudis *in vitro* com *in silico* van convergir en els mateixos resultats, fet que ofereix un mapa dels productes gènics específics de cada espècie i que suggereix una regulació gènica molt fina a nivell de la retina i altres teixits, que pot servir d'ajuda per fer estudis de correlació genotip-fenotip en els casos de distròfia retinal en els quals *CERKL* és el gen causal.

NOTA: El material suplementari es troba disponible en el CD adjunt al final d'aquesta Tesi. Per una millor visualització, el desplegable que es troba a continuació d'aquest article, es correspon a la Figura 2 de la PUBLICACIÓ 2.

APORTACIÓ PERSONAL AL TREBALL

Aquest treball ha estat realitzat per diverses persones del grup d'RP i del grup del Dr. Josep F. Abril. La meva aportació a aquesta publicació ha estat la totalitat de la part experimental i anàlisi corresponent realitzada sobre mostres de ratolí, i que ha consistit en: a) dissecció de teixits, extracció d'RNA i la realització de les RT-PCRs per caracteritzar els transcrits (Figura 1B); b) identificació dels transcrits majoritaris (Figura 3B); c) semiquantificació de l'expressió de *Cerkl* en teixits murins (Figura 5B); d) cerca de nous promotors, així com la seva especificitat tissular (Figura 6), i e) dissecció i realització dels talls de retina per dur a terme la detecció de la proteïna en les cèl·lules d'aquest teixit (Figura 7).

High Transcriptional Complexity of the Retinitis Pigmentosa *CERKL* Gene in Human and Mouse

Alejandro Garanto,[1,2,3,4] *Marina Riera,*[1,2,3,4] *Esther Pomares,*[1,2,3] *Jon Permanyer,*[1,2] *Marta de Castro-Miró,*[1] *Florentina Sava,*[1] *Josep F. Abril,*[1,2] *Gemma Marfany,*[1,2,3] *and Roser Gonzàlez-Duarte*[1,2,3]

Purpose. To shed light on the pathogenicity of the mutations in the retinitis pigmentosa gene *CERKL*, the authors aimed to characterize its transcriptional repertoire and focused on the use of distinct promoters and alternative splicing in human and mouse tissues.

Methods. In silico genomic and transcriptomic computational customized analysis, combined with experimental RT-PCRs on different human and murine tissues and cell lines and immunohistochemistry, have been used to characterize the transcriptional spectrum of *CERKL*. In the mouse retina, Cerkl is detected primarily in ganglion cells and cones but can also be observed in rods. Cerkl is mainly cytosolic. It localizes in the outer segments of photoreceptors and in the perinuclear regions of some cells.

Results. An unexpected multiplicity of *CERKL* transcriptional start sites (four in each species) plus a high variety of alternative splicing events primarily affecting the 5′ half of the gene generate >20 fully validated mRNA isoforms in human and 23 in mouse. Moreover, several translational start sites, compatible with a wide display of functional domains, contribute to the final protein complexity.

Conclusions. This combined approach of in silico and experimental characterization of the *CERKL* gene provides a comprehensive picture of the species-specific transcriptional products in the retina, underscores highly tuned gene regulation in different tissues, and establishes a framework for the study of *CERKL* genotype-phenotype correlations. (*Invest Ophthalmol Vis Sci.* 2011;52:5202–5214) DOI:10.1167/iovs.10-7101

Spatiotemporal differential splicing, often related to developmental events or tissue differentiation processes, affects >95% of the human genes, as recently unveiled after massive sequencing of the human transcriptome.[1,2] Alternative splicing and the use of alternative promoters and transcriptional splice sites are instrumental for the generation of complexity, as proteins with different functions are encoded by the transcript variants produced. Cells can thus deploy a wide array of proteins, all arising from a single genomic sequence.[3,4]

Misregulation of alternative splicing is often at the basis of human disease, given that distortions in the splicing process either directly alter the domains displayed by proteins or, more relevant to pathology, cause frameshifts that are frequently associated with premature stop codons.[5] Therefore, prior knowledge of all the physiologically produced transcripts from a gene of interest is crucial to draw genotype-phenotype correlations in hereditary diseases and to infer the degree of pathologic severity.[6–8] This is even more relevant when considering genetic disorders of the mammalian central nervous system (CNS) and derived neurologic tissues, such as the retina, in which the highest degree of alternative splicing events occurs.[9–11]

Retinitis pigmentosa (RP) is a hereditary neurodegenerative disorder with extremely high genetic heterogeneity. It affects 1:4000 people worldwide, and it is the major cause of nontraumatic adult blindness.[12] Although >45 genes have been identified as causative of RP (Retnet, http://www.sph.uth.tmc.edu/Retnet/), approximately 40% of the genetic cases remain unassigned, highlighting the relevance of identifying new candidates because each gene will presumably explain very few cases. The molecular diagnosis becomes even more complex under the light of recent reports that reveal new mutations in known RP genes, which alter retina-specific splicing events either by changing the number of exons included in the mature product or by modifying the relative proportion of the spliced isoforms.[13–15] These findings widen the range of molecular mechanisms underlying tissue-restricted abnormalities, decrease the number of unknown RP genes, illuminate new scenarios for tissue-specific gene function, and emphasize the need for accurate characterization of candidate splicing products, particularly because 70% of the exons in the human genome are tissue specific.[1,16]

Our group first identified *CERKL* as an RP gene[17] by detecting a homozygous nonsense mutation (R257X) that cosegregated in consanguineous Spanish families. *CERKL* was widely expressed, and the highest transcription levels were observed in the retina.[17,18] Interestingly, the R257X mutation was embedded in an alternatively spliced exon; therefore, some of the *CERKL* isoforms were a priori functional in the patients.[19] These results prompted us to undertake a more accurate characterization of the *CERKL* transcripts in human and mouse. Our work unveils an unexpectedly high complexity of the *CERKL* transcripts, particularly at the 5′ end of the gene, with alternative first exons, inclusion/exclusion of alternatively spliced exons, intron retention, and additional splice sites.

From the [1]Departament de Genètica, Facultat de Biologia, and the [2]Institut de Biomedicina, Universitat de Barcelona, Barcelona, Spain; and [3]CIBERER, Instituto de Salud Carlos III, Barcelona, Spain.

[4]These authors contributed equally to the work presented here and should therefore be regarded as equivalent authors.

Supported by Grants SAF2009-08079 (Ministerio de Ciencia e Innovación) and SGR2009-1427 (Generalitat de Catalunya), CIBERER (U718), Fundaluce and ONCE (RG-D) and BFU2010-15656 (GM). AG, MR, and MC-M were in receipt of the fellowships FPI BES-2007-15414, FPU AP2007-00805, and FPI BES-2010-030745, respectively. EP was under contract by CIBERER.

Submitted for publication December 20, 2010; revised March 31, 2011; accepted April 11, 2011.

Disclosure: **A. Garanto**, None; **M. Riera**, None; **E. Pomares**, None; **J. Permanyer**, None; **M. de Castro-Miró**, None; **F. Sava**, None; **J.F. Abril**, None; **G. Marfany**, None; **R. Gonzàlez-Duarte**, None

Corresponding author: Roser Gonzàlez-Duarte, Departament de Genètica, Facultat de Biologia, Universitat de Barcelona, Avenida Diagonal 645, 08028 Barcelona, Spain; rgonzalez@ub.edu.

Overall, these results, together with the bioinformatics analysis, strongly support the generation of many protein isoforms and the different roles of CERKL in retinal cells and other tissues, and they provide a molecular framework for genotype-phenotype correlations because the location of the mutation in the *CERKL* gene would affect the number and type of transcripts and, hence, be related to the progression and severity of the disease.

Materials and Methods

Animal Handling, Tissue Dissection, and Preparation of Samples

All animal handling and procedures were performed according to the ARVO Statement for the Use of Animals in Ophthalmic and Vision Research and the regulations of the animal care facilities at the University of Barcelona. In brief, C57BL/6J mice (Charles River Laboratories, Davis, CA) were euthanatized with CO_2 followed by cervical dislocation, and specific tissues and organs were dissected and immediately frozen in liquid nitrogen. Human blood and saliva samples were collected from nonaffected subjects with RP, after they provided informed consent, in accordance with the tenets of the Declaration of Helsinki. Retina and brain total RNA samples were supplied by Clontech Laboratories, Inc. (Mountain View, CA), and liver cDNA was provided by BD Biosciences (San Jose, CA).

Cell Culture and Constructs

Human embryonic kidney cells 293T (HEK293T, Bethyl Laboratories, Montgomery, TX) and wild-type fibroblasts (kindly provided by Daniel Grinberg and Lluïsa Vilageliu) were grown in DMEM with 4 mM L-glutamine. The human lung adenocarcinoma epithelial cell line (A549; Abcam, Cambridge, MA) was cultured in Ham's F12 L-glutamine (PAA Laboratories GmbH, Pasching, Austria). Both media were supplemented with 10% fetal bovine serum (FBS), 100 U/mL penicillin, and 100 μg/mL streptomycin (Invitrogen Life Technologies, Carlsbad, CA).

RNA Extraction and RT-PCR

For total RNA extraction, a tissue kit (High Pure RNA Tissue Kit; Roche Diagnostics, Indianapolis, IN) was used in accordance with the manufacturer's instructions. Human and mouse blood RNA was mixed (RNA*later*; Ambion/Applied Biosystems, Foster City, CA) before extraction (RiboPure-Blood Kit; Ambion/Applied Biosystems). Saliva samples were treated as indicated (Oragene/RNA protocol; DNA Genotek Inc., Ontario, Canada), and RNA was extracted from human cultured cells (RNeasy kit; Qiagen, Germantown, MD). RT-PCR assays were performed for human and mouse samples (Mint Kit [Evrogen, Moscow, Russia] or Transcriptor High Fidelity cDNA Synthesis Kit [Roche Diagnostics, Indianapolis, IN]). For tissue expression analysis, all reaction mixtures (50 μL) contained 10 μM each primer pair, 2 μM dNTPs, 1.5 mM $MgCl_2$, and 1 U polymerase (Go*Taq*; Promega, Madison, WI). Primer localizations are depicted in Figures 1A2 (human) and 1B2 (mouse), and the sequences are given in Supplementary Table S1, http://www.iovs.org/lookup/suppl/doi:10.1167/iovs.10-7101/-/DCSupplemental. *CERKL* was amplified using primers A and B for human and a and b for mouse (120 seconds at 94°C followed by 35 cycles of 94°C for 20 seconds, 60°C for 30 seconds, and 72°C for 30/20 seconds). *GAPDH* was used for normalization (120 seconds at 94°C and 30 cycles of 94°C for 20 seconds and 63°C for 120 seconds).

Analysis of the 5′ and 3′ UTRs of human and murine *CERKL* retina isoforms was performed, using either the Plug adaptor or oligo-d(T) primers (provided in the Mint Kit; Evrogen) paired with suitable *CERKL*-specific internal primers under the indicated PCR conditions. The characterization of alternatively spliced variants and promoters was performed using a combination of the internal primers located in different exons. The primers were designed to share the same amplification conditions: 120 seconds at 94°C followed by 40 cycles of 94°C for 20 seconds, 58°C for 30 seconds, and 72°C for 90 seconds. All sequences have been submitted to GenBank (accession numbers are shown in Supplementary Tables S2A and S2B, http://www.iovs.org/lookup/suppl/doi:10.1167/iovs.10-7101/-/DCSupplemental).

Transfections and Recombinant Protein Expression and Immunodetection

For protein expression, HEK293T cells (2×10^5 cells) were seeded and transfected using reagent (Lipofectamine 2000; Invitrogen Life Technologies, Carlsbad, CA), according to the manufacturer's protocol. The recombinant constructs were obtained by cloning representative human cDNA isoforms (h2, h13, h18 in Figs. 1A and 4A) with and in-frame HA epitope fused at the C terminus into pcDNA 3.1 (Clontech Laboratories, Inc., Mountain View, CA). After 48 hours, cells were lysed with protein loading buffer ×1 and boiled for 5 minutes. Protein lysates were loaded onto 12% SDS-PAGE gels that were transferred and analyzed by Western blot. Immunodetection was performed with a primary monoclonal anti-HA (1:1000) and HRP-conjugated anti-mouse secondary antibody (1:3000). Tubulin immunodetection was used as a loading control.

Immunohistochemistry on Mouse Retina Cryosections

Eyes from 8-week-old C57BL/6J mice were fixed in 4% paraformaldehyde (PFA) and 0.5% glutaraldehyde (2 hours at room temperature), cryoprotected in acrylamide, and embedded in OCT (Tissue-Tek, Sakura Finetek, Torrance, CA). Sixteen-micrometer sections on polylysine–covered slides were used for immunostaining, as described[20] with some modifications. Incubation with peanut agglutinin (PNA) conjugated to Alexa Fluor 647 (40 mg/mL; Invitrogen Life Technologies) and the primary antibodies mouse anti-rhodopsin 1:500 (Abcam), mouse anti-PKCα 1:500 (Santa Cruz Biotechnology, Inc., Santa Cruz, CA), and preabsorbed rabbit anti-CERKL 1:50, was performed overnight. Subsequently, slides were incubated with the corresponding secondary antibodies (1:300) conjugated to either Alexa Fluor 488, 546, or 568 (Invitrogen Life Technologies). Sections were mounted with reagent (Fluoprep; Biomérieux, Marcy l'Etoile, France) and photographed with a confocal microscope (SP2; Leica Microsystems, Wetzlar, Germany).

Bioinformatic Analysis of the Genomic Human CERKL Locus

Most of the computational analyses were performed using the genomic sequence of the human *CERKL* locus at chromosome 2 (March 2006 assembly version [NCBI36/hg18)]) within the interval 182,029,864 bp to 182,259,440 bp (including the *ITG4* and *NEUROD1* loci), which was retrieved from the UCSC human genome browser.[21] However, for the purpose of comparative genomics and to determine the conservation among human and other vertebrates (such as *Macaca mulatta*, *Mus musculus*, *Gallus gallus*, and *Takifugu rubripes*), precomputed whole genome alignments were analyzed through the VISTA UCSC browser mirror, which provides the VISTA track feature.[22] The syntenic region of the mouse genome was also retrieved. BLASTN and TBLASTX alignments were performed on the syntenic sequences using the NCBI bl2seq algorithm[23] for a more in-depth comparison between human and mouse.

Previously described *CERKL* isoforms were retrieved from several databases: RefSeq,[24] GenBank,[25] dbTSS,[26] and VEGA.[27] Some of the dbTSS transcripts were already mapped on the human *CERKL* genomic region at the VEGA Web site. These sequences, as well as experimentally validated *CERKL* cDNAs (this work), were mapped onto the analyzed sequence interval using Exonerate,[28] following the est2genome model algorithm for easier comparison of all the exonic structures from both the database and experimental evidence (complete visualization is shown in Supplementary Fig. S1, http://www.iovs.org/lookup/suppl/doi:10.1167/iovs.10-7101/-/DCSupplemental).

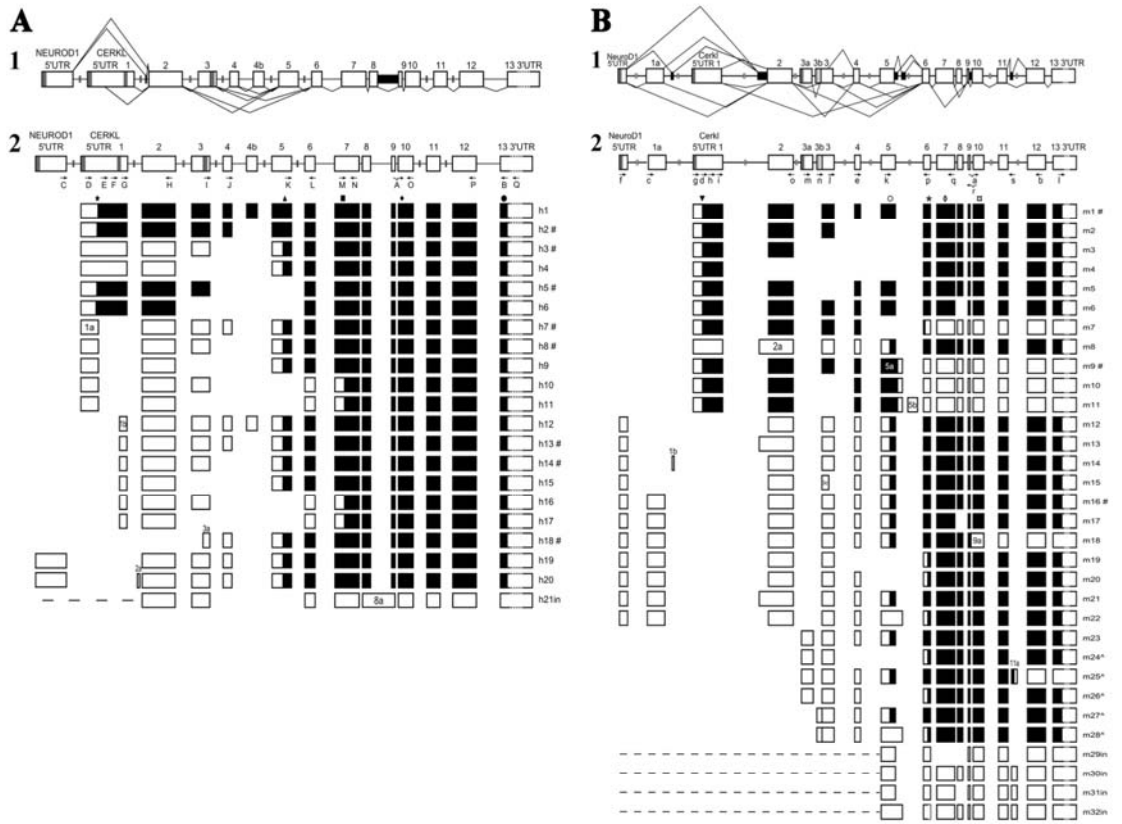

FIGURE 1. Alternately spliced *CERKL* isoforms in human and mouse retina. Extremely high complexity of the splicing events in human (**A1**) and mouse (**B1**) *CERKL* transcripts. *Open boxes*: exons. *Filled boxes*: retained introns or cryptic noncoding exons. *Angled lines* above and below the gene structure indicate validated splicing events. Scheme depicting all the human (**A2**) and mouse (**B2**) spliced variants observed in the retina. Exons are indicated as *boxes* and the coding sequence (CDS) for each isoform, considering the higher likelihood of first methionine, is shown in *black*. *Dark gray*: TSS found in retina. *Light gray*: nonretinal TSS. #Main isoforms in each species. *Arrows*: letters indicate the position and direction of the primers used for PCR reactions (complete list and sequence in Supplementary Table S1, http://www.iovs.org/lookup/suppl/doi:10.1167/iovs.10-7101/-/DCSupplemental). ^Nonretinal isoforms found in mouse liver and spleen. The scores of the Kozak's motif hits containing putative TIS methionines for human are: ⋆ 12.003; ▲ 5.248; ■ 8.389; ♦ 5.281; ● 8.852. For mouse they are: ▼ 13.384; ○ 9.620; *10.662; ◊ 8.389; ¤ 8.863 (the complete list of all Kozak's scores are contained in Supplementary Table S5, http://www.iovs.org/lookup/suppl/doi:10.1167/iovs.10-7101/-/DCSupplemental).

Although a track for the First-Exon-Finder program[29] on the UCSC genome browser was already available, an additional attempt was performed to predict more CpG islands, promoters, and first exons on the *CERKL* genomic region (cutoff value for the first-exon a posteriori probability [APP] = 0.5, cutoff value for the promoter APP = 0.4, and cutoff value for the promoter APP = 0.4).

Genomic sequences for a set of 49 genes related to RP, classified into 10 distinct functional classes, were downloaded from GenBank: *RHO*, *PDE6A*, *PDE6B*, *CNGA1*, *CNGB1*, *SAG*, *GUCA1B*, and *GUCY2D* (phototransduction); *ABCA4*, *LRAT*, *RPE65*, *RLBP1*, *RGR*, *RDH12*, and *RBP3* (retinol metabolism); *PRPH2*, *PROM1*, *EYS*, and *ROM1* (photoreceptors structure); *CRX*, *NR2E3*, *NRL*, and *OTX2* (transcription factors); *SEMA4A*, *MERTK*, *CRB1*, and *USH2A* (cellular interaction); *PRPF3*, *PRPF8*, *PRPF31*, *RP9*, *SNRNP200* (mRNA processing); *TULP1*, *RPGRIP*, *RPGR*, *RP2*, *FSCN2*, *RP1*, *AIPL1*, *CEP290*, and *LCA5* (transport); *KLHL7* and *TOPORS* (ubiquitin/proteasome pathway); *IMPDH1*, *CA4*, and *IDH3B* (several types of enzymatic activities); and, finally, *RD3*, *SPATA7*, and *PRCD* (unknown function). Up to 10-kbp upstream sequences of these genes were searched for overrepresented motifs by running MEME.[30] The first analysis was performed over the whole set of sequences; then, in the following round, MEME was run separately for the sequences of each functional class. Two sets of parameters were used to characterize long and short motifs. To search for long motifs, the "*anr*" model was used, with a minimum width of 8 and a maximum width of 20, and a total of 200 iterations (-mod anr -nmotifs 20 -minw 8 -maxw 20 -maxiter 200). To identify the short ones, the same model was applied, but the maximum width was reduced to 10 (-mod anr -nmotifs 10 -minw 8 -maxw 10 -maxiter 200). Both sets of parameters were applied to the whole data set analysis and to the split group consisting of 10 different functional classes. For each characterized motif, a log likelihood matrix was derived using two background models, the random model (equiprobability for all four nucleotides) and the model considering the GC content bias (40% GC for the whole *CERKL* genomic sequence, including the neighboring loci). We extended the analysis to the promoters (1 kb upstream) of the cone-rod dystrophy (CRD) genes using the TRANSFAC matrices with particular emphasis on the retina-related transcription factor. The genes were grouped according to the disease to which they contributed most: RP (*RHO*, *PDE6A*, *PDE6B*, *CNGA1*, *CNGB1*, *SAG*, *GUCA1B*, *LRAT*, *RPE65*, *RLBP1*, *RGR*, *RDH12*, *RBP3*, *ROM1*, *EYS*, *NR2E3*, *NRL*, *OTX2*, *MERTK*, *CRB1*, *USH2A*, *PRPF3*, *PRPF8*, *PRPF31*, *RP9*, *SNRNP200*, *TULP1*, *RPGR*, *RP2*, *FSCN2*, *RP1*, *CEP290*, *LCA5*, *KLHL7*, *TOPORS*, *IMPDH1*, *CA4*, *IDH3B*, *RD3*, *SPATA7*, and *PRCD*), CRD (*GUCA1A*, *PITPNM3*, *RIMS1*, *UNC119*, *ADAM9*, *CACNA2D4*, *RAX2*,

CDHR1, and *CACNA1F*), and the two retinal disorders (*ABCA4*, *GUCY2D*, *PROM1*, *PRPH2*, *CRX*, *SEMA4A*, *RPGRIP1*, *AIPL1*, and *CERKL*). Unfortunately, no clear pattern of single/clustered transcription factor sites emerged considering any of the three gene groups, either on general or on retina-specific transcription factor matrices (Supplementary Fig. S2, http://www.iovs.org/lookup/suppl/doi:10.1167/iovs.10-7101/-/DCSupplemental).

In addition to those generated by MEME, a new set of matrices corresponding to a selection of known transcription initiation factors (including TATA, CAAT, USF, INI, SRF, SP1, and TFIIA) was downloaded from TransFac.[31] Retina-related transcription factor matrices (for PAX6, AP1, ZF5, AP2REP, AP2ALPHA, AP2GAMMA, TBP, MAZR, CRX, GATA4, SP3, ETF, KROX, WT1, NR2E3, V-MAF, and WT1) were also gathered from TransFac, Promo,[32] and Jaspar.[33] All the matrices were mapped into the analyzed genomic region of *CERKL* using custom Perl scripts with the specific purpose of defining potential novel alternative transcription starting sites (TSS) for *CERKL* isoforms. The score hits on the genomic sequence were normalized between 0 and 1; then a threshold was defined as the score above 95% of the distribution for all those scores. Only hits of matrices showing a normalized score equal to or greater than the threshold were considered (a summary of those found on the 1 kbp upstream for every reported human and mouse *CERKL* exons that included a TSS is provided on Supplementary Tables S4A (human) and S4B (mouse), http://www.iovs.org/lookup/suppl/doi:10.1167/iovs.10-7101/-/DCSupplemental.

Putative translation start sites were evaluated using the Kozak matrix[34] under the same terms. Moreover, the ENCODE H3K4Me3 track[35] on the UCSC genome browser was also considered as additional transcriptional evidence, given that histone modification correlates with transcriptionally active sites.[36] The distribution of SNPs across the exons of the *CERKL* gene was analyzed using dbSNP31, over the hg19 database.

Results

Comprehensive Identification of Alternatively Spliced *CERKL* Isoforms

Evidence of different alternatively spliced isoforms of *CERKL* have been reported, but a comprehensive prioritized list of the physiologically relevant transcript is still missing.[19,37] Furthermore, its wide tissular expression[17,18] appears to be inconsistent with the tissue-restricted phenotype of *CERKL* mutations because only the retina was affected. In this case, as happens with other retina-associated disease genes, tissue-specific isoforms might have reconciled this apparent paradox.[14]

Thus, we first aimed to exhaustively characterize the *CERKL* alternatively spliced isoforms generated in human and murine retinas and to perform an interspecific comparative analysis. Two different methods for the synthesis of the cDNAs (detailed description in Materials and Methods) were used to replicate the experiments, validate the sequences, and avoid technical biases. For a comprehensive isoform characterization, we performed 5′ and 3′ RACE reactions to identify initial and terminal UTRs on endogenously expressed retinal transcripts and subsequently used a battery of internal PCR primers (listed in Supplementary Table S1 [http://www.iovs.org/lookup/suppl/doi:10.1167/iovs.10-7101/-/DCSupplemental] and located in Figs. 1A2 [human] and 1B2 [mouse]) to unveil the combinatorial network of alternative promoters and exons displayed in *CERKL* transcripts. From these data we designed specific primers to identify fully processed transcripts encompassing the first to the last exon and thus depict the complete repertoire of *CERKL* aligned with the genomic primary structure as a means to validate each transcript variant.

Overall, the retinal *CERKL* isoforms generated by alternative splicing events showed an unexpected complexity because >20 transcripts were identified in human and mouse retinas. The genomic organization of *CERKL* with the splicing events (depicted as angled lines) and 5′UTRs (gray boxes) identified are shown in Figures 1A (human) and 1B (mouse). The most abundant transcripts are indicated by the # symbol. For each human and mouse transcript, the 3′UTR was unique, although murine transcripts contained a longer 3′UTR than previously reported, pointing to two polyadenylation signals. Notably, in the two species, the 5′ UTRs showed an unexpected multiplicity of TSS that contributed to the combinatorial complexity of the mature transcripts. This heterogeneity called for a rational and comprehensive nomenclature of all *CERKL* variants in human and mouse. Therefore, sequences from published reports, databases, and this work were gathered and systematized. Our proposal is presented in Supplementary Tables S2A and S2B (http://www.iovs.org/lookup/suppl/doi:10.1167/iovs.10-7101/-/DCSupplemental).

In detail, the analysis of the 20 fully validated human transcripts provided solid evidence of four different *CERKL* TSS (Fig. 1A). Eleven transcripts were expressed from the previously reported 5′ UTR; two from the starting site of the adjacent upstream *NEUROD1* gene (known to be highly expressed in the CNS and transcribed in the same direction than *CERKL*); six from an internal, previously unknown initiation site within exon 1 (referred to as exon 1b in the text and Supplementary material, http://www.iovs.org/lookup/suppl/doi:10.1167/iovs.10-7101/-/DCSupplemental); and one started from an internal sequence of exon 3 (referred to as exon 3a). Of note, the TSS of exon 1b was also supported in silico by the First-Exon-Finder, which, among other structural features, mapped a CpG island within this genomic region, and by the clustering of peaks of the H3K4Me3 track, indicative of transcriptionally active chromatin sites (Fig. 2). Yet we cannot rule out that *CERKL* is transcribed from unknown TSS in other tissues. In this context, the UCSC genome browser has recently incorporated an ENCODE track that corresponds to manually annotated genes, based primarily on sequenced full-length cDNAs from dbTSS plus reports from independent sources. Twelve of the 15 ENCODE *CERKL* variants fully overlapped with some retinal transcripts described in this work. Of the remaining three, one (OTTHUMT00000334820) started at a TSS extremely close to the reported *CERKL* 5′ UTR and possibly was structurally equivalent; the other two (OTTHUMT00000334817 and OTTHUMT00000334818) started at completely different internal sites, suggesting two additional TSS. If the latter two isoforms were validated, the number of *CERKL* TSS in human would amount to six.

In contrast, in the murine retina, only three *Cerkl* start sites were experimentally identified (Fig. 1B, dark gray): 11 (of 23) fully validated transcripts started from the previously reported *Cerkl* site, 11 from the upstream *NeuroD1* gene (as in human), and the last from the novel exon 3a, located in intron 2. The latter is also supported by the dbTSS database. Moreover, RT-PCR assays performed in a panel of several tissues provided evidence for an additional TSS within intron 2, which generated exon 3b (not found in the retina). A complete list specifying the contribution (presence or absence) of every exon in each *CERKL/Cerkl* isoform is presented in Supplementary Table S3, http://www.iovs.org/lookup/suppl/doi:10.1167/iovs.10-7101/-/DCSupplemental.

To identify the more abundant transcripts and approach their relative physiological relevance (Figs. 3A [human] and 3B [mouse]), we used a battery of primers, located either at the different TSS or the alternative exons at the 5′ of *CERKL*, paired with a unique reverse primer in exon 10 (human) or exon 12 (mouse). The location of the primers is indicated in Figure 3C. For isoform assignment, each amplified product was isolated and sequenced. The RT-PCRs were replicated several

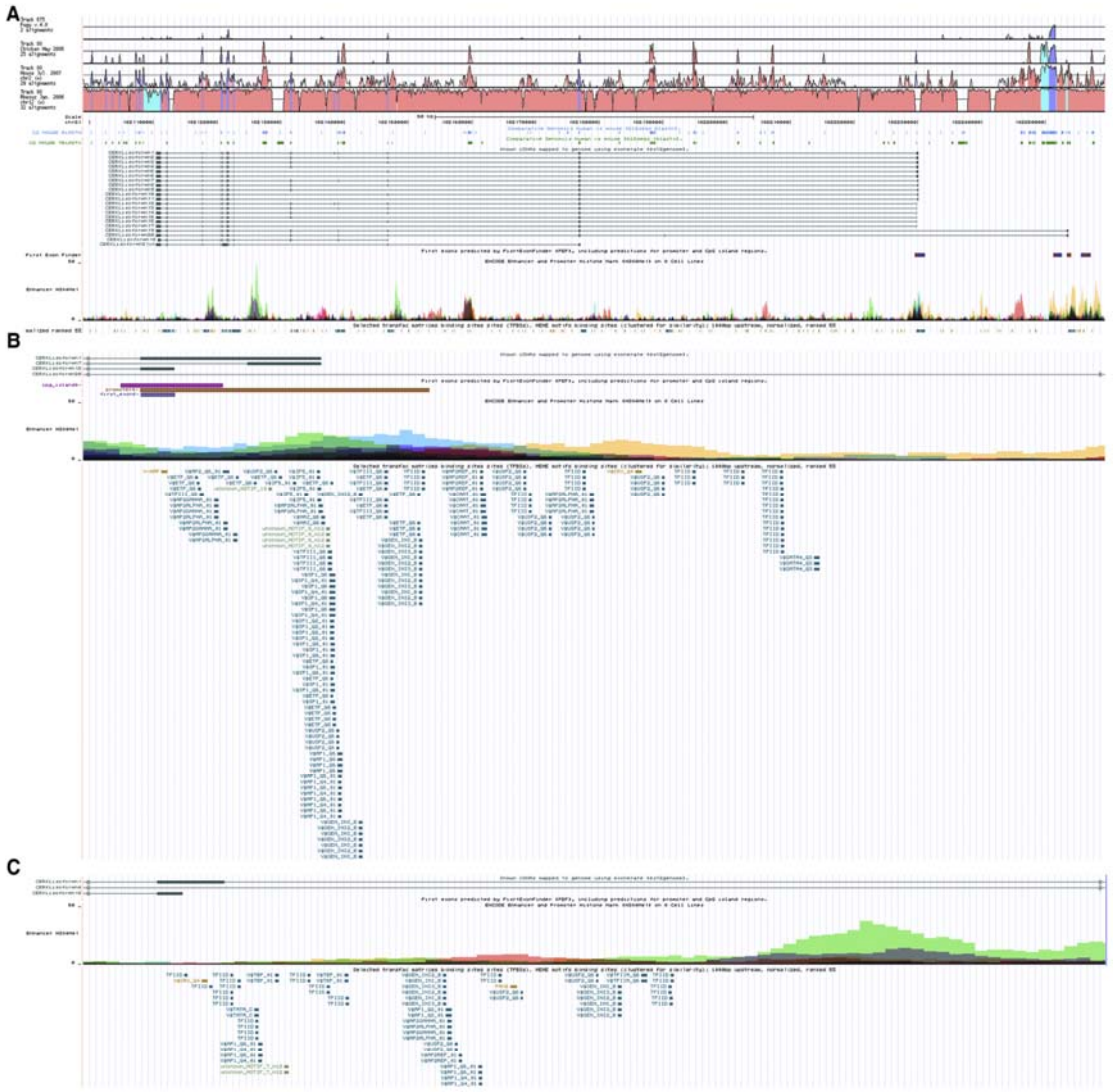

FIGURE 2. Summary of annotated and custom feature tracks on the UCSC genome browser. (**A**) An overall view of the whole genomic neighborhood of human *CERKL*, including upstream *NEUROD1* (*ITGA4* downstream gene is shown in Supplementary Fig. S1, http://www.iovs.org/lookup/suppl/doi:10.1167/iovs.10-7101/-/DCSupplemental). Homology to various species, including mouse, is depicted on the topmost tracks. Exonic structure of all the experimentally validated *CERKL* isoforms described in this article. FirstExonFinder predicted TSS; the ENCODE histone track H3K4Me3, a custom track of hits to different position weight matrices for known and predicted transcription factor binding sites, and some further evidence of transcriptional activity on neural tissues are shown. (**B**, **C**) Magnifications of the regions around exons 1 and 3, respectively, containing a more detailed view of the TFBS sites. The same track distribution is depicted on all three panels. Matrix hits overlapping homopolymer stretches larger than 5 bp were discarded.

times. The interspecific comparison of the more abundant transcripts in the retina revealed a higher number of *CERKL* variants in human (8 of 20 transcripts, with a comparable level of expression) than mouse (3 of 23 transcripts, with one major variant).

Concerning the CERKL/Cerkl protein isoforms, our data reveal that the combination of TSS multiplicity with the high number of alternative splicing events affecting the first exons (exons 1–6) generates a complex pattern of mature transcripts that differ at the 5′ end but share the 3′ moiety (exons 6–13), as shown in Figures 3A (human) and 3B (mouse). The alternative 5′ exons encode the nuclear localization signals,[18,38] the putative pleckstrin homology (PH) domain, and the diacylglycerol kinase (DAGK) signatures.[17,18,38,39] In addition, the human gene includes an in-frame species-specific alternative exon (4b) embedded in the predicted DAGK domain that interrupts the DAGK consensus signature. The comparison of human and mouse *CERKL* mature mRNAs showed that although the number of isoforms is similar, intron retention is more frequent in mouse than in human (Figs. 1A2, 1B2, isoforms m9, m10, m11). These transcripts bear premature stop codons and may be candidates to be degraded by the nonsense-mediated decay mechanisms (NMD) but, if translated, would encode a C-terminal–truncated protein.

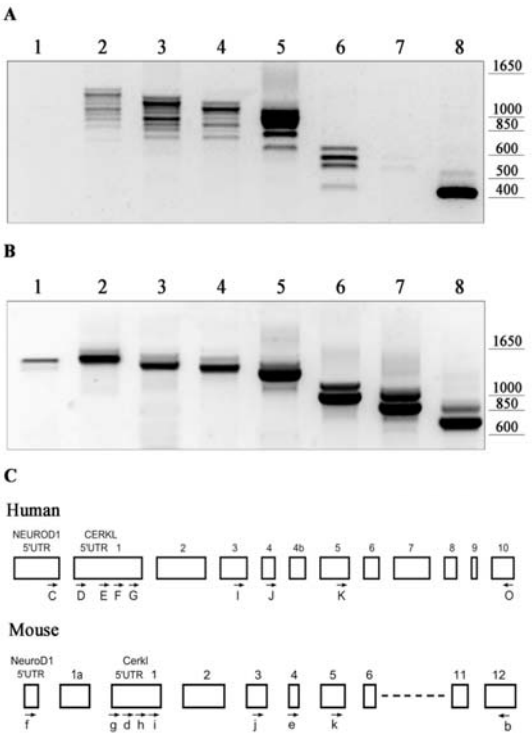

FIGURE 3. Evaluation of *CERKL* main transcripts. RT-PCR from human (**A**) and mouse (**B**) retina total RNA, to identify the main isoforms. (**C**) Scheme depicting the structure of *CERKL* in human and mouse, with the location of the primers used to generate the PCR reactions. For the sake of clarity, exons not relevant to this assay are not shown. For all amplicons, the same reverse oligonucleotide (human: O; mouse: b) was used, paired with the corresponding forward primers. For human: *lane 1*, C; *lane 2*, D; *lane 3*, E; *lane 4*, F; *lane 5*, G; *lane 6*, I; *lane 7*, J; *lane 8*, K. For mouse: *lane 1*, f; *lane 2*, g; *lane 3*, d; *lane 4*, h; *lane 5*, I; *lane 6*, j; *lane 7*, e; *lane 8*, k. Primer sequences are provided in the Supplementary Table S1, http://www.iovs.org/lookup/suppl/doi:10.1167/iovs.10-7101/-/DCSupplemental.

Evidence for CERKL Alternative Translational Initiation Sites

Interestingly, one of the consequences of the use of alternative TSS is that the previously reported initiation Met codon is not always included in the mature transcript. Then, additional translation initiation sites (TIS) should be considered. In silico sequence analyses using motif searches with a Kozak matrix predicted several TIS along the *CERKL* transcripts (Supplementary Table S5, http://www.iovs.org/lookup/suppl/doi:10.1167/iovs.10-7101/-/DCSupplemental). Of these, only two encoded long peptide sequences, whereas the remaining putative TIS yielded a lower score value or would generate very short peptides. Initiation codons with significant TIS scores are indicated in Figures 1A2 and 1B2. For each isoform, only the longest open-reading frame starting with a high-score Met is depicted (filled boxes).

As proof of principle, we tried to express three human highly expressed isoforms (h2, h13, and h18) harboring different in-frame methionines with a high Kozak score. The h2 encompassed the complete *CERKL* sequence, starting at the previously described 5′UTR, whereas the h13 and h18 cDNAs started at different TSS. The two latter did not contain the first in-frame methionine in exon 1, but they both shared an in-frame Met residue at exon 5 having a high Kozak score. Of note, other out-of-frame methionines located upstream in exon 5 showed comparable Kozak values (Fig. 4A). For each construct the CERKL coding sequence was fused at the 3′ end to an HA epitope to facilitate protein immunodetection. HEK293T cells were transfected with each construct, and RT-PCR was performed to assess the level of the recombinant *CERKL* transcription. Notably, we observed a high yield of the CERKL protein from 2 of 3 constructs (h2 and h18), each starting from the corresponding highlighted high Met score (Figs. 4B, 4C). Indeed, the size of the expressed CERKL-HA proteins was in agreement with their expected molecular mass (60 and 32 kDa).

Exploring the Promoter Landscape of *CERKL TSS*

To shed light on the architecture of the *CERKL* promoters and to define in silico potential novel alternative TSS, we aimed to map conserved transcription factor binding sites (TFBS) on the 1-kb upstream region of every human *CERKL* exon. To this end, we used position weight matrices from reported general transcription initiation motifs, retina-related transcription factors, and matrices obtained by MEME after analysis of the 49 promoters of RP genes to underscore conserved retina-specific regulatory motifs (subfunctionalized MEMEs) (for a detailed description of these analyses, see Materials and Methods). The outcome of this search along the upstream sequences of every exon depicted three different scenarios that corresponded to the patterns yielded by exons with a TSS function in retina (NeuroD1, 5′CERKL UTR, 1b, and 3a), exons with TSS not found in the retina (corresponding to the starting exons in the ENCODE transcripts OTTHUMT00000334817 and OTTHUMT00000334818), and the remaining internal exons, which are not used as TSS (Table 1).

Notably, a more focused analysis of the target sites of retina-specific transcription factors revealed several hits that are worth mentioning: a high-scoring hit for PAX6, right upstream exon 3, and some significant hits for CRX upstream *NEUROD1*. However, no hits within the 1-kb upstream region of each exon were found for NR2E3 or V-MAF (used to detect NRL-binding sites), although some were scattered along the *CERKL* genomic region. Overall, the evidence points to distinct promoter architecture concerning TSS, probably reflecting tissue-specific expression. Supplementary Tables S4A and S4B (http://www.iovs.org/lookup/suppl/doi:10.1167/iovs.10-7101/-/DCSupplemental) show the detailed list of TFBS, MEME, and subfunctionalized MEME hits upstream of each exon.

Given that *CERKL* mutations also contribute to CRD, we extended the analysis to the promoters (1 kb upstream) of the CRD genes using the TRANSFAC matrices, with particular emphasis on the retina-related transcription factor. The genes were grouped according to the disease to which they contributed most: RP (already listed), CRD, and a group of genes involved in both retinal disorders. Unfortunately, no clear pattern of single/clustered—general or retina-specific—transcription factor sites emerged in any of the three gene groups (Supplementary Fig. S2, http://www.iovs.org/lookup/suppl/doi:10.1167/iovs.10-7101/-/DCSupplemental).

Genomic Conservation of the *CERKL* Region among Vertebrates

VISTA tracks on Figure 2 clearly outline evolutionary conservation of the *CERKL* syntenic regions among vertebrates (human, *Homo sapiens;* rhesus chimp, *Macaca mulatta;* mouse, *Mus musculus;* chicken, *Gallus gallus;* and fugu, *Takifugu rubripes*). The degree of sequence conservation is high, close to 100% between human and rhesus. Among

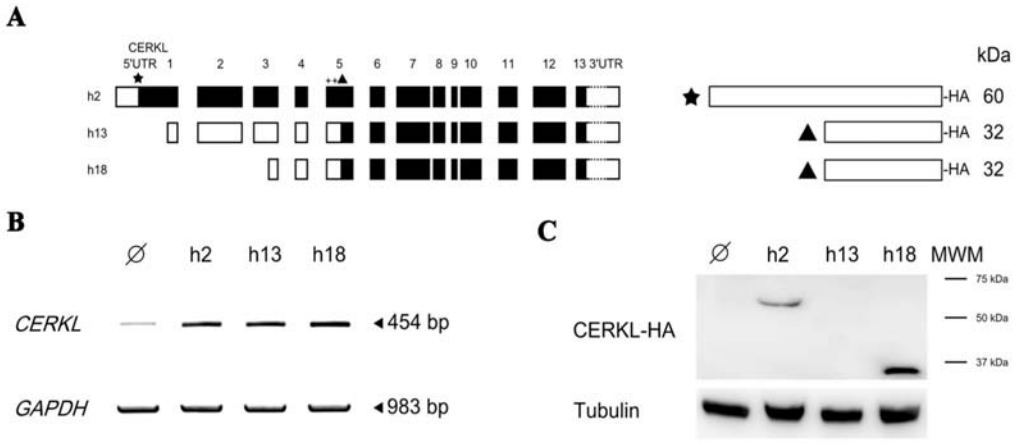

Figure 4. Evidence for additional initiating methionines in alternatively spliced human CERKL isoforms. (**A**) Diagram of the three different HA-tagged constructs from isoforms h2, h8, and h13, as well as the structure and molecular mass of the predicted encoded proteins. Methionines showing high Kozak scores are indicated by an *asterisk* (methionine in exon 1) and a *filled triangle* (internal methionine in exon 5), whereas other out-of-frame significantly scored Met are marked with a *cross*. *Filled boxes*: putative CDS. (**B**) RT-PCR showing expression of the *CERKL* constructs in transfected HEK293T cells. Lower endogenous *CERKL* levels were also detected in nontransfected cells (Ø). *GAPDH* gene was used for normalization. (**C**) CERKL-HA–fused proteins were immunodetected with an anti-HA monoclonal antibody. α-Tubulin was used as a loading control.

tetrapods, the average degree of conservation is above 70% for all exons but drops significantly in introns and intergenic regions. However, exon 4b could be an innovation in the ape lineage leading to humans because it is unique to the human genome. The comparison with fugu reveals an expected lower degree of conservation because only *NEUROD1* exons rank above 70% whereas most *CERKL* exons (2, 3, 5, 7, 8, 9, 10, 11, and 12) and *ITGA4* exons (3, 4, 5, 6, 7, 8, 9, 10, 11, 12, 13, 17, 19, 20, and 21) range between 50% and 70% similarity. Surprisingly, the *CERKL* exon 1 was among the least conserved. These results agreed with those obtained from bl2seq comparisons between human and mouse syntenic regions both at the nucleotide (BLASTN) and the translated (TBLASTX) levels. Thus far, no evidence supporting additional exons for *CERKL* apart from those described in this work could be obtained.

CERKL Expression in a Collection of Human and Mouse Tissues

Semiquantitative RT-PCR analysis of *CERKL* expression was performed in a collection of tissues and cell lines of human and mouse, with a pair of primers located in the exons shared by all isoforms (forward in exon 9 and reverse in exon 13 in human; exon 12 in mouse; see Figs. 1A2 and 1B2 for locations; details are given in Materials and Methods). The results are shown in Figures 5A and 5C (human) and 5B and 5D (mouse). At least three independent replicates were performed and quantified for each tissue. *GAPDH* expression was used for normalization.

In humans, the retina was by far the tissue in which *CERKL* expression was the highest. In fact, among the other tissues, only the brain showed some detectable expression (at levels below 10% of those in retina). Sequence analysis of the brain transcript revealed that gene expression was driven by the *NEUROD1* TSS (data not shown). Of interest for future functional studies, some human cell lines showed detectable levels of *CERKL* transcription, as is the case with HEK293T and A549 (Fig. 5C).

In mouse, *Cerkl* was also highly expressed in the retina, although the liver showed even slightly higher levels of expression (Fig. 5D). Sequence analysis of the murine liver isoform (marked with an asterisk) showed that it corresponded to m30in variant. This isoform would generate a prematurely truncated protein because it retained a noncoding fragment of intron 11. Other mouse tissues, such as testis and spleen, also showed high to moderate levels of *Cerkl* expression.

As mentioned, in addition to the reported mouse *Cerkl* promoter (heretofore, UTR), retinal transcripts were produced from the *NeuroD1* promoter and an internal TSS in intron 2 (named 3a). Direct sequencing of RT-PCRs from other tissues led us to identify another TSS, 3b, also within intron 2. We performed RT-PCR assays to assess the relative contribution of these TSS in the retina: UTR, NeuroD1, 3a and 3b to *Cerkl* expression (Fig. 6). Tissular comparison showed a wide range of expression from each TSS: the *Cerkl* UTR contribution was indeed major in the retina, moderate in the kidney, faint in the brain, and undetectable in the blood and spleen. In addition, in

Table 1. Distribution of Motifs among 1 kbp Upstream of Every *CERKL* Exon Showed a Differential Pattern, Depending on the Kind of Exon

Scenario	Transfac Motifs	MEME Motifs	Subfunctionalized MEME Motifs	TSS Type
1	>40	0	<5	Retinal TSS (NEUROD1, 1/1a, 1b, and 3a)
2	<35	≈10	>75	Nonretinal TSS (OTTHUMT00000334817 first exon and OTTHUMT00000334818 first exon)
3	≈25	0	<5	No TSS exons

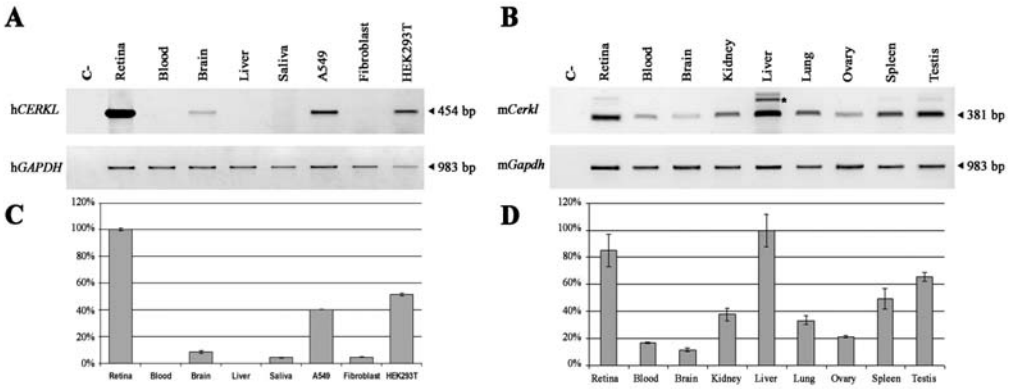

FIGURE 5. *CERKL* semiquantitative expression analysis in human and mouse tissues. *CERKL* expression identified by RT-PCR in several tissues and cell lines of human (**A**) and mouse (**B**) origin. Semiquantitative analysis of all *CERKL* transcripts in human (**C**) and mouse (**D**). At least three replicates were performed. *GAPDH* expression was used for normalization. Maximum *CERKL* levels were arbitrarily set as 100% (retina in human, liver in mouse). *CERKL* was amplified using primers A and B in human and primers a and b in mouse, as located in Figures 1A2 and 1B2. The amplicon size is indicated in each case. The *asterisk* in the murine liver sample corresponds to the alternative isoform m30in. Primer sequences are provided in Supplementary Table S1, http://www.iovs.org/lookup/suppl/doi:10.1167/iovs.10-7101/-/DCSupplemental. Notably, the primers used for the amplification of *CERKL* transcript were located in the common region at 3′ of the gene; therefore, the bands observed are the result of the transcripts produced from all TSS in each tissue.

agreement with previous reports, *NeuroD1*-driven expression was tissue restricted and was observed only in the retina in our panel. In contrast, the 3a TSS-driven transcript was expressed more widely but showed very low levels in the retina. Although the 3b TSS was silent in the mouse retina, it was the most active in the liver (Fig. 6). Isoforms m24 to m28 in Figure 1B, which started at either 3a or 3b TSS, were isolated and sequenced in the spleen and liver but were undetectable in the retina. Of note, in some tissues, the RT-PCRs specific for these four promoters did not explain the total *Cerkl* transcriptional levels (as revealed by the amplification of the 9 to 12 exon region common to all isoforms), again pointing to additional TSS.

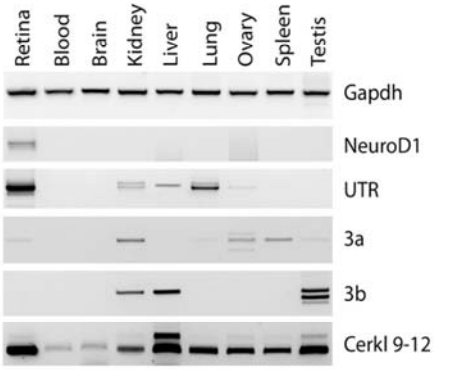

FIGURE 6. Tissue-specific *Cerkl* promoter in adult mice. RT-PCRs were performed on several murine samples to determine the active promoters in each tissue. Forty-five cycle amplifications were carried out using the same reverse oligonucleotide in exon 12 and different forward primers located in each TSS identified (*NeuroD1* UTR, *Cerkl* UTR, 3a, and 3b) as well as exon 9 to amplify the common region. *Gapdh* was used to normalize between samples. Primer location is depicted in Figure 1B, and sequences are listed in Supplementary Table S1, http://www.iovs.org/lookup/suppl/doi:10.1167/iovs.10-7101/-/DCSupplemental.

Cerkl Localization in Mouse Retina by Immunohistochemistry

Previous results based on in situ mRNA hybridization showed that *Cerkl* was expressed mainly in the ganglion cell layer, though a fainter level of expression was detected in other retinal layers, including photoreceptors.[17] To accurately assess the localization of the Cerkl protein in the retina, fluorescent immunohistochemistry using different cell-specific antibodies and markers was performed on serial sagittal cryosections of adult mouse retinas (2 months old). An in-house rabbit polyclonal anti-Cerkl antibody raised against an exon 2 peptide sequence was affinity purified and preabsorbed before use. Double coimmunodetection with this polyclonal anti-Cerkl antibody and either anti-rhodopsin (specific for rods) or anti-PKCα (which primarily labels bipolar cells and rods), plus counterstaining with DAPI (nuclei) and Alexa Fluor 647–conjugated PNA (which labels cones) were performed in parallel to allow a more detailed localization (Fig. 7).

Cerkl expression was found at the ganglion cell layer (GCL), in the photoreceptors (PhR), and in some cell bodies at the outer nuclear layer (ONL) and inner nuclear layer (INL) (Fig. 7). Magnification of the photoreceptor cell layer showed a strong immunodetection of Cerkl in cones and, faintly, in rods. Of interest, Cerkl localized primarily in the outer segments of both types of photoreceptors, as shown by its colocalization with rhodopsin (rods) and cone (Figs. 7H, 7I) staining. In addition, Cerkl showed perinuclear staining in some cell bodies at the ONL, extremely close to the photoreceptor layers, probably corresponding to cones (Figs. 7I, 7J, white arrows). Concerning other neuronal retinal types, Cerkl was detected in a population of bipolar cells (white arrowheads in Fig. 7N) as well as in other cell types at the INL, as yet undetermined.

DISCUSSION

One of the major breakthroughs from interspecific sequence comparisons of whole genomes is that the complexity of a particular organism depends not only on the number of genes but also on the diversity of the proteins produced and the regulation of transcription. An increasing amount of evidence

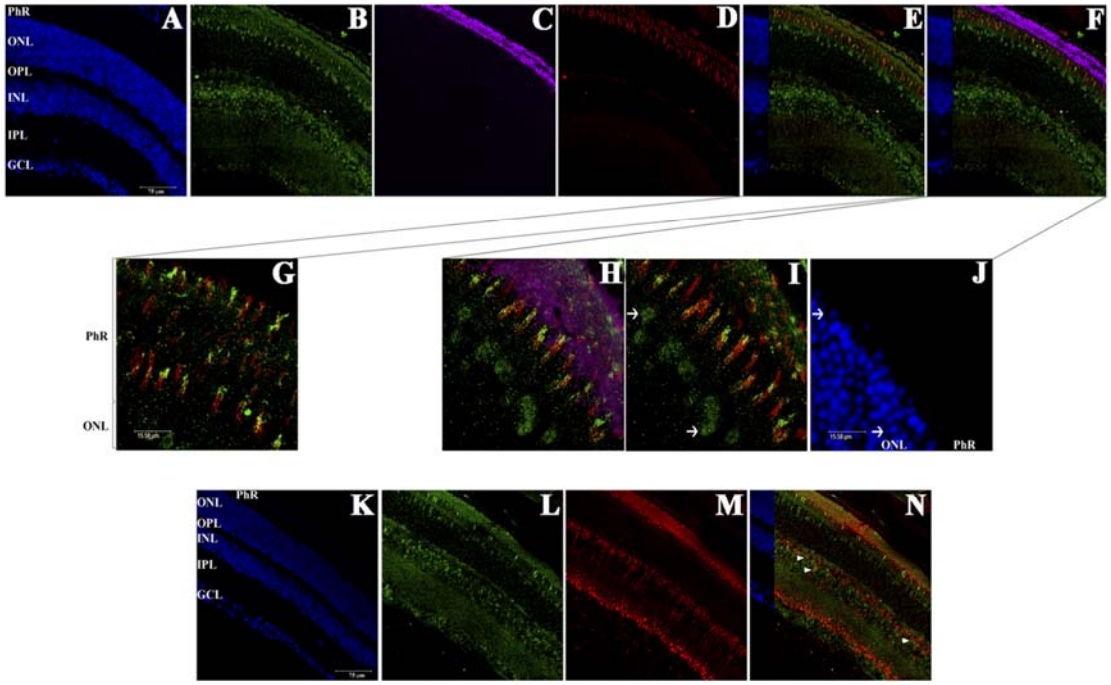

FIGURE 7. Immunohistochemistry on mouse retina cryosections. (**A–J**) Localization of Cerkl in photoreceptor cells. Nuclei are stained with DAPI (*blue*, **A**); Cerkl (**B**) and Rhodopsin (**C**) proteins are detected in *green* and *magenta*, respectively; cones appear in *red* (**D**) using PNA staining. Two merged images (**E**, **F**) and the magnification of some sections show clear localization of Cerkl in cones (*yellow*, **G**) and, more faintly, in rods, colocalizing with rhodopsin (**H**). Although Cerkl localizes mainly in the outer segments, some perinuclear staining could be also observed in the nuclei of the cones at the ONL, indicated by *white arrows* (**I**, **J**). (**J**) DAPI counterstaining of the nuclei. (**K–N**) Expression of Cerkl in other retinal layers. Nuclei are stained with DAPI (*blue*, **K**), Cerkl protein is detected in *green* (**L**), bipolar cells and rods expressing PKCα are labeled in *red* (**M**). Cerkl is expressed in the ganglion cells (GCL), some cells in the INL and ONL, and in the photoreceptors. The merged image (**N**) shows expression of Cerkl in some bipolar cells (*white arrowheads*) while confirming localization in rods. Scale bars show magnifications.

in the human genome supports that alternative splicing is more the rule than the exception because >95% of the multiexon genes undergo alternative splicing events, often related to developmental or tissue differentiation processes and differential physiological functions. Many bioinformatic efforts are now being devoted to decipher "the splicing code," which is intended to characterize the regulatory splicing strategies on a genomewide scale to predict the specific transcripts from every gene.[40,41] However, these in silico predictions must be substantiated in vivo to identify the physiologically relevant isoforms, their regulation, and eventually their contribution to disease. Within this framework, we have combined both in vivo and in silico approaches to analyze the expression of *CERKL*, a retinitis pigmentosa gene of an as yet unknown function. Our data show unexpectedly high transcriptional complexity in human and mouse tissues arising from the combination of tissue-specific promoters and alternative splicing events, particularly in the retina. A large multiplicity of retina transcripts has also been reported for other genes, such as *RPGR*, *RPGRIP1*, and *CPEB3*[42–44]. In agreement with these results, a recent accurate transcriptional characterization focused on the PRPF gene family (proteins associated with spliceosome formation and responsible for retinal dystrophies) showed that the processed pre-mRNA levels were highest in the retina than in other tissues and organs. Their results pointed to a particularly increased splicing activity at the base of the high multiplicity of retinal transcripts and called for sophisticated quality control mechanisms.[45]

This high repertoire of CERKL transcript and protein isoforms suggests distinct roles for the alternatively displayed domains. The first two exons of *CERKL* encode a PH domain and two nuclear localization signals, whereas exons 3 to 7 encompass the DAGK domain[17–19,38,39] (Fig. 8). Notably, the use of the different promoters and 5′UTRs affects the inclu-

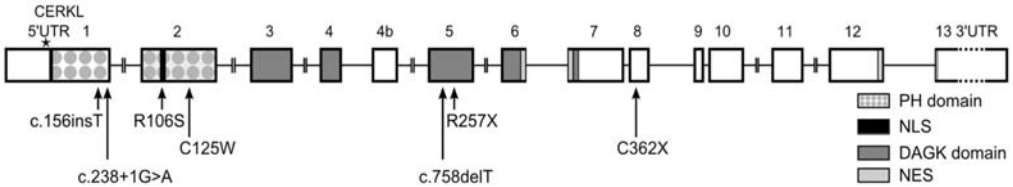

FIGURE 8. Scheme of the reported causative mutations on the CERKL gene. The location of the mutations identified thus far is shown on a diagram of the CERKL protein. The CERKL domains described by either sequence homology (PH, pleckstrin; DAGK, diacylglycerol kinase domain) or functional analysis (NLS, nuclear localization signals; NES, nuclear export signals) are also depicted.

sion/exclusion of the first exons in the final transcript and generates variability at the N-terminal peptide moiety, with a potential impact in the protein function, which supports a finely tuned regulation of the 5′ splicing events. In contrast, the exons encoding the C-terminal domains are maintained in all isoforms, even in the transcripts from nonretinal tissues, arguing in favor of a basic function.

The comparison between human and mouse retina major *CERKL* isoforms reveals higher complexity for the human transcripts. In fact, the most abundant isoforms are species-specific (except for h2 and m1, which are structurally equivalent). For example, the *NeuroD1* promoter contributes to the highly expressed isoforms in mouse, whereas its relevance in the human adult retina appears to be minor. This holds true for the least abundant isoforms (e.g., h1, h12, h15–h17 and m5, m7, m8, m10, m11, m13) (Fig. 1A2, 1B2). Interspecific differences in the levels of expression and identification of species-specific isoforms have also been reported for other visual disorder genes, such as *IMPDH1*, *OPA1*, and *PRPF31*, suggesting distinct functional requirements for each species.[46–48] Remarkably, one-third of the murine isoforms (12 of 32) compared with 1 of 21 human isoforms are produced by missplicing (with partial retention of intron sequences). Most of these misspliced transcripts would encode a truncated protein, unless degraded by NMD. Other reports analyzing human versus murine transcripts identified other retinal dystrophy genes with preferential or unique intron retention in the mouse, among them *RPGR* (intron 14),[49] *RPGRIP1* (intron 13),[42] and *PRPF31* (intron 7).[48] If extended to other genes, these results would argue in favor of either a more precise splicing machinery or a less permissive mRNA integrity control, in human, at least in retina; even though it has been shown that relevant splicing events associated with NMD remain conserved through mammalian genomes, reflecting a common clearance mechanism of transcripts that might compromise cell viability.[50]

One of the relevant findings of our work is the use of tissue-specific TSS in mouse. Among the tissues analyzed, the *NeuroD1* promoter was only active in the retina, where the reported *Cerkl* UTR promoter also showed the highest transcriptional activity. Instead, the additional alternative internal promoters were highly expressed in nonneuronal tissues (Fig. 6, liver, testis, kidney). The combination of different promoters and shared splicing events in both species hindered isoform quantification by real-time RT-PCR (which relies on small probes) to evaluate their contribution to the *CERKL* transcript population. Thus, a relative quantification by specific amplification of each isoform was performed (Figs. 3, 5, 6). Of note, the retina is the tissue in which higher expression and greater display of *CERKL* transcript variability is observed. In addition to the multiplicity of promoters and alternative splicing events, another layer of complexity is provided by other in-frame methionines, which direct the synthesis of shortened CERKL protein isoforms, with a downstream start in exon 5. In vitro experimental evidence strongly supports this starting Met in the h18 isoform, though no expression could be detected for the h13 variant. Whether this apparent discrepancy could be explained by other upstream out-of-frame methionines in h13 (not present on the h18 alternative 5′UTR exons) that affect the translational initiation complex formation remains to be elucidated (Fig. 4). Although the CERKL function is as yet undetermined, such a high repertoire of transcripts and proteins, while making functional assignment a real challenge, hints at a very crucial role in retinal cell survival. Indeed, in a more general view, these results open new scenarios for the human proteome complexity associated with a multiplicity of isoforms.

The in silico analysis of binding sites for transcription initiation factors across the *CERKL* genomic neighborhood (approximately 230 kbp) revealed a high number of hits (>15,000). However, they were not randomly distributed but were clustered just upstream of *ITGA4*, *NEUROD1*, and *CERKL* canonical TSS. If we focus on the retina-specific TFBS, no significant scores for OTX2 or NR2E3 could be found upstream of the promoters of these genes. In contrast, binding sites for CRX, PAX6, and NRL upstream of *NEUROD1* TSS, for NRL in *CERKL* exon 1b, and for PAX6 and CRX upstream of exon 3 TSS were identified. These results provide evidence for retina-specific regulatory enhancers close to *CERKL*. Overall, the differential patterns observed for the in silico predicted enhancers, the TSS experimentally confirmed in the retina, and the identification of nonretinal transcriptional products clearly support a highly tuned, tissue-specific regulation of *CERKL* expression.

Notably, Cerkl immunohistochemistry showed high expression in cones and moderate expression in rods, ganglion cells, and other retinal INL cell types. A specific perinuclear staining was observed at the INL and ONL. Hitherto, *CERKL* mutations have been associated with both conventional RP and CRD. Regarding this clinical heterogeneity, our findings of expression in cones and rods are consistent with the two clinical entities but also highlight the need to establish a more accurate scenario. Therefore, full characterization of the transcriptional map of isoforms, the type and location of the mutations, the accurate subcellular localization of proteins, and the action of modifier genes is required to comprehend the contribution of *CERKL*/CERKL variants to retinal degeneration disorders.

To establish a more precise relationship between mutations and the relative pathogenicity of each isoform, the distribution of SNPs along the coding gene structure was analyzed in silico. A priori, a homogeneous distribution of both mutations and SNPs should be expected when all the exons and encoded domains contribute equally to function. The results of this analysis showed that not all the domains harbored the same frequency of SNPs because some showed higher SNP frequencies than the observed average, whereas others were devoid of polymorphic variants, thus suggesting differential selection pressures (Supplementary Fig. S3, http://www.iovs.org/lookup/suppl/doi:10.1167/iovs.10-7101/-/DCSupplemental). For instance, the alternately spliced exons that encompassed the DAGK domain contained fewer SNPs, whereas the exons that encoded the pleckstrin homology domain showed more SNPs than average. The biological meaning of this differential distribution remains to be assessed.

Meanwhile, as more mutations are being identified, a genotype-phenotype correlation pattern is emerging (Fig. 8, Table 2). The first pathogenic variant described, p.R257X—a nonsense homozygous mutation in exon 5—generates a truncated protein that abrogates the putative DAGK domain. Interestingly, only 1 of the 8 major isoforms remains unaffected after alternative splicing. The phenotype associated with this variant ranges from canonical RP to more severe CRD features.[53] Another RP-associated mutation, p.R106S, is localized in 1 of the 2 putative nuclear localization signals, probably compromising its import and function in the nucleus.[55] However, all other protein domains remain unaltered, in accordance with a moderate RP phenotype. Other alleles are associated with more severe retinal disorders, with clear cone-rod dystrophy features and early macular degeneration. One of them, c.238+1G>A,[37] affects the splicing of the first intron, abrogating the generation of the putative protein isoforms produced from exon 1 and 1b. Thus, only the isoforms starting in exon 3 or the spliced variants of exon 1a would be produced. The other mutation, p.C125W[54] (also affecting the conformation of the protein isoforms encoded from the methi-

TABLE 2. Genotype-Phenotype Correlations of Reported *CERKL* Mutations

Mutation*/Exon	Protein Domain/Molecular Effect	Allelic Status	Major Affected Isoforms (Fig. 1A)	Phenotype†	Allele Frequency among CERKL Reported Mutations *n* (%)	References
p. R257X/exon 5	Lipid kinase/protein truncated	Homozygous and compound heterozygous	7 of 8 (h2, h3, h7, h8, h13, h14, h18)	RP, with some patients showing phenotypes closer to CRD; peripheral pigment deposits plus macular dystrophy	30/40 alleles (20 families or patients) (~75%)	Tuson et al.,[17] Pomares et al.,[51] Avila-Fernández et al.,[52] Aleman et al.,[53] Littink et al.[54]‡
c.238+1G >A/ intron 1	Pleckstrin homology/ abrogates splicing	Homozygous	5 of 8 (h2, h3, h5, h13, h14)	Mixed features of RP and CRD, with early macular degeneration	2/40 alleles (~5%)	Auslender et al.[37]
p.R106S/exon 2	Nuclear localization signal/compromises nuclear import	Homozygous	3 of 8 (h2, h3, h5)	RP features (bone-spicules) with CRD leading to peripheral and central vision deficit	2/40 (~5%)	Ali et al.[55]
c.156_157ins/ exon 1	Pleckstrin homology/ frameshift and protein truncation	Compound heterozygous with C.758delt	3 of 8 (h2, h3, h5)	NC	1/40 (~2.5%)	Tang et al.,[56]
c.758delT/exon 5	Lipid kinase/frameshift and protein truncation	Compound heterozygous with C.156_157/ins	7 of 8 (h2, h3, h7, h8, h13, h14, h18)	NC	1/40 (~2.5%)	Tang et al.,[56]
p.C362X/exon 8	Unknown	Compound heterozygous with P.r257x	All isoforms (h2, h3, h5, h7, h8, h13, h14, h18)	NC	1/40 (~2.5%)	Aleman et al.[53]
p.C125W/exon 2	Pleckstrin homology/ evolutionarily conserved residue	Homozygous	3 of 8 (h2, h3, h5)	CRD (with central scotoma and macular atrophy, retinal thinning)	2/40 (~5%)	Littink et al.,[54]

* The isoform cDNA used for reference is NM_201548.4, corresponding to isoform h2 (Fig. 1A). NC, not considered due to heterozygosity.
† Only the phenotype for homozygous allelic combination is considered of value in genotype-phenotype correlations. NC, not considered.
‡ The reported mutation p.R283X, considered as novel in this study, corresponds to the already reported p.R257X variant (this difference is due to the isoform cDNA taken as reference—NM_001030311.2 and NM_201548.4, respectively).

onine in exon 1), changes an evolutionarily conserved cysteine residue of the pleckstrin domain. Three other clearly pathogenic alleles, two frameshifts (by indels) and a nonsense mutation, have also been reported, but their association with particular features is hindered by their compound heterozygous status. Indeed, this is an ongoing task.

Our comprehensive approach, by characterizing a high number of isoforms expressed in a single tissue, provides an exhaustive transcriptional picture on a hitherto fragmentary collection of data and builds a reference framework to assess the severity of new mutations. Considering the high number of *CERKL* isoforms, undertaking accurate analysis for localization or functional specificity, or both, at the subcellular level remains a key challenge to understand the contribution of this gene to retinal degeneration.

Acknowledgments

The authors thank Andrés Mayor (Fundaluce, Hospital Central de Asturias) for the generous support; Ana Méndez-Zunzúnegui (IDIBELL, Universitat de Barcelona) for generous support and technical advice on the use of eye cryosections; and the ENCODE project for making publicly available, through the UCSC Genome browser, the H3K4Me3 and the GENCODE manual gene annotations (including VEGA) tracks.

References

1. Sultan M, Schulz MH, Richard H, et al. A global view of gene activity and alternative splicing by deep sequencing of the human transcriptome. *Science*. 2008;321:956–960.
2. Pan Q, Shai O, Lee LJ, Frey BJ, Blencowe BJ. Deep surveying of alternative splicing complexity in the human transcriptome by high-throughput sequencing. *Nat Genet*. 2008;40:1413–1415.
3. Nilsen TW, Graveley BR. Expansion of the eukaryotic proteome by alternative splicing. *Nature*. 463:457–463.
4. Licatalosi DD, Darnell RB. RNA processing and its regulation: global insights into biological networks. *Nat Rev Genet.* 2010;11:75–87.
5. McGlincy NJ, Smith CW. Alternative splicing resulting in nonsense-mediated mRNA decay: what is the meaning of nonsense? *Trends Biochem Sci.* 2008;33:385–393.
6. Tazi J, Bakkour N, Stamm S. Alternative splicing and disease. *Biochim Biophys Acta.* 2009;1792:14–26.
7. Raponi M, Baralle D. Alternative splicing: good and bad effects of translationally silent substitutions. *FEBS J*. 2010;277:836–840.
8. Ward AJ, Cooper TA. The pathobiology of splicing. *J Pathol.* 2010;220:152–163.
9. Xu X, Liu Y, Weiss S, Arnold E, Sarafianos SG, Ding J. Molecular model of SARS coronavirus polymerase: implications for biochemical functions and drug design. *Nucleic Acids Res.* 2003;31:7117–7130.
10. McCullough RM, Cantor CR, Ding C. High-throughput alternative splicing quantification by primer extension and matrix-assisted laser desorption/ionization time-of-flight mass spectrometry. *Nucleic Acids Res.* 2005;33:e99.
11. Licatalosi DD, Darnell RB. Splicing regulation in neurologic disease. *Neuron.* 2006;52:93–101.
12. Hartong DT, Berson EL, Dryja TP. Retinitis pigmentosa. *Lancet.* 2006;368:1795–1809.
13. Beit-Ya'acov A, Mizrahi-Meissonnier L, Obolensky A, et al. Homozygosity for a novel ABCA4 founder splicing mutation is associated with progressive and severe Stargardt-like disease. *Invest Ophthalmol Vis Sci.* 2007;48:4308–4314.
14. Schmid F, Glaus E, Cremers FP, Kloeckener-Gruissem B, Berger W, Neidhardt J. Mutation- and tissue-specific alterations of RPGR transcripts. *Invest Ophthalmol Vis Sci.* 2010;51:1628–1635.
15. Riazuddin SA, Iqbal M, Wang Y, et al. A splice-site mutation in a retina-specific exon of BBS8 causes nonsyndromic retinitis pigmentosa. *Am J Hum Genet*. 2010;86:805–812.
16. Wang Y, Juranek S, Li H, Sheng G, Tuschl T, Patel DJ. Structure of an argonaute silencing complex with a seed-containing guide DNA and target RNA duplex. *Nature.* 2008;456:921–926.
17. Tuson M, Marfany G, Gonzalez-Duarte R. Mutation of CERKL, a novel human ceramide kinase gene, causes autosomal recessive retinitis pigmentosa (RP26). *Am J Hum Genet.* 2004;74:128–138.
18. Bornancin F, Mechtcheriakova D, Stora S, et al. Characterization of a ceramide kinase-like protein. *Biochim Biophys Acta.* 2005;1687:31–43.
19. Tuson M, Garanto A, Gonzalez-Duarte R, Marfany G. Overexpression of CERKL, a gene responsible for retinitis pigmentosa in humans, protects cells from apoptosis induced by oxidative stress. *Mol Vis.* 2009;15:168–180.
20. Mendez A, Lem J, Simon M, Chen J. Light-dependent translocation of arrestin in the absence of rhodopsin phosphorylation and transducin signaling. *J Neurosci.* 2003;23:3124–3129.
21. Rhead B, Karolchik D, Kuhn RM, et al. The UCSC Genome Browser database: update. *Nucleic Acids Res*. 2010;38:D613–D619.
22. Frazer KA, Pachter L, Poliakov A, Rubin EM, Dubchak I. VISTA: computational tools for comparative genomics. *Nucleic Acids Res.* 2004;32:W273–W279.
23. Tatusova TA, Madden TL. BLAST 2 Sequences, a new tool for comparing protein and nucleotide sequences. *FEMS Microbiol Lett.* 1999;174:247–250.
24. Pruitt KD, Tatusova T, Klimke W, Maglott DR. NCBI Reference Sequences: current status, policy and new initiatives. *Nucleic Acids Res.* 2009;37:D32–D36.
25. Benson DA, Karsch-Mizrachi I, Lipman DJ, Ostell J, Sayers EW. *GenBank Nucleic Acids Res.* 2009;37:D26–D31.
26. Wakaguri H, Yamashita R, Suzuki Y, Sugano S, Nakai K. DBTSS: database of transcription start sites, progress report 2008. *Nucleic Acids Res.* 2008;36:D97–D101.
27. Harrow J, Denoeud F, Frankish A, et al. GENCODE: producing a reference annotation for ENCODE. *Genome Biol.* 2006;7(suppl 1):S41–S49.
28. Slater GS, Birney E. Automated generation of heuristics for biological sequence comparison. *BMC Bioinformatics.* 2005;6:31.
29. Davuluri RV, Grosse I, Zhang MQ. Computational identification of promoters and first exons in the human genome. *Nat Genet*. 2001;29:412–417.
30. Bailey TL, Boden M, Buske FA, et al. MEME SUITE: tools for motif discovery and searching. *Nucleic Acids Res.* 2009;37:W202–W208.
31. Matys V, Fricke E, Geffers R, et al. TRANSFAC: transcriptional regulation, from patterns to profiles. *Nucleic Acids Res.* 2003;31:374–378.
32. Messeguer X, Escudero R, Farre D, Nunez O, Martinez J, Alba MM. PROMO: detection of known transcription regulatory elements using species-tailored searches. *Bioinformatics.* 2002;18:333–334.
33. Portales-Casamar E, Thongjuea S, Kwon AT, et al. JASPAR: the greatly expanded open-access database of transcription factor binding profiles. *Nucleic Acids Res*. 2010;38:D105–D110.
34. Kozak M. An analysis of 5′-noncoding sequences from 699 vertebrate messenger RNAs. *Nucleic Acids Res.* 1987;15:8125–8148.
35. Celniker SE, Dillon LA, Gerstein MB, et al. Unlocking the secrets of the genome. *Nature.* 2009;459:927–930.
36. Ruthenburg AJ, Allis CD, Wysocka J. Methylation of lysine 4 on histone H3: intricacy of writing and reading a single epigenetic mark. *Mol Cell.* 2007;25:15–30.
37. Auslender N, Sharon D, Abbasi AH, Garzozi HJ, Banin E, Ben-Yosef T. A common founder mutation of CERKL underlies autosomal recessive retinal degeneration with early macular involvement among Yemenite Jews. *Invest Ophthalmol Vis Sci.* 2007;48:5431–5438.
38. Inagaki Y, Mitsutake S, Igarashi Y. Identification of a nuclear localization signal in the retinitis pigmentosa-mutated RP26 protein, ceramide kinase-like protein. *Biochem Biophys Res Commun.* 2006;343:982–987.
39. Rovina P, Schanzer A, Graf C, Mechtcheriakova D, Jaritz M, Bornancin F. Subcellular localization of ceramide kinase and ceramide kinase-like protein requires interplay of their pleckstrin homology domain-containing N-terminal regions together with C-terminal domains. *Biochim Biophys Acta.* 2009;1791:1023–1030.
40. Barash Y, Calarco JA, Gao W, et al. Deciphering the splicing code. *Nature.* 2010;465:53–59.
41. Tejedor JR, Valcarcel J. Gene regulation: Breaking the second genetic code. *Nature.* 2010;465:45–46.

42. Lu X, Ferreira PA. Identification of novel murine- and human-specific RPGRIP1 splice variants with distinct expression profiles and subcellular localization. *Invest Ophthalmol Vis Sci.* 2005;46:1882–1890.
43. Neidhardt J, Glaus E, Barthelmes D, Zeitz C, Fleischhauer J, Berger W. Identification and characterization of a novel RPGR isoform in human retina. *Hum Mutat.* 2007;28:797–807.
44. Wang XP, Cooper NG. Characterization of the transcripts and protein isoforms for cytoplasmic polyadenylation element binding protein-3 (CPEB3) in the mouse retina. *BMC Mol Biol.* 2009;10:109.
45. Tanackovic G, Ransijn A, Thibault P, et al. PRPF mutations are associated with generalized defects in spliceosome formation and pre-mRNA splicing in patients with retinitis pigmentosa. *Hum Mol Genet.* 2011;20:2116–2130.
46. Spellicy CJ, Daiger SP, Sullivan LS, et al. Characterization of retinal inosine monophosphate dehydrogenase 1 in several mammalian species. *Mol Vis.* 2007;13:1866–1872.
47. Akepati VR, Muller EC, Otto A, Strauss HM, Portwich M, Alexander C. Characterization of OPA1 isoforms isolated from mouse tissues. *J Neurochem.* 2008;106:372–383.
48. Tanackovic G, Rivolta C. PRPF31 alternative splicing and expression in human retina. *Ophthalmic Genet.* 2009;30:76–83.
49. Kirschner R, Rosenberg T, Schultz-Heienbrok R, et al. RPGR transcription studies in mouse and human tissues reveal a retina-specific isoform that is disrupted in a patient with X-linked retinitis pigmentosa. *Hum Mol Genet.* 1999;8:1571–1578.
50. de Lima Morais DA, Harrison PM. Large-scale evidence for conservation of NMD candidature across mammals. *PLoS One.* 5:e11695.
51. Pomares E, Marfany G, Brión MJ, et al. Novel high-throughput SNP genotyping cosegregation analysis for genetic diagnosis of autosomal recessive retinitis pigmentosa and Leber congenital amaurosis. *Hum Mutat.* 2007;28:511–516.
52. Avila-Fernandez A, Riveiro-Alvarez R, Vallespin E, et al. CERKL mutations and associated phenotypes in seven Spanish families with autosomal recessive retinitis pigmentosa. *Invest Ophthalmol Vis Sci.* 2008;49:2709–2713.
53. Aleman TS, Soumittra N, Cideciyan AV, et al. CERKL mutations cause an autosomal recessive cone-rod dystrophy with inner retinopathy. *Invest Ophthalmol Vis Sci.* 2009;50:5944–5954.
54. Littink KW, Koenekoop RK, van den Born LI, et al. Homozygosity mapping in patients with cone-rod dystrophy: novel mutations and clinical characterizations. *Invest Ophthalmol Vis Sci.* 2010;51:5943–5951.
55. Ali M, Ramprasad VL, Soumittra N, et al. A missense mutation in the nuclear localization signal sequence of CERKL (p.R106S) causes autosomal recessive retinal degeneration. *Mol Vis.* 2008;14:1960–1964.
56. Tang Z, Wang Z, Wang Z, et al. Novel compound heterozygous mutations in CERKL cause autosomal recessive retinitis pigmentosa in a nonconsanguineous Chinese family. *Arch Ophtalmol.* 2009;127:1077–1078.

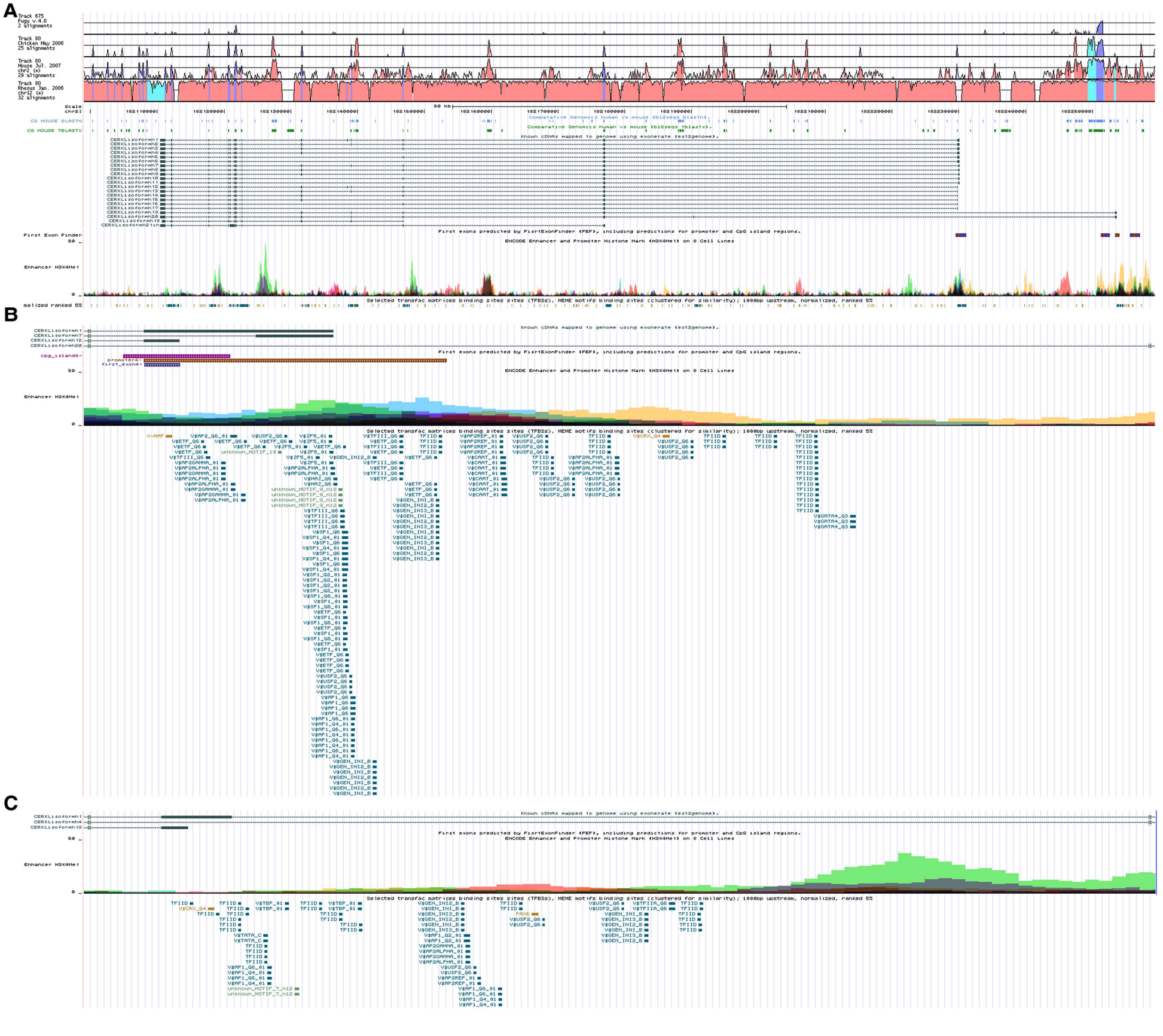

FIGURE 2. Summary of annotated and custom feature tracks on the UCSC genome browser. **(A)** An overall view of the whole genomic neighborhood of human CERKL, including upstream NEUROD1 (ITGA4 downstream gene is shown in Supplementary Fig. S1, http://www.iovs.org/lookup/suppl/doi:10.1167/iovs.10-7101/-/DCSupplemental). Homology to various species, including mouse, is depicted on the topmost tracks. Exonic structure of all the experimentally validated CERKL isoforms described in this article. FirstExonFinder predicted TSS; the ENCODE histone track H3K4Me3, a custom track of hits to different position weight matrices for known and predicted transcription factor binding sites, and some further evidence of transcriptional activity on neural tissues are shown. **(B, C)** Magnifications of the regions around exons 1 and 3, respectively,containing a more detailed view of the TFBS sites. The same track distribution is depicted on all three panels. Matrix hits overlapping homopolymer stretches larger than 5 bp were discarded.

Cerca del substrat de CERKL

CERCA DEL SUBSTRAT DE CERKL

ANTECEDENTS

CERKL és un gen que el nostre grup va identificar l'any 2004 com a causant d'arRP. La proteïna CERKL té una elevada similitud amb la proteïna CERK, presentant totes dues un domini quinasa de lípids conservat i una regió específica del grup de les quinases de ceramides. Des de l'inici, aquestes evidències han suggerit que CERKL podria tenir un paper clau dins del metabolisme dels esfingolípids, concretament, exercint una funció molt semblant a la de CERK (FIGURA 18), tot i que, experimentalment, encara no s'ha pogut demostrar [38, 39].

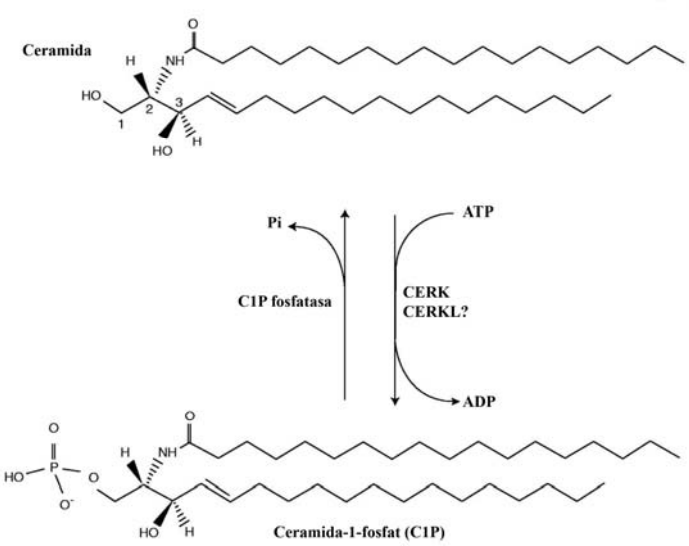

FIGURA 18 - Representació de la reacció que catalitza CERK. Formació de C1P a partir de la ceramida per l'enzim CERK. La semblança de CERK i CERKL suggereix que CERKL podria realitzar una funció similar, encara no descrita. Adaptada de Lamour et al. 2005 [199].

Els esfingolípids no són únicament components estructurals de membrana. En els darrers anys, s'ha pogut observar que tenen un paper clau com a grup de molècules senyalitzadores i que són essencials per la viabilitat de les cèl·lules, ja que poden dirigir el destí d'aquestes. La ceramida és el component central del metabolisme dels esfingolípids, a partir de la qual es sintetitzen altres metabòlits més simples, com l'esfingosina (SPH), o més complexos, com l'SM i els glucoesfingolípids (GlcCer, GalCer, etc.). A dia d'avui, podem dir que les ceramides intervenen en la mort cel·lular i en la resposta a l'estrès oxidatiu, promovent l'apoptosi, entre d'altres [64]. En canvi els diferents derivats de la ceramida: SM, GlcCer, GalCer, així com també les formes fosforilades de la ceramida (C1P) i de l'esfingosina (S1P), causen un efecte contrari, fet que indueix la supervivència cel·lular, gràcies a un balanç regulat acuradament (FIGURA 19) [67, 69].

Actualment, es sap ben poc del paper dels esfingolípids en la retina, però sí s'ha pogut demostrar que la ceramida és un mediador de l'apoptosi en la degeneració dels fotoreceptors [80], i que la inhibició de la via de síntesi provoca una degeneració més lenta d'aquestes neurones [109]. D'altra banda, en quant a la composició de lípids de la retina, l'esfingomielina i els gangliòsids serien els components majoritaris,

tot i que encara resta molta feina per realitzar sobre l'estudi de la composició d'esfingolípids en la retina. Altres patologies causades per deficiències en enzims d'aquest metabolisme (Gaucher, Niemann-Pick, etc), poden acabar generant neurodegeneració de la retina entre d'altres símptomes [93].

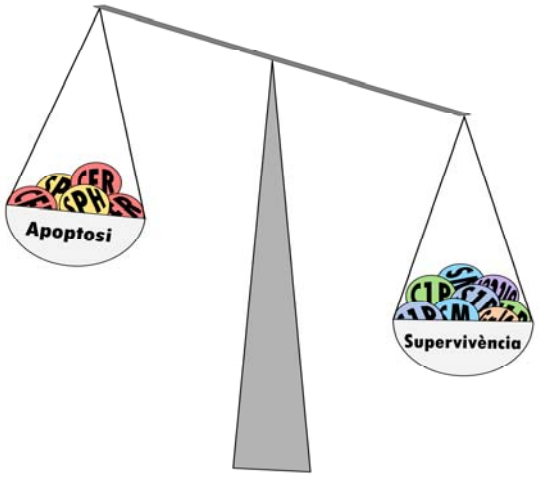

FIGURA 19 - El balanç entre la supervivència i la mort cel·lular. La ceramida i l'esfingosina afavoreixen l'apoptosi, mentre que les formes fosforilades d'aquestes i altres esfingolípids derivats de la ceramida són anti-apoptòtics.

Així doncs, ens vam proposar com a principal objectiu, la cerca del(s) substrat(s) i la caracterització de l'activitat enzimàtica de CERKL. Aquest apartat engloba la feina realitzada en col·laboració amb l'equip del Dr. Robert E. Anderson, director del Dean McGee Eye Institute a la Universitat d'Oklahoma.

MATERIAL I MÈTODES

Plasmidis

Les 4 isoformes descrites per CERKL (a: 532, b: 558, c: 2/6 i d: 3/6), així com CERK van ser clonades en el vector d'expressió eucariota pcDNA3.1. Totes elles contenien en la regió codificant de l'extrem C-terminal l'epítop HA. També, per poder generar adenovirus recombinants, es van clonar totes aquestes isoformes sense epítop en un pDNR-CMV, afegint la seqüència Kozak (CCACC) abans de l'ATG com indica el proveïdor (Clontech). Totes les construccions es seqüenciaren per tal de descartar possibles mutacions. Endemés, la seva expressió va ser comprovada per immunodetecció en *Western-blot*.

Cultius cel·lulars

Per dur a terme els diferents assaigs, es van utilitzar cèl·lules embrionàries humanes de ronyó -HEK293-, les mateixes cèl·lules però transformades amb l'adenovirus humà 5 -HEK293 E1/E3-, i cèl·lules humanes de Müller –MIO-M1- sembrades en DMEM suplementat amb un 10% de sèrum fetal boví (FBS), 100 U/ml de penicil·lina i 100 µg/ml estreptomicina. També es van sembrar cèl·lules precursores de fotoreceptors -661W- (cedides pel Dr. Al-Ubaidi) en DMEM complementat amb un 10% de FBS, 0.3 g/l de glutamina, 40 µl/l 2-Mercaptoetanol, més 100 U/ml penicil·lina i 100 µg/ml estreptomicina.

Transfeccions

Es van utilitzar dos protocols diferents de transfecció pels diversos assaigs. El primer va ser la transfecció amb *Lipofectamine 2000™*, seguint el protocol del fabricant (Invitrogen). L'altre protocol que es va emprar va ser la transfecció amb fosfat càlcic, la qual es duu a terme partint d'una gran quantitat de plasmidi precipitat (2-10 μg), posteriorment resuspés en 10 μl de TE pH 8 que es barreja amb 100 μl de $CaCl_2$ 2.5M i 890 μl d'H_2O. En un tub diferent es posa 1 ml d'HeBS 2x pH 7.2 (274 mM NaCl, 10 mM KCl, 1.4 mM $Na_2HPO_4 \cdot 7H_2O$, 15 mM D-Glucosa, 42 mM Hepes) i s'escalfa a 37 °C. Finalment, es deixa caure la barreja de DNA/ $CaCl_2$/ H_2O gota a gota sobre l'HeBS 2x, mentre s'agita el tub en el vòrtex. Es deixa reposar 30 min a temperatura ambient i s'afegeix a les cèl·lules crescudes en medi amb antibiòtic, canviant el medi després de 12-16 hores.

Generació d'adenovirus

Per generar els adenovirus vam utilitzar el *kit Adeno-X™ ViraTrak™ Expression System 2* (Clontech), seguint cadascun dels passos. De manera resumida: es varen barrejar 200 ng del vector donador (pDNR-CMV) amb 1 μl de recombinasa Cre i 18 μl de la barreja de reacció *Adeno-X LP*. La reacció es va incubar 15 min a temperatura ambient i, posteriorment, es va aturar, escalfant-la 5 min a 70 °C. Un microlitre de la reacció es va electroporar en cèl·lules electrocompetents *Supercharge EZ10* (Clontech) i es van deixar créixer en plaques d'LB amb ampicil·lina i cloramfenicol. Al dia següent, es va fer l'escrutini de les colònies mitjançant una reacció de PCR amb oligonuclòtids informatius. El plasmidi va ser amplificat i purificat a partir dels clons positius. Un cop purificat es va digerir amb *Pac*I per linealitzar-lo i es va transfectar amb fosfat càlcic en cèl·lules HEK293 E1/E3, que permeten la replicació i encapsidació del virus. El vector utilitzat va acoblat a fluorescència de manera que, expressa la proteïna DsRed, que actua com un indicador de la transfecció/transducció. Un cop vam arribar a un títol en que en 24 h totes les cèl·lules estaven infectades, es congelaven els pellets amb medi (uns 3 ml) per lisar les cèl·lules, posteriorment, es tornaven a centrifugar i s'utilitzava el medi per transduir altres línies cel·lulars.

Manipulació d'animals

Es van fer servir rates de les soques SD (Sprague Dawley) i Wistar de 2 mesos d'edat. Tota la manipulació dels animals es va fer seguint les normes de la Universitat d'Oklahoma i la declaració d'ARVO per a la utilització d'animals d'experimentació en el camp de la visió. L'estrès lumínic es va realitzar posant cada animal en una sola gàbia i exposant-los durant 6 hores a diferents intensitats de llum, en el cas de les Wistar, a 1000 lux, i en el de les SD, a 2700 lux. Posteriorment, els animals van ser sacrificats amb CO_2 més dislocació cervical i, finalment, es van extreure les retines.

Extracció de lípids

Les extraccions de lípids es van dur a terme a partir de retines de vaca i de rata (100-200 mg de teixit), cèl·lules en cultiu, així com també esperma de bou. L'extracció de Folch [200] va ser la més utilitzada. Breument, es va homogeneïtzar el teixit en 4 ml de Cloroform/Metanol 2:1, es tapa sota nitrogen (N_2), i es sonica durant 10 min. Es centrifuga durant 10 min a 1000 rpm. El sobrenedant es passa a un segon tub, mentre el pellet proteic es renta dues vegades amb 1 ml Cloroform/Metanol 1:1 seguit d'una centrifugació de 10 min a 1000 rpm. Es barregen els tres sobrenedants en el segon tub i s'afegeixen 1,2 ml d'una solució 1 mM DTPA, en un ambient de N_2, es barreja en el vòrtex i, finalment, es centrifuga a 1000 rpm durant 5 min. Es descarta la fase aquosa (superior) i s'addiciona una solució anomenada fase superior teòrica de Folch (Cloroform/Metanol/1 mM DTPA 3:48:47) i es va tapar sota N_2, per després barrejar i centrifugar els tubs 5 min a 1000 rpm. Es descarta la fase aquosa i s'asseca la fase orgànica sota N_2. Els lípids es van guardar a -20 °C fins la seva utilització.

Preparació de microsomes

S'homogeneïtzen 6 retines de 3 rates de 2 mesos d'edat en un 1 ml de tampó de sucrosa pH 7.5 (0.25 M sucrosa, 1 mM EGTA, 10 mM Tris-HCl pH 7.5, còctel d'inhibidors de proteases i 1 mM PMSF -afegit just abans d'utilitzar-se-). Una primera centrifugació de 10 min a 500 g va permetre un enriquiment en nuclis; posteriorment, es centrifuga 10 min a 17000 g per tal d'enriquir en mitocòndries. Finalment, el sobrenedant obtingut d'aquesta última centrifugació es torna a centrifugar durant 2 h a 100000 g a 4 °C. Els microsomes es van resuspendre en el tampó TEGM pH 7.5 (1 mM EGTA, 50 mM Tris-HCl pH 7.5, 1 mM β-mercaptoetanol, còctel d'inhibidors de proteases i 1 mM PMSF -afegit just abans d'utilitzar-se- i 33% de glicerol). Es quantifica la proteïna per BCA™ (Thermo Scientific) de les mostres, que posteriorment, s'aliquoten i congelen en N_2 líquid, i es conserven a -80 °C fins el moment de la seva utilització.

Reacció enzimàtica de fosforilació de lípids

El cultius cel·lulars transfectats amb les diferents construccions es lisen en tampó de lisi (20 mM MOPS pH 7.2, 2 mM EGTA, 10% glicerol i 1 mM DTT). Es mesura la concentració de proteïna per BCA™ i es fan alíquotes de 50 µl (200 µg). Les micel·les es van generar a partir de 150 mg de β-octilglucòsid amb 20 µl de DTPA 0.1 M pH 6.6 i 1980 µl d'H_2O, la barreja es sonica 40 min i es guarden fins la seva utilització a -20 °C. El tampó de reacció consistia en 75 mM MOPS pH 7.2, 250 mM NaCl, 15 mM $CaCl_2$, 5 mM EGTA, 2.5 mM DTT en H_2O. Entre 50 i 100 µg dels diversos lípids utilitzats s'assequen sota N_2 i es resuspenen en 20 µl de micel·les. Aquesta barreja es sonica durant 10 min i s'afegeix a la reacció que contenia: 50 µl de lisat, 21 µl de tampó de reacció, 5 µl de $MgCl_2$ 10 mM i ATP (en el cas de les reaccions amb radioactivitat, s'afegien 10 µl de γ-ATP^{32} 10 mCi/ml; en la resta de casos 12 µl d'una solució 1 mM d'ATP) i s'incuba durant 20-30 min a 37 °C. La reacció s'atura directament amb $HClO_4$ pels assajos de quantificació de fòsfor, o amb 2 ml de Cloroform/Metanol/Aigua 1:1:0.5, per tal d'extreure els lípids després de centrifugar 5 min a 6000 rpm, descartant-ne la fase aquosa i assecant l'orgànica sota N_2 per finalment, carregar-los en una TLC.

Reacció de fosforilació de proteïnes

Per les reaccions enzimàtiques, s'utilitzen lisats de cèl·lules transfectades amb pcDNA i pcDNA-*CERKLa*, així com cèl·lules transfectades amb les mateixes construccions, però estressades durant 24 hores amb 300 µM d'H_2O_2. A 50 µg de proteïna (lisat) s'addicionen 8 mM d'ATP i 20 mM de $MgCl_2$ (volum final de la reacció 40 µl). S'incuba durant 30 min a 37 °C i s'atura la reacció afegint tampó de càrrega de proteïnes 2x. Un cop bullides, es carreguen 25 µl de cada una de les mostres en un gel d'acrilamida del 10%. Després de la transferència a una membrana de PVDF, el bloqueig consisteix en 5% de BSA durant 1 h i s'incuba tota la nit a 4 °C amb els anticossos que detecten fosforilacions en diferents posicions: PY20 (1:4000) i PY99 (1:500). Finalment, s'incuba la membrana durant 1 h amb l'anticòs secundari i es revela, després de 3 rentats, mitjançant l'ús d'ECL.

Cromatografies en capa fina

Es van emprar tres tipus diferents de cromatografies en capa fina (TLC). En la primera, els lípids es carreguen sobre plaques de sílice gel 60 i, posteriorment, es corren en una fase que conté Cloroform/Acetona/Metanol/Acètic/Aigua en les proporcions següents 10:4:3:2:1. La segona, que anomenarem TLC en 2 dimensions, consisteix en plaques HPTLC HL de 10x10 cm tractades amb 3% d'acetat de magnesi i incubades 90 min a 100 °C on, a l'extrem esquerre, a 2 cm de cada extrem, es carrega la mostra en petits volums. La primera i segona corregudes es fan en la fase mòbil formada per Cloroform/Metanol/Amoni 65:25:5 en la mateixa direcció de la primera fase mòbil, després s'asseca la cromatografia, i mitjançant l'ús d'una espàtula es dibuixa una línia a 2 cm de l'extrem superior, es gira 90 ° i es corre en l'altre sentit en Hexà:Èter (60:40). Finalment, un cop seca, amb l'espàtula s'elimina la sílice de l'extrem inferior dret i es posa a migrar en la mateixa direcció en Cloroform/Acetona/Metanol/Acètic/Aigua 3:4:1:1:0.5. El tercer tipus de TLC, que anomenem TLC de 3 corregudes, consisteix en carregar els lípids en una placa d'HPTLC de 10x20 cm prèviament netejada en Cloroform/Metanol/Aigua 60:30:4 i activada a 100 °C durant un mínim de 12 h. Es dibuixen 4 línies, la primera a 1 cm de la part inferior (on es carreguen les mostres), la segona a 4 cm d'aquesta, la tercera a 10 cm i, finalment, una altra a 17 cm. Un cop s'han carregat els lípids, la primera correguda es fa en Cloroform/Metanol/Aigua 40:10:1 fins la línia de 4 cm, s'asseca a 60 °C i es torna a córrer en el mateix dissolvent fins la línia de 10 cm. Un cop assecada a 60 °C, es posa en Cloroform/Metanol/Acètic 47:2:0.5 i es deixa córrer fins que el front arriba a la línia de 17 cm. La última correguda es fa en Hexà:Dietilèter:Acètic 30:15:0.5 fins a la línia de 17 cm. Per revelar les plaques radioactives, es van exposar en films o en pantalles. Les no radioactives, es van revelar amb diclorofluoresceïna 0.05% en metanol al 75%, amb tinció de iode o per *charring*, submergint uns minuts la placa en una solució (8.5% v/v àcid fosfòric i 3.3% w/v acetat de coure monohidratat en H_2O).

Protein-lipid overlay

Diferents quantitats de lípids comercials (50-100 µg) es van assecar i resuspendre posteriorment en 5 µl de Cloroform/Metanol/Aigua 1:2:0.8. Basant-nos en l'assaig del *Protein-lipid overlay* de Dowler et al. 2002 [201], es dipositen gota a gota sobre una membrana Hybond C-extra els lípids, i els deixem

assecar durant 1 h a temperatura ambient. Es bloqueja durant 1 h la membrana en TBS (50 mM Tris-HCl pH 7.5, 150 mM NaCl) suplementat amb 1% BSA i 1% de llet en pols sense greix. Els lisats proteics es dilueixen a una concentració 1 μg/μl i s'incuben amb la membrana a 4 °C durant 16 h. Passat aquest temps, es fan 10 rentats de 5 min en TBST (TBS amb 0,1% Tween-20) i es torna a incubar la membrana amb anti-HA (1.1000) en solució de bloqueig durant 1 h, es fan 10 rentats de 5 min en TBST i s'incuba 1 h amb l'anticòs secundari conjugat a la peroxidasa (1.3000) en solució de bloqueig. Finalment, es realitzen 12 rentats de 5 min en TBST i es revela mitjançant l'ús d'ECL.

Assaig de quantificació de fòsfor

Els estàndards per fer la recta patró estaven preparats a partir de Na_2HPO_4 a 0.1 μg/μl de fòsfor. Es va partir de diferents reaccions enzimàtiques (20 μg de lisat) on s'havien utilitzat diferents substrats comercials. S'afegeix 0.26 ml d'àcid perclòric al 70% a la reacció i es va barrejar molt bé amb el vòrtex. Durant una hora s'incuba a 160-185 °C i, posteriorment, es refreda en gel durant 5 min i s'afegeixen 0.92 ml d'H_2O. La reacció química es realitza afegint 0.4 ml d'àcid molíbdic seguit de l'addició de 0.4 ml d'àcid ascòrbic, es barreja bé i es posa 5 min exactes a 100 °C. Passats els 5 min, es refreden les mostres ràpidament en gel durant 5 min i es mesura la densitat òptica a λ=797 nm.

Assaig d'activitat ATPasa

A partir dels lisats obtinguts es preparen reaccions de 25 μl afegint diferents quantitats de proteïna (0, 1, 5, 10, 50 i 100 μg). Es duu a terme la reacció enzimàtica descrita anteriorment, afegint tampó de reacció fins un volum final de 450 μl. Es refreden els tubs en gel i s'incuben 10 min amb 1 ml de solució II preparada al moment a partir d'1,5 g d'àcid ascòrbic en 17,5 ml d'H_2O, amb 25 ml d'àcid clorhídric 1 M, més 2.5 ml d'una solució 10% de molibdat d'amoni i 7.5 ml d'una solució 20% SDS. El color resultant ha de ser groguent. Després, s'afegeixen 1,5 ml de solució III (1.75 g de citrat de bismut en 50 ml d'àcid clorhídric 1 M amb 3.5 g de citrat de sodi) i s'incubar 10 min a 37 °C. Es mesura l'absorbància a λ=710 nm.

RESULTATS

Generació d'adenovirus

La troballa d'uns àcids grassos de cadena llarga (>26C) a la retina produïts per la proteïna ELOVL4 (FIGURA 20)[124], la importància dels quals en aquest teixit sembla ser essencial, atès que, una mutació en aquest gen causa un tipus d'Stargardt d'herència dominant molt poc freqüent, va suggerir que aquests àcids grassos podrien formar part de la fosfatidilcolina (grup polar de l'esfingomielina) o de les ceramides i els seus derivats, essent l'àcid gras que s'uniria a la base esfingoide per formar la dihidroceramida [93].

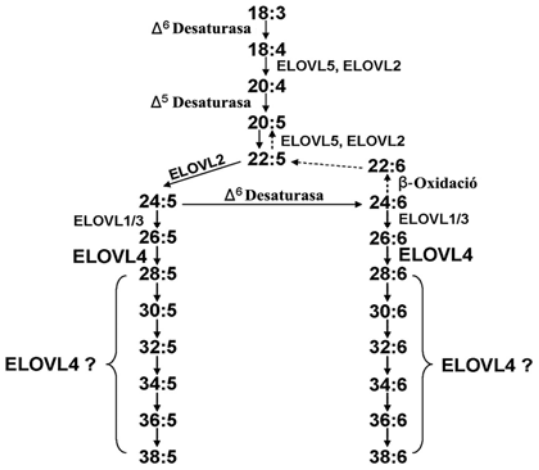

FIGURA 20 - Síntesi de àcids grassos de cadena llarga. Representació de la formació dels àcids grassos de cadena llarga a partir d'un precursor, mitjançant l'activitat de diferents elongases i desaturases. Adaptat de Agbaga et al. 2008 [124].

En base a totes aquestes dades, vam hipotetitzar que CERKL podria ser l'encarregada de fosforilar les ceramides que contenien àcids grassos de cadena llarga, ja que en experiments anteriors, no s'havia detectat fosforilació de les ceramides convencionals, de 16 i 18 carbonis (vegeu PUBLICACIÓ 1).

Degut a què les cèl·lules d'origen neuronal tenen una molt baixa eficiència de transfecció, el primer pas que es va dur a terme va ser la generació d'adenovirus recombinants. Un cop obtinguts es van poder transduir diferents línies cel·lulars (HEK293), algunes d'elles d'origen neuronal (661W). Endemés, l'experiment més important consistia en co-transduir adenovirus de *CERKL* i *ELOVL4* per veure si l'augment en la generació d'àcids grassos de cadena llarga donava alguna diferència en el patró de fosforilació. Aquests adenovirus que contenien el cDNA de *CERKL*, expressaven a la vegada la proteïna DsRed, la qual cosa permetia calcular l'eficiència de transducció mitjançant l'observació de les cèl·lules en el microscopi de fluorescència. A més a més, es va comprovar per *Western blot* l'expressió de la proteïna a partir dels adenovirus recombinants (FIGURA 21).

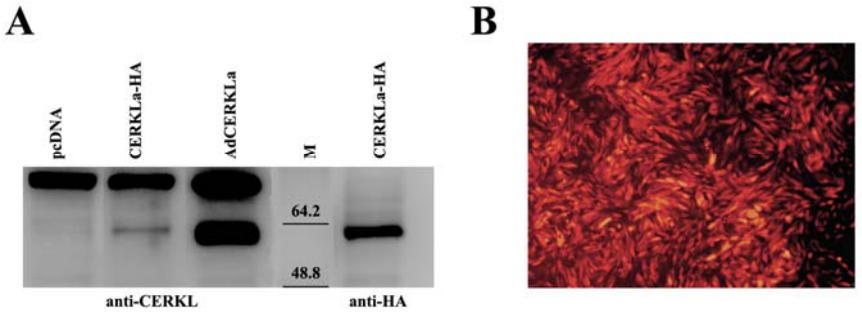

FIGURA 21 - Transducció i expressió de CERKLa. *Western blot* per detectar la correcta expressió de CERKLa mitjançant transfecció de la construcció CERKLa-HA i el vector buit, i de la transducció amb AdCERKLa, revelat contra un anticòs policlonal contra l'exó 1 de CERKL i l'anticòs monoclonal anti-HA (**A**). Cèl·lules MIO-M1 transduïdes amb AdCERKLa (**B**).

Un cop obtinguts els virus, per comprovar que seria possible transduir dos virus simultàniament, es va fer una prova amb dos adenovirus diferents. Amb aquesta fita en ment, es van infectar les cèl·lules amb els AdCERKLa (que expressen també la proteïna DsRed) i els adenovirus control que utilitzaven en el grup d'Oklahoma que expressen la GFP (AdGFP), per separat i conjuntament. El resultat obtingut va mostrar que quan s'afegeixen els dos adenovirus al mateix temps, es pot donar la co-infecció a la mateixa cèl·lula amb eficiència (FIGURA 21).

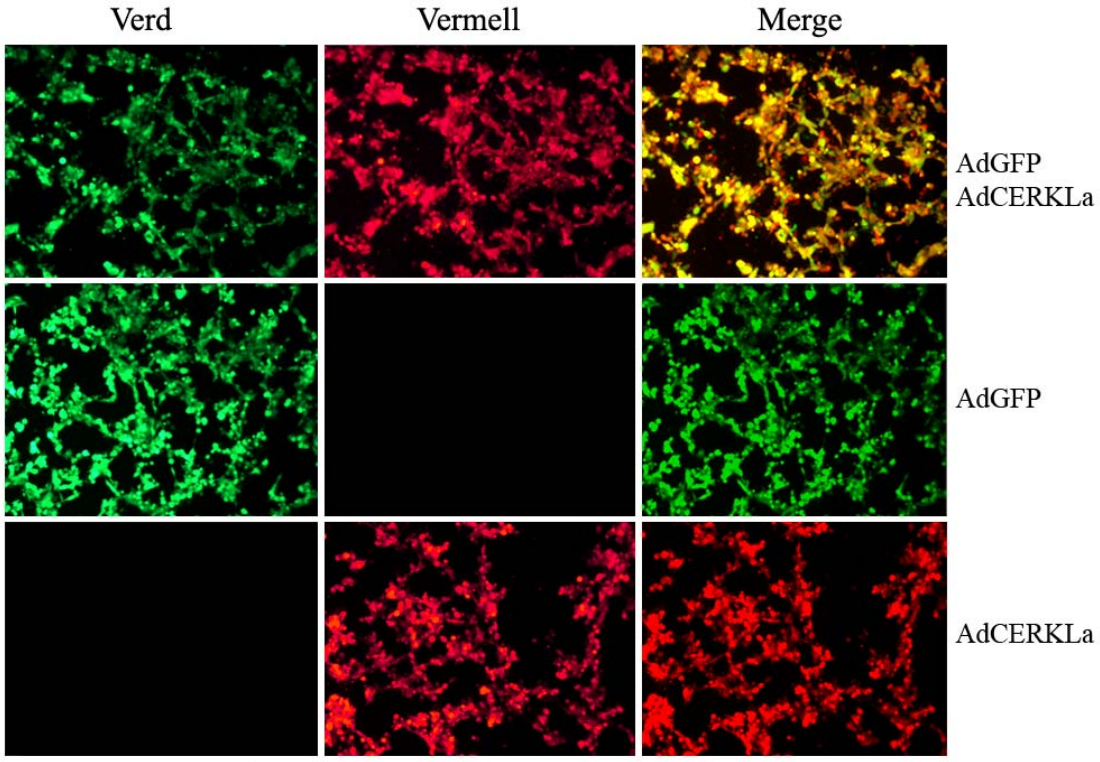

FIGURA 22 - Co-transducció d'AdCERKLa i AdGFP en cèl·lules HEK293. En verd es mostren les cèl·lules transduïdes amb els AdGFP, mentre que en vermell, els AdCERKLa que expressen també la DsRed. Com es pot observar, es pot produir la co-infecció sobre la mateixa cèl·lula de manera eficient.

Activitat quinàsica

CERKL té un domini quinasa de lípids conservat, tot i que encara no s'ha pogut demostrar la seva funcionalitat. Per tal de detectar i estudiar aquesta activitat quinàsica, es van dissenyar tot un seguit de reaccions utilitzant una àmplia varietat de compostos i de lisats proteics com a font de substrat i de la proteína. L'obtenció dels adenovirus va requerir força temps, tot i que un cop obtinguts, es van poder transduir diferents línies cel·lulars que ens van permetre, a més a més, analitzar per TLC els lípids de diverses línies cel·lulars transduïdes amb AdCERKLa i AdGFP. D'igual manera, també es van incubar les cèl·lules infectades amb ortofosfat marcat radioactivament, i es va intentar administrar SM i GlcCer exògena. Totes les combinacions queden reflectides a les TAULA 6 i TAULA 7.

Reaccions enzimàtiques per la cerca de la funció quinasa		
Font enzimàtica	**Substrat**	**Font de fòsfor**
Lisats de HEK293 transfectades amb CERKLa	Lípids de retina de rata	ATP-P^{32}
	Lípids de retina de vaca	
	Lípids de pell de la rata	
	Lípids de cèl·lules HEK transduïdes amb AdELOVL4	
	Micel·les de *cis*-retinol i àcid retinoic	
	Lípids de rata sotmesa a dany lumínic	
	Lisats proteics de retina de rata	
	Lisats proteics de retina de rata sotmesa a estrès lumínic	
	Microsomes de retines de rata	
	Micel·les amb Cer, GlcCer i SM	
	Lípids de retina de rata	ATP
	Microsomes de retines de rata	
	Micel·les amb Cer, GlcCer i SM	
	Micel·les amb GlcCer, SM, gangliòsids, Cer, LacCer i PI	
	Micel·les amb Cer, GlcCer i SM	GTP
	Micel·les amb GlcCer, SM, gangliòsids, Cer, LacCer i PI	
	Micel·les de *cis*-retinol i àcid retinoic	
Lisats de HEK293 transduïdes amb Ad-CERKLa	Lípids de retina de rata	ATP-P^{32}
	Lípids de pell de la rata	
	Lípids de cèl·lules HEK tranduïdes amb AdELOVL4	
	Lisats proteics de retina de rata	
	Lisats proteics de retina de rata sotmesa a estrès lumínic	
	Micel·les amb Cer, GlcCer i SM	
	Micel·les amb GlcCer, SM, gangliòsids, Cer, LacCer i PI	
	Micel·les amb SM	
	Micel·les amb GlcCer i SM	
	Lisats proteics de retina de rata	ATP
	Lisats proteics de retina de rata sotmesa a estrès lumínic	
	Micel·les amb Cer, GlcCer i SM	
	Micel·les amb GlcCer, SM, gangliòsids, Cer, LacCer i PI	
	Micel·les amb SM	
	Micel·les amb GlcCer i SM	
Lisats de HEK293 transfectades i estressades amb H_2O_2	Lisats proteics de retina de rata	ATP-P^{32}
	Lisats proteics de retina de rata sotmesa a estrès lumínic	
	Micel·les amb Cer, GlcCer i SM	
	Lisats proteics de retina de rata	ATP
	Lisats proteics de retina de rata sotmesa a estrès lumínic	
	Micel·les amb Cer, GlcCer i SM	

TAULA 6 - Reaccions enzimàtiques *in vitro*.

Anàlisi lipídica cèl·lules		
Cèl·lules transduïdes	**Addició de substrat**	**Font de fosfat**
HEK293	Endògens de la cèl·lula	Endògena
HEK293	SM i GlcCer exògenes	Endògena
HEK293	Endògens de la cèl·lula	Ortofosfat-P^{32}
HEK293	SM i GlcCer exògenes	Ortofosfat-P^{32}
MIO-M1	Endògens de la cèl·lula	Endògena
661W	Endògens de la cèl·lula	Endògena

TAULA 7 - Cèl·lules transduïdes amb AdCERKLa a les quals s'ha realitzat una anàlisi lipídica per TLC.

A continuació es mostren un recopilatori de diverses TLCs que resumeixen part d'aquesta feina, reflectint els experiments en cèl·lules en cultiu, reaccions quinàsiques *in vitro* i anàlisi de lípids directe sobre cèl·lules, tant per assaigs amb o sense radioactivitat.

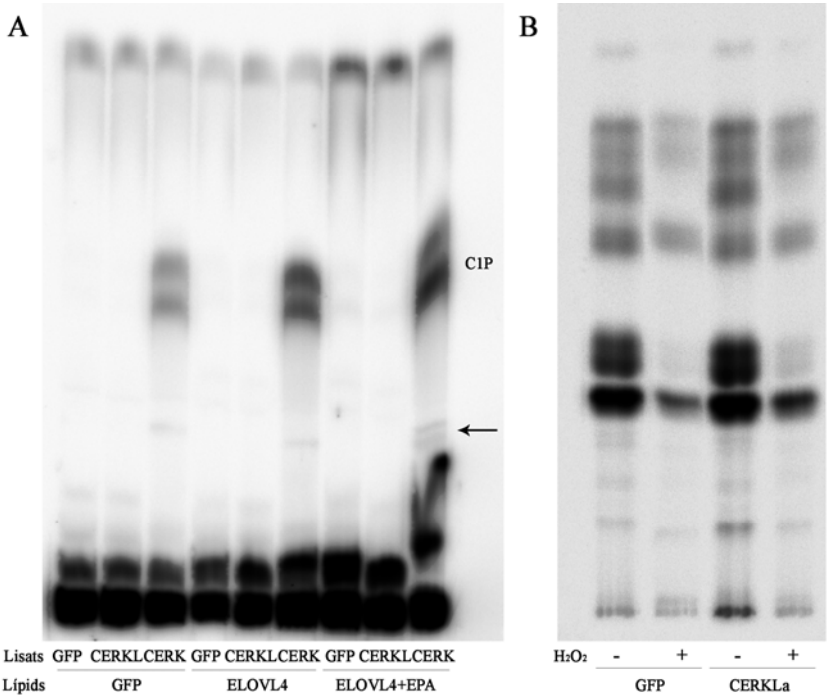

FIGURA 23 - Cromatografia en capa fina de reaccions enzimàtiques *in vitro* (A) i cèl·lules transduïdes amb AdGFP i AdCERKLa en presència d'H_2O_2 (B) amb P^{32}. (**A**) Lisats proteics de cèl·lules HEK293 transfectades amb la GFP, CERKLa i CERK es van incubar amb micel·les que contenien lípids extrets de cèl·lules transduïdes amb AdGFP, AdELOVL4 i AdELOVL4 en presència del seu substrat 20:5 n-3 (àcid eicosapentanoic). CERK va mostrar activitat quinasa generant C1P, incloent unes possibles ceramides de cadena llarga (bandes indicades amb la fletxa). En canvi, els lisats de CERKL i GFP no van mostrar cap indici de fosforilació. (**B**) Lípids de cèl·lules MIO-M1 transduïdes amb AdGFP i AdCERKLa en presència/absència d'H_2O_2 (1 mM durant 4 h) incubades amb ortofosfat marcat radioactivament. La fase mòbil en ambdós va consistir en Cloroform/Acetona/Metanol/Acètic/Aigua 10:4:3:2:1.

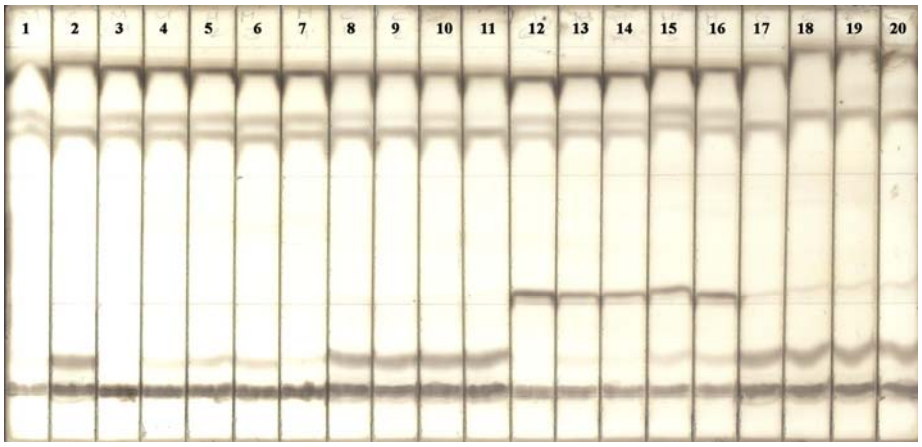

FIGURA 24 - Cromatografia després de l'addició d'SM i GlcCer acomplexades amb BSA en cèl·lules en cultiu. Per tal de poder determinar si seria viable addicionar a les cèl·lules alguns esfingolípids, es van incubar cèl·lules HEK293 en presència d'SM i GlcCer a diferents temps (1, 2, 3 i 4 h). Posteriorment, es van extreure els lípids del medi i de les cèl·lules i es va procedir a realitzar una cromatografia de 3 corregudes. En els carrils 1 i 2 es mostren els lípids del medi i de les cèl·lules sense tractar. Els carrils 3 i 12 mostren el medi amb SM i GlcCer, respectivament a temps 0. Els carrils del 4 al 6 (SM) i del 13 al 16 (GlcCer) pertanyen als lípids del medi de les cèl·lules incubades a 1, 2, 3 i 4 h respectivament. En canvi, els carrils del 8 al 11 (SM) i del 17 al 20 (GlcCer) es corresponen amb els dels pellets cel·lulars dels temps mencionats. L'observació dels lípids es va fer revelant la TLC pel mètode de *charring*. Com es pot observar, cap dels dos esfingolípids acomplexats amb BSA van ser capaços d'entrar a les cèl·lules.

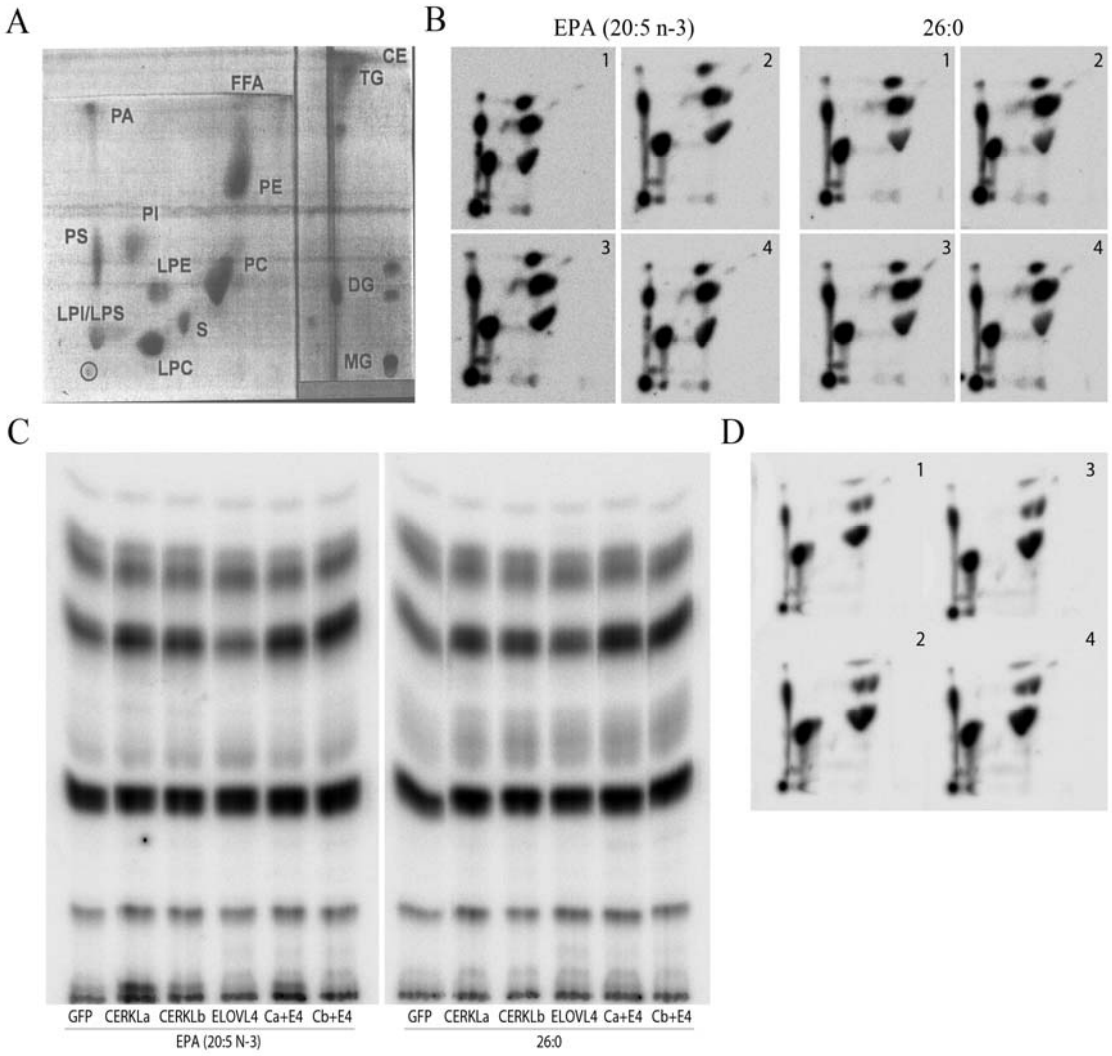

FIGURA 25 - TLCs on es mostren els lípids de diverses línies cèl·lulars incubades en presència d'ortofosfat-P^{32} transduïdes amb AdCERKLa i AdCERKLb. **(A)** Patró d'on localitzen els diferents lípids en la TLC de 2 dimensions. **(B)** TLC de 2 dimensions on es mostren els lípids obtinguts de cèl·lules HEK293 transduïdes amb AdGFP -1-, AdELOVL4 -3- i AdCERKLa -2- i AdCERKLb -4- en presencia de dos substrats diferents de la proteïna ELOVL4 -l'àcid eicosapentanoic (20:5 n-3) i l'àcid ceròtic (26:0). **(C)** Els mateixos extractes en un altre tipus de cromatografia, utilitzant com a fase mòbil: Cloroform/Acetona/Metanol/Acètic/Aigua 10:4:3:2:1. **(D)** Lípids de cèl·lules MIO-M1 no transduïdes -1-, transduïdes amb AdGFP -2-, AdCERKLa -3- i AdCERKLb -4- incubades amb ortofosfat-P^{32} separats per una cromatografia de 2 dimensions. En aquests tipus d'assaig es marcaven tots aquells compostos que contenen fòsfor, ja sigui com a component estructural (per exemple, l'SM presenta com a grup polar una fosfatidilcolina) o degut a fosforilació. En cap dels casos es va poder observar diferències en la incorporació de fòsfor. FFA: àcids grassos lliures, CE: colesterol èster, TG: triacilglicerol, DG: diacilglierol, MG: monoacilglicerol, PE: fosfatidiletanolamina, PC: fosfatidilcolina, PI: fosfatidilinositol, PS: fosfatidilserina, S: esfingomielina, LPI/LPS: lisofosfatidilinositol/lisofosfatidilserina, LPC: lisofosfatidilcolina.

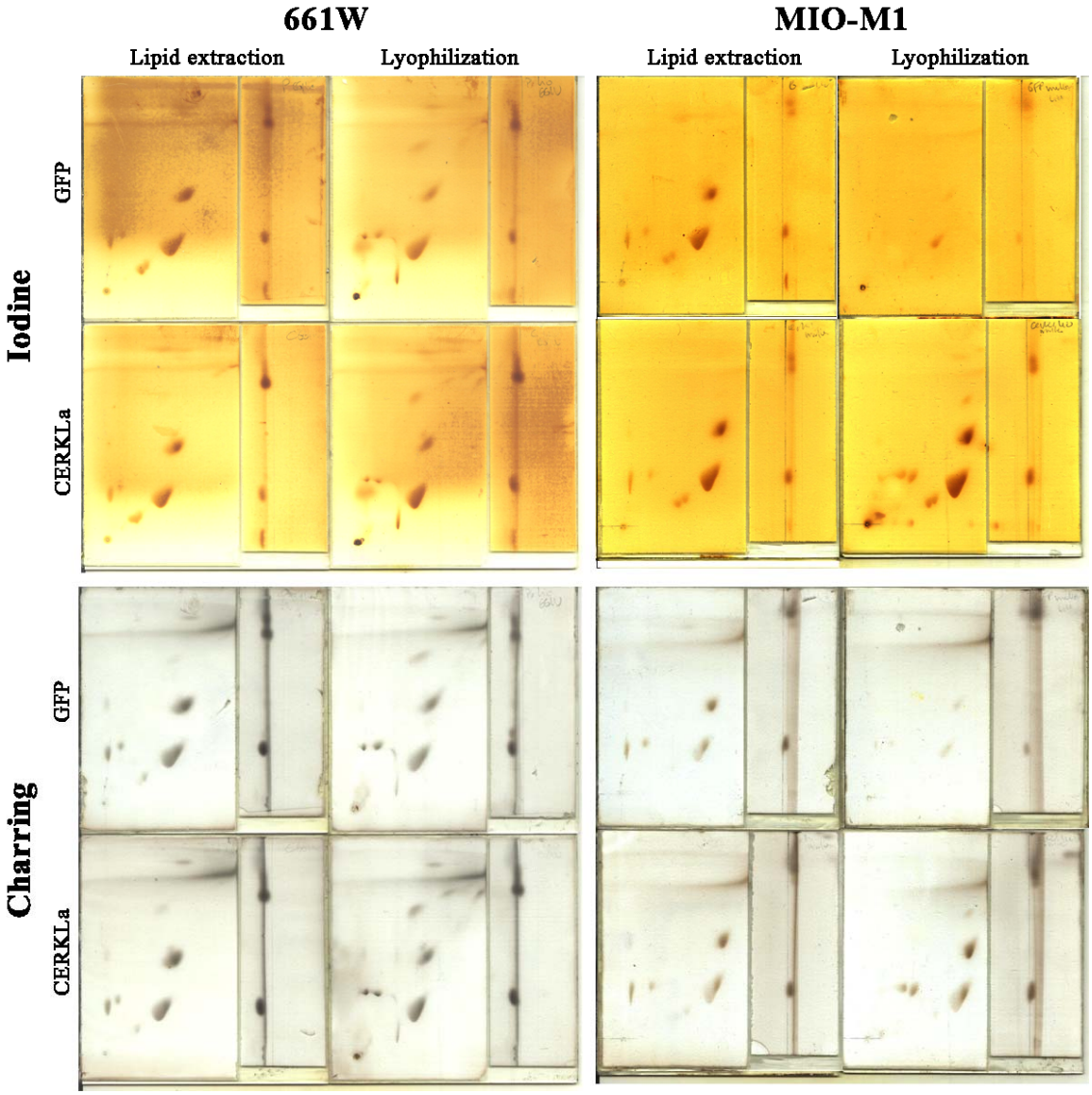

FIGURA 26 - Separació dels lípids de cèl·lules d'origen retinal (661W i MIO-M1) transduïdes amb AdGFP i AdCERKLa. En una cromatografia de 2 dimensions es van analitzar els compostos obtinguts a partir de l'extracció de lípids de Folch i la liofilització dels lisats cel·lulars obtinguts a partir d'aquestes cèl·lules. En aquest últim cas, un cop liofilitzat es va resuspendre el pellet en Cloroform/Metanol (1:1), es va centrifugar i es va assecar en N_2. Les plaques es van revelar mitjançant iode -permet el marcatge reversible de gairebé tots els compostos orgànics, a excepció d'alguns alcans saturats- i per el procès irreversible de carbonització o *charring* -tècnica que permet marcar en marró-negre els compostos orgànics en un fons blanc quan es posa a 120 °C després de tractar la placa amb una solució que conté 3% d'acetat de coure i 8% d'àcid fosfòric-.

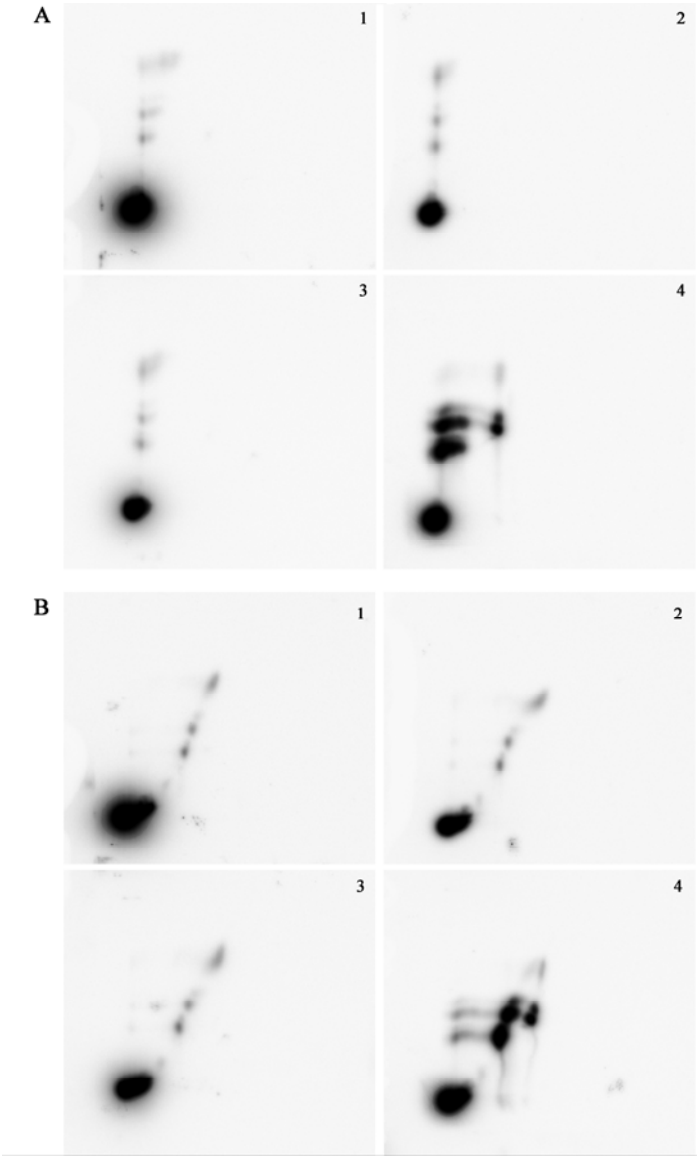

FIGURA 27 - TLC en 2 dimensions de la reacció enzimàtica *in vitro* de lisats proteics de cèl·lules HEK293 transduïdes en presència d'SM, PI, GalCer, GlcCer i Cer. Es van transduir cèl·lules HEK293 amb AdGFP -1-, AdCERKLa -2- i AdGFP+AdCERKLa -3- i transfectades amb CERK -4-. Es van generar micel·les que contenien SM, PI, GalCer, GlcCer i Cer per ser incubades amb els lisats. Es va analitzar el resultat de la reacció mitjançant una cromatografia en 2 dimensions (**A**). Per poder separar millor els compostos que es van quedar retinguts a la part esquerra de la placa, es van girar 90° cap a l'esquerra i es van córrer novament en la fase mòbil anomenada Rouser II: Cloroform/Acetona/Metanol/Acètic/ Aigua 3:4:1:1:0.5 (**B**). Tot i la clara activitat de CERK, no es va poder observar cap tipus d'activitat quinasa en les reaccions de lisats d'AdCERKLa.

Tot i el gran número de reaccions enzimàtiques realitzades, utilitzant múltiples substrats i fonts enzimàtiques, en cap cas hem pogut observar la fosforilació de cap producte lipídic dels estudiats, i no hem pogut demostrar que CERKL tingui activitat quinasa. Els nostres resultats estan d'acord amb la infructuosa cerca d'activitat quinasa realitzada per altres grups de recerca. Per tant, CERKL continua essent una proteïna òrfena d'activitat enzimàtica.

Protein-Lipid overlay

Una altra estrategia per abordar la cerca del substrat de CERKL va consistir en la utilització del mètode del *protein-lipid overlay*. Aquest assaig es basa identificar una possible interacció entre proteïnes en solució i els lípids d'interès ancorats sobre una membrana de nitrocel·lulosa en condicions no desnaturalitzants. Es va emprar com a control positiu CERK, que com s'esperava s'unia a les ceramides i als lípids totals de retina. Un cop validada la tècnica, es va procedir a realitzar l'experiment d'unió de CERKL a lípids amb lisats de cèl·lules HEK293 transfectades amb CERKLa-HA. Els lípids que es van utilitzar van ser els següents:

- Esfingolípids: Cer (hidroxi- i no hidroxi-), SM, GlcCer, GalCer, Gangliòsids, LacCer
- Àcids grassos: VLCFA, FFA
- Altres: PI, RA, RL, *cis*-retinol

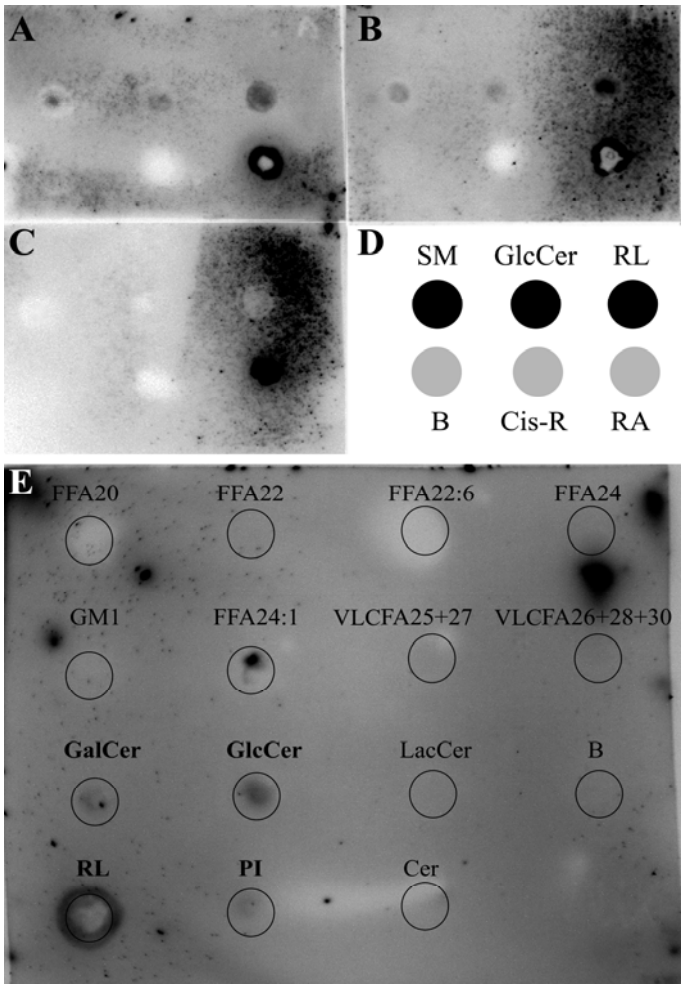

FIGURA 28 - Resultat del *Protein-Lipid Overlay*. Lisats de cèl·lules transfectades amb CERKLa (**A**), amb les 4 isoformes juntes (**B**) o amb el vector buit (**C**), van ser incubades en membranes que contenien 50 µg dels lípids indicats a (**D**). En negre els marquen aquells en els que es va detectar senyal, mentre que en els que no estan indicats en gris. Membrana en la qual es va incubar un lisat de cèl·lules transfectades amb CERKLa (**E**). En negreta s'indiquen els lípids als quals CERKL es va unir. B: blanc, RL: lípids totals de retina de rata, FFA: àcid gras lliure (el número indica el número de carbonis), VLCFA: àcid gras de cadena llarga (el número indica el número de carbonis), Cis-R: *cis*-retinol, RA: àcid retinoic.

Després de la incubació de les membranes amb els lisats proteics i la realització de la immunodetecció contra l'epítop HA fusionat a CERKLa, es va observar de manera repetitiva la unió a la GlcCer així com a l'SM, i en alguns casos als PIs i la GalCer, tot i que de manera més dèbil (FIGURA 28). En tots els casos, CERKL va unir-se al control positiu (tots els lípids de retina de rata, RL). Encara que el senyal detectat mostra una unió de CERKL amb els lípids mencionats, i donat que estem utilitzant lisats totals de cèl·lules transfectades, mitjançant aquest assaig no es pot afirmar fefaentment que la interacció entre l'esfingolípid i la proteïna sigui directa, ja que podria donar-se el cas que fos una altra proteïna present en el lisat la que interaccionés amb CERKL i, a la vegada, pogués unir-se al substrat. Tot i que l'àcid retinoic va donar positiu, caldria aclarir que aquest senyal es deu a que aquest producte estava resuspés en DMSO, i no es va poder evaporar del tot sota N_2, fet que va provocar que, en entrar en contacte amb la membrana, aquesta es desfés, de manera que el que es va observar va ser un forat, que també es detecta en el control negatiu (FIGURA 28), per la qual cosa no es pot concloure que aquesta unió sigui real.

Quantificació de fòsfor

L'estudi de la quantificació de fòsfor va consistir en una reacció química en la qual, mitjançant un assaig colorimètric, es podia quantificar la quantitat de fòsfor incorporat, independentment de quin tipus de molècula (lípid o proteïna) sigui fosforilada. Per realitzar aquests assaigs, inicialment es van preparar les reaccions d'activitat quinàsica utilitzant cèl·lules transfectades amb el vector buit i amb la proteïna CERK, i com a substrat micel·les que contenien ceramides. Un cop aturada la reacció, es va procedir a la quantificació del fòsfor incorporat, mostrant un augment significatiu en les reaccions que contenien CERK (FIGURA 29).

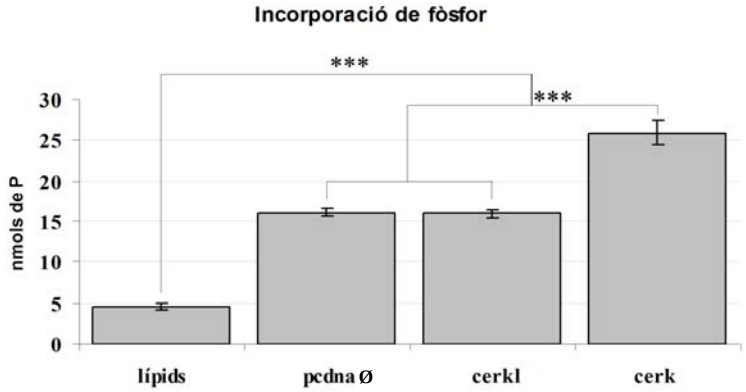

FIGURA 29 - Representació gràfica del fòsfor incorporat. Es mostra els nanomols de fòsfor incorporats en les reaccions enzimàtiques on només hi havia les micel·les que contenien els lípids de retina (lípids), i micel·les amb lisats de pcDNA buit, CERKL i CERK. *** indica significació estadística ($p<0.001$) mitjançant el test t-Student.

Un cop observada la sensibilitat d'aquest assaig, es van agrupar els lípids comercials disponibles al laboratori agrupats segons les seves propietats i la semblança entre ells (TAULA 8). Es va realitzar la reacció enzimàtica i es va analitzar el fòsfor incorporat. Tal i com es pot veure en la FIGURA 30, no van observar-se diferències en els nanomols de fòsfor entre els lisats transfectats amb el vector buit i els transfectats amb CERKLa, la qual cosa indica que, o bé CERKL no és una quinasa de lípids, bé el seu substrat és un lípid desconegut o minoritari, o bé no hem trobat les condicions ideals per la reacció.

Grups de lípids	
Grup	**Lípids**
Grup 0	Cap lípid
Grup 1	GlcCer, GalCer, GM1, LacCer
Grup 2	SPH, SM
Grup 3	PS, PA, PC, PI, PE
Grup 4	LPA, LPC, LPI, LPE
Grup 5	Colesterol, colesterol èster
Grup 6	MAG, DAG, TAG
Grup 7	FFA12, FFA14, FFA16, FFA18
Grup 8	FFA20, FFA22, FFA24

TAULA 8 - Llista de grups de lípids utilitzats per a les reaccions enzimàtiques.

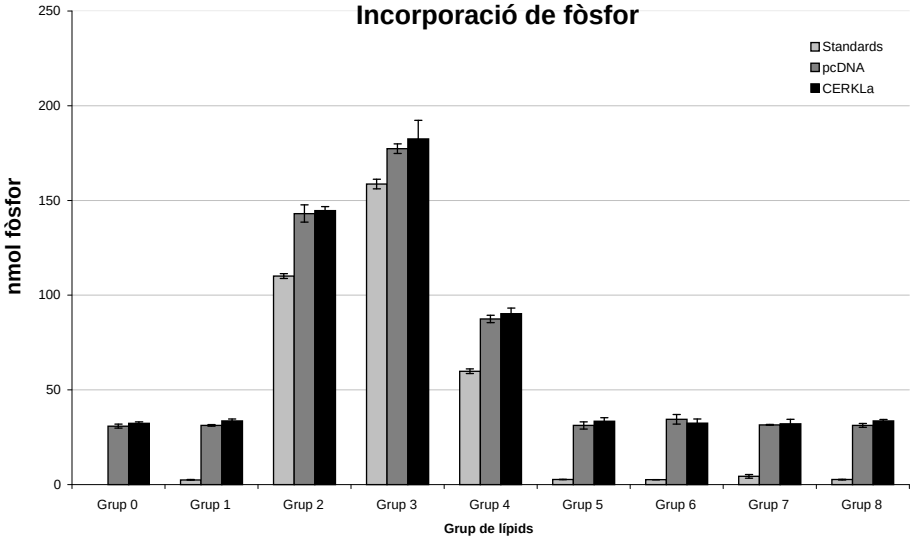

FIGURA 30 - Resultat de la quantificació de fòsfor incorporat en les reaccions enzimàtiques realitzades amb diversos lípids agrupats. La composició de cada grup s'indica a la TAULA 8.

Novament, aquests experiments van posar de manifest que CERKL, sota les condicions utilitzades, no té funció quinasa, atès que no es van poder observar increments significatius en la incorporació de fòsfor.

Fosforilació de proteïnes

Com tots els experiments de fosforilació de lípids van ser negatius, ens plantejàrem si CERKL podia ser, en comptes d'una quinasa de lípids, una quinasa de proteïnes. Així doncs, vam agafar lisats proteics de cèl·lules transfectades i els incubàrem en presència o absència d'ATP. També vam utilitzar lisats de cèl·lules sotmeses a condicions d'estrès oxidatiu (addicionant H_2O_2). Es van carregar les mostres en un gel d'acrilamida i es va realitzar una immunodetecció, mitjançant l'ús de dos anticossos que reconeixen residus de tirosina fosforilats: PY20 i PY99 (FIGURA 31). No es va poder observar cap diferència entre els lisats que sobreexpressaven CERKLa i els que havien estat transfectats amb el plasmidi buit.

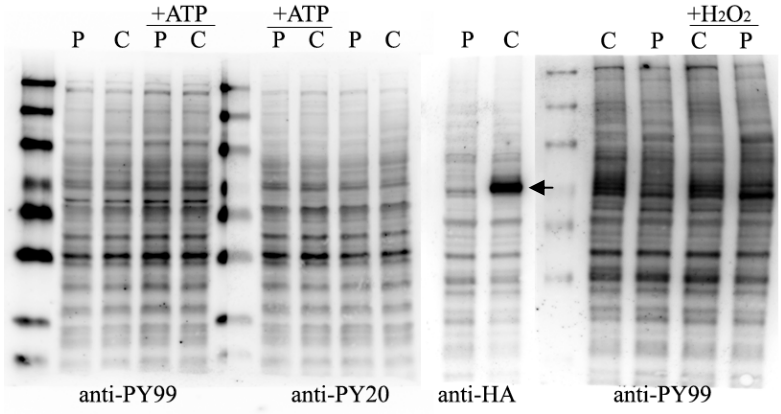

FIGURA 31 - Anàlisi per *Western blot* del patró de fosforilació. Reaccions de fosforilació utilitzants lisats de cèl·lules transfectades amb el vector pcDNA buit -P- i pcDNA-*CERKLa*-HA -C-, amb i sense ATP, pels 2 anticossos (anti-PY99 i anti-PY20). També es va fer el control de transfecció, mitjançant la immunodetecció per l'antigen HA on es pot detectat (fletxa) la producció de CERKLa. A més, es van provar altres condicions com per exemple, emprant lisats estressats amb H_2O_2. En cap cas hi ha diferències entre les cèl·lules transfectades amb *CERKL*a-HA i el vector buit.

Assaig d'activitat ATPasa

Degut a que l'assaig de quantificació de fòsfor no va donar diferències en quant a fosforilació i, per tant, no hi havia canvis en la incorporació de fòsfor, i atès que CERKL té un domini conservat d'unió a ATP, es va intentar veure si, en comptes d'una quinasa, podia ser una ATPasa, ja que en vàries ocasions al fer els experiments d'incorporació de fòsfor vam veure una tendència a disminuir la quantitat de fòsfor incorporat. Per tal d'estudiar si CERKL podia ésser una ATPasa, es va realitzar un altre assaig colorimètric que permetia la quantificació del fòsfor lliure. En aquests cas, es van utilitzar diferents concentracions de lisats proteics i es va realitzar una reacció d'activitat quinasa sobre lípids de retina.

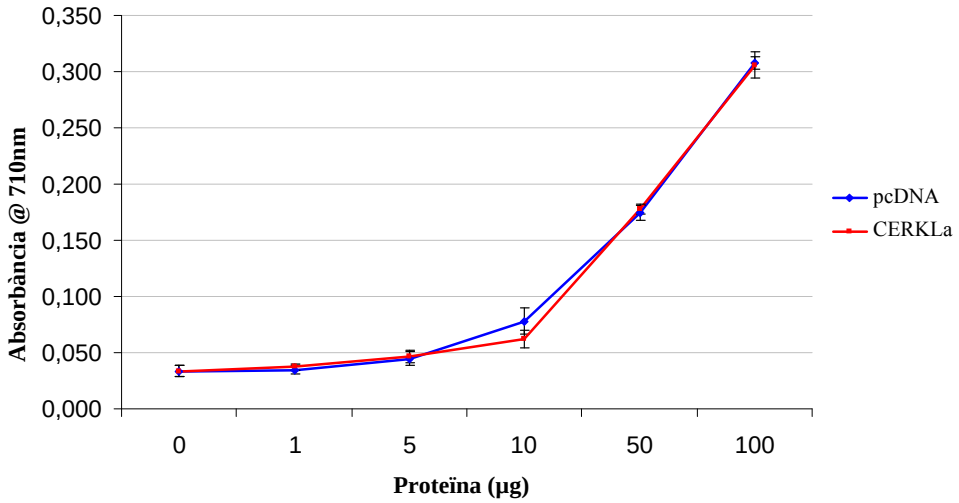

FIGURA 32 - Resultat de la quantificació de fòsfor lliure. Reaccions que es van dur a terme amb diferents concentracions de proteïna de lisats transfectats amb el vector buit o CERKLa. Totes dues mostres es comporten de manera idèntica.

El comportament entre les cèl·lules transfectades amb el vector buit i *CERKL*a va resultar idèntic, i indica que CERKL no té activitat ATPasa o fosfatasa (FIGURA 32).

Cerca d'interaccions proteiques

CERCA D'INTERACCIONS PROTEIQUES

ANTECEDENTS

CERKL, com ja hem esmentat en vàries ocasions, continua essent avui en dia una quinasa òrfena de substrat. S'han descrit fins el moment 9 transcrits, els quals generen 4 isoformes proteiques [40]. D'altra banda, en el metabolisme dels esfingolípids intervenen diversos enzims, l'activitat dels quals ve regulada per la dimerització. Entre aquestes proteïnes, s'ha observat que la CERT, una proteïna que transporta la ceramida de l'ER al Golgi, per tal de produir, principalment, SM [202], pot formar homotrímers que provoquen la inactivació de la proteïna, podent regular així els nivells d'SM. Aquests complexes s'han observat al tractar les cèl·lules amb UV i estrès oxidatiu, i queda per establir si realment aquest fenòmen es dóna *in vivo* de forma natural [203]. Altres enzims també regulen la seva activitat formant heterodímers: d'una banda, la Serina-palmitoïl transferasa (SPT), enzim encarregat d'unir un palmitoïl-CoA amb la serina per generar la 3-cetoesfinganina, constaria d'un heterodímer format per la subunitat SPTLC1 i la SPTLC2 [204]. Endemés, recentment, s'ha trobat una tercera subunitat SPTLC3 encarregada de generar les bases esfingoides de 16 carbonis, de les quals es generen esfingolípids que es troben particularment enriquits en el plasma humà [205]. D'altra banda, sembla ser que vàries transferases implicades en la síntesi de glucoesfingolípids a partir de la ceramida, podrien formar homo- o heterodímers i oligòmers per dur a terme la glicosilació. Endemés, alguns estudis han demostrat que la GCS pot formar heterodímers amb una proteïna desconeguda de 15 kDa [206, 207]. Nogensmenys, altres enzims de la via interaccionen amb proteïnes que activen o augmenten la seva activitat. Aquest és el cas de la Calmodulina, una proteïna que és sensible a les concentracions de Ca^{2+} i que pot regular l'activitat de CERK [59]. Per últim, recentment s'ha descrit que la S1P liasa, enzim encarregat d'hidrolitzar de manera irreversible la S1P en *trans*-2-hexadecenal i etanolamina fosfat, també podria dimeritzar [208].

Tot plegat, ens va fer pensar que CERKL podria estar formant complexes entre les 4 isoformes, mitjançant diferents combinacions d'aquestes. A més a més, ens vam proposar explorar si CERKL interactuava amb altres proteïnes, així com si podia estar modificada post-traduccionalment per fosforilació o ubiquitilació.

MATERIAL I MÈTODES

Clonatges

Mitjançant una sèrie de clonatges, es va introduir el cDNA de les 4 isoformes de *CERKL* en el vector pACT2 i pGBKT7. El cDNA de *CERK* es va clonar també en el pACT2. El canvi en *cassette* es va validar per digestió test i posterior seqüenciació dels clons positius. Els clonatges es van realitzar de la següent manera: inicialment es van clonar els cDNAs de *CERKL* en el vector pACT2 a partir d'una construcció pRSET-*CERKL*. Per dur a terme el clonatge, es va digerir el vector amb *Sfi*I i posteriorment es va aprofitar l'activitat 3'-5' exonucleasa de la Klenow per eliminar els nucleòtids de l'extrem 3' protuberant generat per l'enzim de restricció. Finalment, es va digerir per *Xho*I. En el cas del clonatge a

pGBKT7 es va digerir per *Sfi*I, seguit de la incubació amb Klenow i la digestió per *Sal*I. D'altra banda, l'insert es va obtenir digerint les construccions pRSET-*CERKL* per *Bam*HI, seguit de *fill-in* mitjançant l'activitat 5'-3' polimerasa de la Klenow i, per últim, una digestió per *Xho*I. En el cas de *CERK*, es va digerir a partir del clon original (cedit pel Dr. Bornancin) per *Nco*I, obtenint un fragment de 850 pb de bases que es va clonar utilitzant el mateix enzim en el vector pACT2. Posteriorment, utilitzant els oligos CERK_For (GAG GAC GCA GAG GAG CGC CG) i CERK_Rev_*Bam*HI (CGG GAT CCA CCA CTT TGT ACA AGA AAG CT) es va amplificar part de *CERK* per PCR (2 min a 94 °C, 35 cicles 30 seg a 94 °C, 30 seg a 63 °C i 1 min a 68 °C). Tant el fragment de PCR, com el fragment de 850 pb de la construcció pACT2-*CERK* es van digerir per *Bsa*B1i *Bam*HI, i lligar per recomposar el clon complet.

Doble híbrid

Per realitzar l'assaig de doble híbrid es va utilitzar la soca AH109 de *S. cerevisiae*. Breument, les cèl·lules es van créixer en medi ric YPDA, i es van preparar per la seva transformació seguint el protocol estàndard. Es van fer dues proves, en les que es va obtenir el mateix resultat, d'una banda la co-transformació dels dos plasmidis a la vegada, i d'altra, la transformació primer d'un vector i, després, l'altre. Es van créixer els llevats en medi SD sense leucina ni triptòfan, per tal d'observar l'eficiència de la transformació i, posteriorment, per comprovar si hi havia interacció, es van sembrar en un medi selectiu SD sense leucina, triptòfan, adenina ni histidina. Per a la transformació, es van emprar 100 ng de plasmidi seguint el protocol convencional de transformació de llevats. Les combinacions dels diferents vectors es mostren en la TAULA 9. Com a control positiu de la interacció, es van utilitzar dos plasmidis, la interacció dels quals va ser descrita anys enrere en el grup de la Dra. Marfany [209].

Co-immunoprecipitació i *Western blot*

Es van utilitzar les construccions pcDNA-*CERKL*-HA i pGFP-*CERKL* generades en el grup prèviament a l'inici d'aquest treball. Es sembren cèl·lules HEK293T en plaques de 10 cm (1 x 10^5 cèls/placa). L'endemà es transfecten amb Lipofectamina, seguint les indicacions de la casa comercial. Les construccions pcDNA-*CERKL*-HA utilitzades corresponen a *CERKLc* i *CERKLd*, que van ésser transformades al mateix temps que el vector buit pGFP i les construccions en pGFP-*CERKL* que contenien els cDNAs de *CERKLa*, *CERKLb*, *CERKLc* i *CERKLd*. Les cèl·lules es recullen a les 48 hores post-transfecció, es renten en PBS i soniquen en tampó de lisi (0.5% Nonidet P40, 50 mM TrisHCl pH 7.5, 1 mM EDTA, 150 mM NaCl, suplementat amb inhibidors de proteases). Els lisats es centrifuguen i els sobrenedants s'incuben amb boles prèviament conjugades amb l'anticòs anti-HA. La incubació es realitza durant 4 h a 4 °C i, finalment, es duen a terme nombrosos rentats, per acabar eluint la mostra en 80 µl en tampó de càrrega de proteïnes. Les mostres es van bullir durant 5 min i es van carregar 15 µl en un gel d'acrilamida del 10%. Un cop transferides les proteïnes a una membrana PVDF es va bloquejar la membrana en 5% llet en pols sense greix i incubar 1 h a temperatura ambient amb els anticossos anti-GFP produït en conill i anti-HA en ratolí (1:1000). Els secundaris DARPO (1:4000) i SAMPO (1:3000) es van incubar 1 h a temperatura ambient. Després dels rentats, es va procedir al revelat mitjançant l'ús d'ECL.

Interaccions proteiques detectades per immunoprecipitació més anàlisi per espectometria de masses

Es sembraren cèl·lules HEK293T en plaques de 10 cm (1 x 10^5 cèls/placa). Passades 16 h es varen transfectar amb pcDNA-*CERKLa* i el vector buit (2 plaques de cada). Les cèl·lules van ser recollides, rentades i sonicades en tampó de lisi (veure apartat de la co-immunoprecipitació). Un cop incubades amb la resina conjugada a anticòs anti-HA es bullen en tampó de càrrega de proteïnes i es carreguen en un gel d'acrilamida del 12.5% (per tal de detectar *partners* de massa petita) i 7.5% (per a la identificació de proteïnes de massa gran). Un cop finalitzada l'electroforesi, es tenyeix en Comassie i totes les bandes diferencials entre les cèl·lules transfectades amb pcDNA buit i pcDNA-*CERKLa* van ser retallades i analitzades per MALDI-TOF. Tots els passos es van realitzar amb molta cura i amb guants per evitar contaminacions per queratina de la pell humana.

Modificacions post-traduccionals

***Fosforilació*:** Es van obtenir lisats proteics en PBS suplementats amb inhibidors de proteases de cèl·lules COS7 transfectades amb les diferents construccions de pcDNA-*CERKL*. Els lisats es van dividir en tres. Una fracció va ser tractada amb la fosfatasa de serina/treonina PP_1, una altra es va incubar amb la fosfatasa de tirosina TC-PTP, ambdues seguint les instruccions del distribuïdor. La tercera fracció no es va tractar. Posteriorment, es van carregar els lisats en un gel d'acrilamida del 10% i es van immunodetectar, incubant les membranes de PVDF amb l'anticòs monoclonal anti-HA (vegeu apartat co-immunoprecipitació i *Western blot*).

***Ubiquitilació*:** Es van co-transfectar cèl·lules HEK293T amb pcDNA-*CERKLa* i una construcció que contenia el cDNA de la ubiquitina fusionat amb una cua d'histidines (pcDNA-*UB*-His). Una de les plaques es va tractar amb 10 μM de MG132 (inhibidor específic del proteasoma) durant les últimes 16 hores abans de recollir les cèl·lules en tampó de lisi (vegeu apartat co-immunoprecipitació) més inhibidors de proteases. Posteriorment, es va realitzar una co-immunoprecipitació, utilitzant boles de resina conjugades a anticòs anti-HA o a Co^{2+} (amb elevada afinitat per les histidines) i es va detectar per *Western blot*, utilitzant l'anticòs primari contrari al que s'havia utilitzat per la co-immunoprecipitació.

RESULTATS

Modificacions post-traduccionals

Durant els controls rutinaris de transfecció realitzats per *Western blot* en el laboratori es van observar unes bandes mirall superiors sobre la proteïna sobreexpressada. Degut a la diferència de massa entre la banda majoritària i la banda superior es va pensar que es podria tractar d'una modificació post-traduccional, com ara una fosforilació. Així doncs, els lisats van ser tractats amb dues fosfatases diferents, PP1 i TC-PTP. En cap dels dos casos, la banda es va reduir o desaparèixer, la qual cosa indica que hauria de ser un altre tipus de modificació (FIGURA 33).

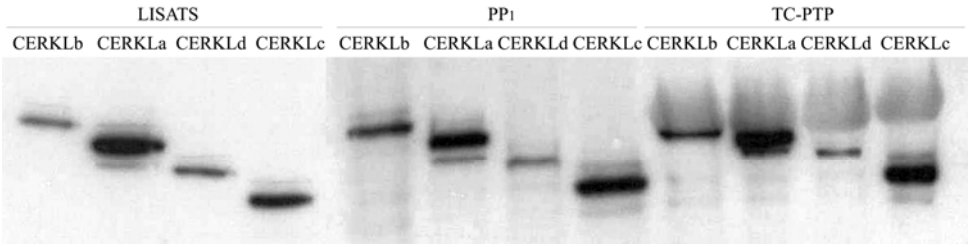

FIGURA 33 - Anàlisi per *Western blot* de les modificacions post-traduccionals. Es van tractar els lisats amb dues fosfatases diferents, per veure si la banda mirall observada es debia a una fosforilació. Cap de les dues fosfatases va fer desaparèixer la banda,i vam concloure, doncs, que havia de ser un altre tipus de modificació.

D'altra banda, l'increment de massa, per mida, també podria correspondre a la unió d'una ubiquitina (aprox. 8 kDa). En aquest cas es va realitzar una co-immunoprecipitació a partir de cèl·lules HEK293T co-transfectades amb pcDNA-*CERKL*-HA i pcDNA-*UB*-His, en la qual es va enriquir gràcies a l'epítop HA de la proteïna CERKL sobreexpressada i després es procedia a la immunodetecció mitjançant la cua d'histidines de les ubiquitines. Malauradament, mai es va poder detectar cap banda amb l'anticòs anti-histidines. A més a més, en el grup es va començar a veure que aquestes construccions que contenien vàries ubiquitines en tàndem fusionades amb l'epítop, anaven perdent unitats, segurament per recombinació dins el bacteri on era transformat el plasmidi, fet que podia contribuir als nostres resultats negatius. No obstant, si que es va observar que la banda mirall superior era més intensa quan s'addicionava la construcció pcDNA-*UB*-His (FIGURA 34).

Per últim, també es va demostrar que CERKL es degrada via proteasoma, ja que, la seva inhibició mitjançant l'ús de MG132, produïa un increment en el rescat de CERKL, així com l'aparició de nombroses bandes superiors corresponents a la proteïna amb diverses unitats d'ubiquitines (FIGURA 34).

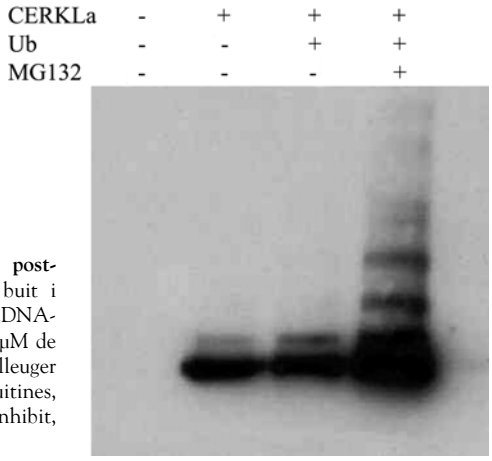

FIGURA 34 - Anàlisi per Western blot de les modificacions post-traduccionals. Es van transfectar cèl·lules HEK293T amb el vector buit i CERKLa-HA. Endemés, aquestes últimes es van co-transfectar amb el pcDNA-UB-His i, a més a més, una mostra va ser tractada durant 16 h amb 10 μM de MG132, un inhibidor específic del proteasoma. Es va observar un lleuger augment en la banda mirall quan es co-transfectava *CERKL* amb les ubiquitines, així com també, un rescat de la proteïna quan el proteasoma estava inhibit, indicant que CERKL es degrada per aquesta via.

Dimerització

L'estudi de la possible dimerització o oligomerització de CERKL, es va realitzar mitjançant tres tècniques diferents. La primera va consistir en un assaig de doble híbrid, en el qual es van transformar les construccions de CERKL en combinacions diferents (TAULA 9) i, a la vegada, també amb CERK. El resultat va mostrar que per aquest mètode no hi ha cap indici de que CERKL pogués interaccionar amb ella mateixa, formant un complex ni amb CERK (FIGURA 35). Els mateixos resultats es van obtenir quan

es van transformar els llevats inicialment amb les construccions derivades de pGBKT7 i, posteriorment, amb les de pACT2.

Combinacions doble híbrid					
Número	**pACT2**	**pGBKT7**	**Número**	**pACT2**	**pGBKT7**
1	CERKLb	pGBKT7	11	CERKLd	CERKLd
2	CERKLb	CERKLb	12	CERKLd	CERKLc
3	CERKLb	CERKLa	13	CERKLc	pGBKT7
4	CERKLb	CERKLd	14	CERKLc	CERKLc
5	CERKLb	CERKLc	15	CERK	pGBKT7
6	CERKLa	pGBKT7	16	CERK	CERKLb
7	CERKLa	CERKLa	17	CERK	CERKLa
8	CERKLa	CERKLd	18	CERK	CERKLd
9	CERKLa	CERKLc	19	CERK	CERKLc
10	CERKLd	pGBKT7	20	USP25	Actina

TAULA 9 - Combinacions de plasmidis utilitzades per les co-transformacions en llevat.

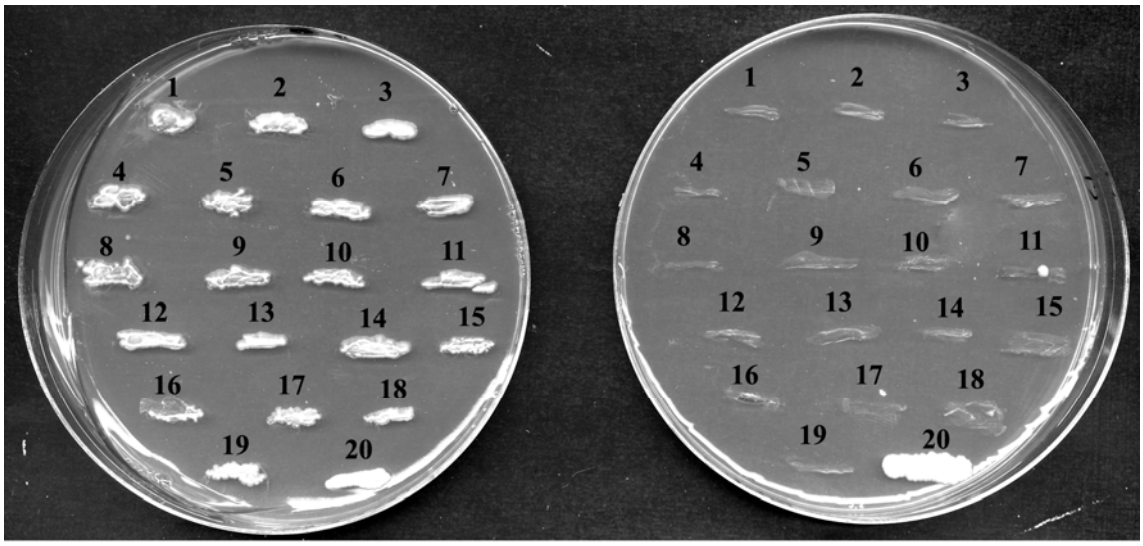

FIGURA 35 - Resultat de l'experiment de doble híbrid. Tots els clons van créixer en medi SD-LT indicant que tots dos plasmidis havien estat transformats, però només el control positiu va créixer en medi SD-LTHA, indicant que no hi havia interacció directa entre les diferents isoformes de CERKL.

La segona tècnica utilitzada va ser una co-immunoprecipitació, en la qual, les cèl·lules eren transfectades amb dues construccions de *CERKL*, però amb epítops diferents. Així, doncs, es va co-transfectar d'una banda pcDNA-*CERKLc*-HA amb els vectors: pGFP, pGFP-*CERKLc*, pGFP-*CERKLd* i pGFP-*CERKLa*; i de l'altra pcDNA-*CERKLd*-HA amb: pGFP-*CERKLd* i pGFP-*CERKLb*. La immunoprecipitació es va realitzar mitjançant unes boles de resina conjugades a anticossos anti-HA, i un cop obtingut el resultat del *Western blot*, no es va observar proteïna immunoprecipitada quan es revelava la membrana amb l'anticòs anti-GFP. Malauradament, s'observà que la GFP, per si mateixa, podia interactuar, bé amb les boles de resina, bé amb l'HA o bé amb la proteïna CERKL, ja que la quantitat de proteïna enriquida va ser molt elevada. Actualment, s'han clonat les 4 isoformes en un vector pcDNA amb una cua d'histidines a N-terminal, per tal de realitzar experiments futurs en els que es pugui comprovar si realment CERKL pot o no oligomeritzar (FIGURA 36).

Per últim, es van co-transfectar combinacions de 2, 3 i de totes 4 construccions en cèl·lules HEK293T i es va intentar, mitjançant una electroforesi en condicions no desnaturalitzants, observar si hi havia formació de complexos. Els resultats no van ser gaire resolutius, tot i que tot semblava apuntar a que no hi havia formació de complexes, atès que no es detectava cap banda d'elevada massa molecular en comparació amb el marcador emprat per aquest tipus de gels (resultats no mostrats).

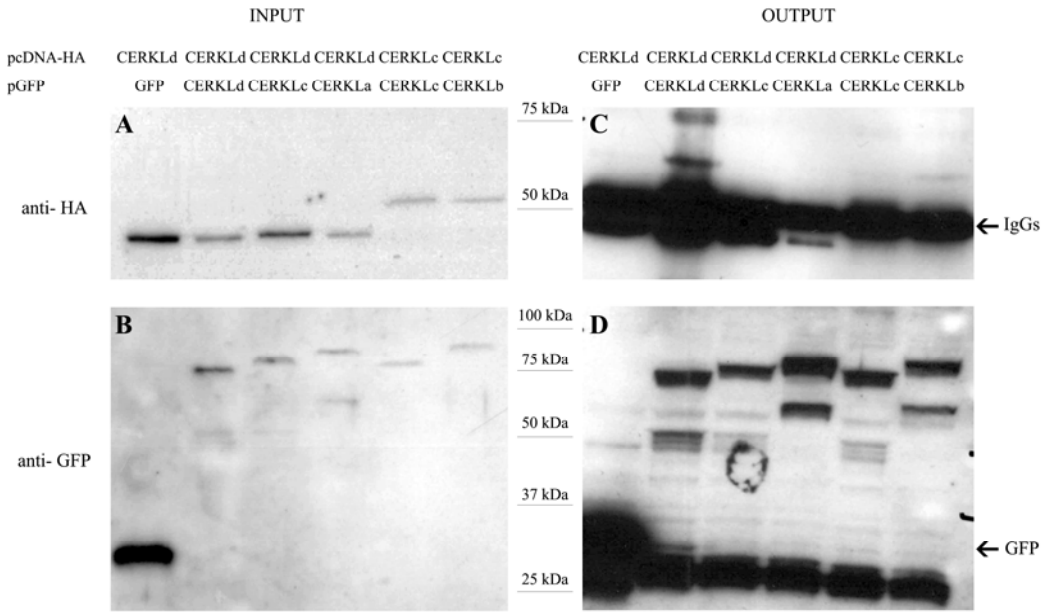

FIGURA 36 - Co-immunoprecipitació de CERKL. Es van co-transfectar dues isoformes de CERKL, una fusionada amb epítop HA i l'altre, amb GFP. Es va realitzar un enriquiment de CERKL-HA i es va veure si CERKL-GFP també es detectava. El resultat, va mostrar que si que era capaç de co-immunoprecipitar, però també tenia la capacitat la proteïna GFP (vector buit),la qual cosa indica que la GFP es pot unir directament a les boles o a CERKL sense necessitat de dimerització entre dues subunitats de CERKL.

Interaccions proteiques

La cerca de la funció de CERKL ha estat l'objectiu principal d'aquest treball. Una manera d'obtenir pistes de quin paper podia estar jugant aquesta proteïna en la cèl·lula va ser estudiar aquelles proteïnes amb les que CERKL podia interactuar (*partners*). Per dur a terme aquest estudi, es va immunoprecipitar CERKLa-HA a partir de cèl·lules HEK293T transfectades amb pcDNA-*CERKL*a-HA i el vector pcDNA buit. Finalment, es va carregar tot l'eluït enriquit d'una placa de 10 cm, en un gel d'acrilamida on es va carregar també l'eluït de la immunoprecipitació de les cèl·lules transfectades amb el vector buit. Per poder separar bé les bandes de mides grans i mides petites, es van utilitzar gens de diferents concentracions d'acrilamida (7.5% i 12.5%). Les bandes diferencials detectades després de la

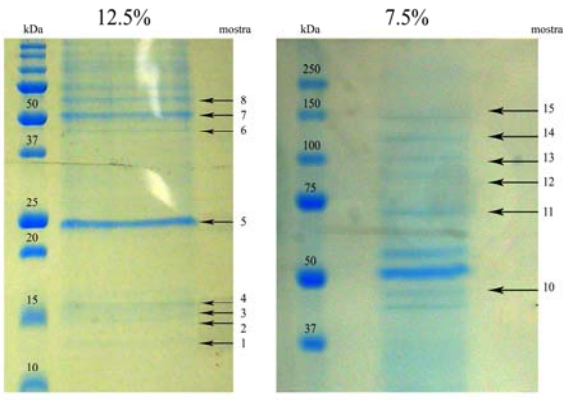

FIGURA 37 - Detecció de partners proteics mitjançant immunoprecipitació, separació per electroforesi i tinció de Comassie. Dos exemples de gels que es van obtenir, indicant les bandes retallades i el número al que correspon en la TAULA 10.

tinció per Comassie, van ser retallades i enviades al servei de Proteòmica del Parc Científic de Barcelona (FIGURA 37). Tot i anar amb la màxima cura possible, utilitzar recipients nous i netejar tot el material bé, no es va poder evitar la contaminació per queratina. Els resultats obtinguts per cada banda retallada es resumeixen a la TAULA 10.

Resultats proteòmica							
M	**Proteïna**	**Massa gel**	**Massa real**	**Cob**	**Sco**	**Loc**	**Comentari**
1	HIST2H4B protein	12,5	11,4	57%	178	N	
	Histone cluster 1, h4a	14	11,4	57%	174	N	
2	Histone cluster 1, h2ai	14	14	35%	286	N	
	Ribosomal protein P2	14	11,7	38%	179	C	
3	Histone H2A.2	15	14	34%	213	N	
	Histone H2B	15	14	35%	196	N	
	Ribosomal protein S16	15	16,5	14%	112	C	
4	Ribosomal protein S25	16	17	24%	196	C	
5	Chain L of the Fab Fragment of the monoclonal antibody	25	24	30%	174		Cadena lleugera dels anticossos de la immunoprecipitació
6	Beta-actin	45	42	26%	430	C	
	NF45 protein	45	45	10%	178	N	
	Creatine kinase-B	45	42,7	8%	159	C	
7	Heavy chain	50	51	17%	248		Cadena pesada dels anticossos de la immunoprecipitació
	Beta-tubulin	50	50,2	12%	184	C	
	2-phosphopyruvate-hydratase alpha-enolase	50	47	11%	179	C	
8	Ceramide kinase-like isoform a	60	60	23%	385	C/N	Control positiu de transfecció
	Heat shock protein 60kDa	60	61,2	11%	260	C*	
10	Heterogeneous nuclear ribonucleoprotein F	47	46	8%	104	N	
11	Heat shock protein	70	70	7%	161	C	
12	90kDa heat shock protein	85	83,6	11%	228	C	
	Heat shock protein HSP 90-alpha 2	85	98	7%	184	C	No coincideix amb la mida esperada
13	Nucleolin	100	76,4	6%	181	N	No coincideix amb la mida esperada
	Eukaryotic translation elongation factor 2	100	96,24	6%	170	C	
14	HnRNP U protein	120	90	11%	336	N	
	Matrin 3	120	96	9%	213	N	No coincideix amb la mida esperada
	Elongation factor Tu GTP binding domain containing 2	120	110	6%	107	N	
15	Clathrin heavy chain 1	150	193	6%	350	C	No coincideix amb la mida esperada
	Eukaryotic translation initiation factor 3, subunit 10 theta, 150/170kda	150	166	3%	128	C	
20	Hypothetical protein LOC126353	90	75	9%	114	D	No coincideix amb la mida esperada
21	Histone h1b	27	21,8	20%	279	N	
	Histone cluster 1, h1c	27	21,4	20%	279	N	
22	Myosin regulatory light chain	18	20	12%	94	C	
23	Growth regulated nuclear 68 protein	70	67,3	19%	411	N	
25	Sterol regulatory element binding protein 3	82	52	53%	319	C	
	LIMA1 protein	82	75	36%	294	C	
26	Protein phosphatase I alpha subunit (PPPIA)	37	36	20%	229	C/N	
	Glyceraldehyde-3-phosphate dehydrogenase	37	36	17%	208	C	
	F-actin capping protein alpha-1 subunit	37	33	15%	171	C	
	Ribosomal protein P0	37	34,4	14%	171	C	
27	Histone h1b	23	21,8	12%	141	N	

TAULA 10 - Resultat de l'anàlisi de possibles *partners* de CERKLa determinada per IP seguida de separació electroforètica i identificació per espectometria de masses (MALDI-TOF). S'indica el número de banda (M), el nom de la proteïna, el pes molecular en el qual es va trobar, així com la massa real que té. La mitjana dels *scores* va ser al voltant de 60, el punt de tall es va posar en un *score* de 100 (Sco). També s'indica el percentatge de cobertura (Cob) i la seva localització (Loc), N: si es nuclear, C: si es citoplasmàtica, D: si es desconeguda. Els colors agrupen les diferents funcions: vermell: implicació en transcripció i *splicing*, groc: biosíntesi de proteïnes (traducció), blau: activitat enzimàtiques diverses, principalment obtenció d'energia per glucòlisi, rosa: transport, verd: citoesquelet o relacionat amb aquest, gris: plegament de proteïnes, lila: funció desconeguda i blanc: controls positius. L'asterisc indica que localitza a mitocondri.

Capítol 2

Construcció i caracterització d'un model animal *knockout* per C*erkl*

Publicació 3

The use of alternative promoters turns a targeted knockout of the Retinitis Pigmentosa gene Cerkl into a knockdown with mild affectation of the retinal ganglion cell layer

PUBLICACIÓ 3

TÍTOL

"*The use of alternative promoters turns a targeted knockout of the Retinitis Pigmentosa gene Cerkl into a knockdown with mild affectation of the retinal ganglion cell layer*"

AUTORS (ANY)

Alejandro Garanto, Javier Vicente-Tejedor, Marina Riera, Roser Gonzàlez-Duarte, Román Blanco i Gemma Marfany

REFERÈNCIA

Investigative Ophtalmology and Visual Science (Sotmès a publicació)

RESUM

Mutacions en *CERKL* causen distròfies retinals hereditàries. Per esbrinar la funció de *CERKL* a la retina i les bases moleculars de la patogenicitat associada a les mutacions descrites en aquest gen vam plantejar-nos generar un model animal *knockout* total (KO) pel gen *Cerkl*, mitjançant deleció d'unes 2.4 kb de la regió genòmica on es troba l'exó 1 i el promotor proximal del gen. En aquest model es van dur a terme: 1) estudis d'expressió del gen delecionat per RT-PCRs i hibridacions *in situ*; 2) les caracteritzacions morfològiques i electroretinogràfiques; 3) anàlisis semiquantitatives de marcadors de tipus cel·lulars de la retina i finalment, 4) immunolocalitzacions de CERKL en retines murines WT i KO. Els ratolins *Cerkl -/-* són viables i fèrtils. L'estudi a nivell transcripcional va revelar una davallada del 65% (respecte al WT) en l'expressió de *Cerkl* a la retina. Estudis més en detall van mostrar que l'ús de promotors adjacents són els causants de la presència de transcrit en els animals *Cerkl -/-*. Els animals *knockdown* generats vàren mostrar una davallada significativa i no progressiva en els nivells de Brn3a (un marcador de cèl·lules ganglionars) així com diferències consistents i repetitives en els electroretinogrames, on els potencials oscil·latoris (OPs) estaven desplaçats, ambdues dades apunten a una possible alteració estructural o funcional de les cèl·lules ganglionars i/o amacrines. D'altra banda, estudis amb la proteïna GFAP, marcador d'estrès retinal, van mostrar que les retines dels ratolins *Cerkl -/-* presentaven nivells més elevats que els WT, i que aquests, a la vegada, es veien augmentats amb l'edat, tot i que la relació de GFAP KO-WT no es veia alterada. A més a més, per hibridació *in situ* es va observar una expressió de *Cerkl* residual en els fotoreceptors, i més dèbil en les cèl·lules ganglionars i en la capa nuclear interna (INL). Les proves immunohistoquímiques confirmaren aquests resultats, ja que CERKL es localitzava en el segment extern dels cons, les cèl·lules ganglionars i cèl·lules de la INL (en WT) i s'observava una clara disminució a nivell de proteïna en els KO. Així doncs, la deleció del promotor i l'exó 1 de *Cerkl* generava de fet un animal *knockdown* (en comptes del *knockout* esperat), i produïa transcrits amb diverses metionines en pauta a partir de promotors alternatius. En resum, l'animal transgènic construït presentava un fenotip retinal lleu, amb canvis consistents en els OPs produïts per la disfunció de les cèl·lules ganglionars i/o amacrines, acompanyats per una davallada dels nivells del

marcador de cèl·lules ganglionars, Brn3a, a les retines dels ratolins *Cerkl -/-*. A més, les retines dels animals KO presentaven un augment del marcador d'estrès retinal, GFAP, indicantiu d'algun tipus d'afectació que caldria estudiar més en detall. A nivell morfològic no es va detectar diferències en quant a l'estructura i gruix de les diverses capes de la retina.

NOTA: El material suplementari es troba disponible en el CD adjunt al final d'aquesta Tesi.

APORTACIÓ PERSONAL AL TREBALL

L'aportació a aquest treball ha estat: a) la generació del vector de direccionament gènic, el posterior escrutini de cèl·lules mare embrionàries per PCR i la realització dels *Southerns* per comprovar que el procés de recombinació homòloga per obtenir el model *knockout* de *Cerkl* (Figura 1); b) obtenció de l'individu KO fundador i el manteniment i augment de la colònia de ratolins; c) l'anàlisi d'expressió de *Cerkl* mitjançant RT-PCR en els diferents teixits, així com la comparativa amb ratolins WT (Figura 2); d) l'anàlisi de l'activitat dels diferents promotors de *Cerkl* identificats, en ratolins *knockout* (Figura 3); e) el comptatge de nuclis i cèl·lules ganglionars (Figura 4B); f) l'estudi comparatiu *Cerkl +/+* i *Cerkl -/-* mitjançant tincions hematoxilina-eosina en ratolins de diferents edats (Figura 4A); g) els estudis d'expressió mitjançant la tècnica d'hibridació *in situ* sobre retines WT i KO (Figura 5); h) lisats proteics i anàlisi de marcadors de retina (Figura 7) i i) immunodetecció de la proteïna GFAP en talls de retina (Figura S1).

The use of alternative promoters turns a targeted knockout of the Retinitis Pigmentosa gene *Cerkl* into a knockdown with mild affectation of the retinal ganglion cell layer

Alejandro Garanto[1,2,3], Javier Vicente-Tejedor[4], Marina Riera[1,2,3], Pedro de la Villa[4], Roser Gonzàlez-Duarte[1,2,3], Román Blanco[5]*, Gemma Marfany[1,2,3]**

From the [1]Departament de Genètica, Facultat de Biologia, [2]Institut de Biomedicina (IBUB), Universitat de Barcelona, Barcelona, Spain; [3]CIBERER, Instituto de Salud Carlos III, Barcelona, Spain; [4]Departamento de Fisiología, Facultad de Medicina, Universidad de Alcalá, Alcalá de Henares, Madrid, Spain; [5]Departamento de Cirugía, Facultad de Medicina, Universidad de Alcalá, Alcalá de Henares, Madrid, Spain

* These authors contributed equally to this work and all are corresponding authors

PURPOSE: To approach the retinal dystrophy *CERKL* gene function in a knockout mouse model generated by targeted deletion of the *Cerkl* first exon and proximal promoter.

METHODS: The gene targeting resulted in the cre-mediated excision of a 2.3 kb-genomic region encompassing the first *Cerkl* exon, upstream sequences including the proximal promoter and part of the first intron. The *Cerkl-/-* retinas were characterized at the morphological and electroretinographic level, and the effects of *Cerkl* deletion were assessed by RT-PCR, in situ hybridization, immunohistochemistry and protein expression analyses.

RESULTS: The *Cerkl-/-* mice were viable and fertile. Basal *Cerkl* expression was still attained in the retina by the use of adjacent alternative promoters. n situ hybridizations and immunohistochemistry showed that the remnant expression was moderate in the photoreceptors and weak in the ganglion and inner cell layers. Morphological analyses did not show any gross changes, even at 12 months of age. Analysis of several retinal proteins detected a significant decrease of the ganglion cell marker Brn3a, as well as an increase of GFAP. At the electroretinographic level, the oscillatory potentials amplitude waveforms were consistently reduced at all ages.

CONCLUSIONS: The targeted *Cerkl* deletion resulted in a knockdown more than a knockout model, retaining some *Cerkl* transcription (35%) from alternative promoters. The *Cerkl-/-* knockdown shows a mild retinal phenotype, with high levels of cellular stress indicators but no detectable morphological alterations. Remarkably, the altered oscillatory potentials in the ERGs indicate a functional alteration of ganglion and/or amacrine cells, consistent with the lower Brn3a levels.

Grant Information: This study was supported by grants BFU2006-04562 (Ministerio de Educación y Ciencia), SAF2009-08079 (Ministerio de Ciencia e Innovación), 2009SGR-1427 (Generalitat de Catalunya), CIBERER (U718), Fundaluce and ONCE to R.G.-D; SAF2007-66175 and SAF2010-21879 (Ministerio de Educación y Ciencia); RD07/0062/0008 (Instituto de Salud Carlos III) to P. de la V., FISS PI11/00533 (Instituto de Salud Carlos III) to R.B. and BFU2010-15656 (Ministerio de Educación y Ciencia) to G. M.

Corresponding authors:
Roser Gonzàlez-Duarte - Tel: +34934021034, rgonzalez@ub.edu; Roman Blanco – Tel: +34918854522, roman.blanco@uah.es; Gemma Marfany- Tel: +34 934021502, gmarfany@ub.edu

Mutations in the *CERKL* gene are associated to autosomal recessive retinal degeneration. First characterized as a retinitis pigmentosa (RP) causing gene[1-6], and later also considered to promote Cone-Rod Dystrophy (CRD)[7, 8], its classification as a RP or CRD gene is still under question. In fact, although the association of *CERKL* mutations with retinal pathology is clear, we are still at the dark concerning its physiological function and contribution to the progressive photoreceptor degeneration.

CERKL[6] was named after the amino acid identity conservation with CERK[9], the reported ceramide kinase enzyme, known to phosphorylate the sphingolipid ceramide to ceramide-1-phosphate[10], whose balance acts as

cellular rheostat between apoptosis versus survival signalling pathways[11-13]. Although CERKL has an intact diacylglycerol kinase domain[6, 14], no kinase activity neither on lipids nor proteins, could be assigned after intense studies from many groups[14-16]. Remarkably, overexpression of CERKL in cultured cells confers protection against apoptosis caused by oxidative stress injury, providing the first experimental clues on its role in retinal cell protection[16].

Very recently, an accurate assessment of the transcriptional products has unveiled that *CERKL* shows a high repertoire of transcript isoforms due to a combination of extensive alternative splicing plus the use of at least three additional promoters[17]. Adding to the complexity of CERKL functional analysis, the protein subcellular localization is extremely dynamic, shifting from the cytoplasm –where it mainly localizes associated to the endoplasmic reticulum and Golgi membranes– to the nucleus and seldomly, at the nucleoli[16].

CERKL shows a wide tissular expression although the tissues where the expression is highest are retina in humans and retina and liver in mouse[17]. In situ mRNA hybridization on mouse retinal sections showed strong *Cerkl* specific expression in the ganglion cell layer, moderate and interspersed staining in the inner nuclear layer and faint detection in the inner segment of photoreceptors, whereas immunohistochemistry with antibodies against specific epitopes strong Cerkl colocalization with cones, fainter in rods, and moderate at the inner nuclear and ganglion cell layers.

Our group first identified the R257X mutation in *CERKL*[6], which it is also the most frequent and accounts for more than half of the reported mutated alleles[17]. This mutation is located on exon 5, one of the alternatively spliced exons, and thus some but not all protein isoforms are compromised. To evaluate the phenotype of this mutation, a mouse model in which exon 5 had been excised was constructed[18]. The homozygous exon 5-deleted mice did not show any apparent phenotype in the retina.

In this context, to shed light on CERKL physiological role and the in vivo consequences of its mutations, we aimed to generate a full knockout *Cerkl*-/- mouse model by targeted deletion of the reported promoter and the first exon, according to the knowledge at that time. However, the use of alternative promoters driving residual transcription at the retina turned our knockout into a knockdown model retaining 30-35% of *Cerkl* mRNA isoforms, all of them lacking the first exon and initiating methionine. The homozygous exon1-deleted *Cerkl*-/- mice show higher level of retinal stress and diminished expression of the ganglion cell marker Brn3a but no gross morphological retinal alterations. Most interestingly, the electroretinographic changes observed in the oscillatory potential waveforms are in accordance with the reduced levels of *Cerkl* mRNA and Brn3a protein levels in the retina of the KO mice.

MATERIAL AND METHODS

Animal handling, tissue dissection and preparation of samples

Murine tissue samples were obtained from *Cerkl*+/+ and *Cerkl*-/- C57BL/6J background mice. All procedures were performed according to ARVO statement for the use of animals in ophthalmic and vision research, as well as the regulations of the Animal Care facilities at the University of Barcelona. Animals were euthanized with CO_2 followed by cervical dislocation. Specific tissues and organs were dissected and immediately frozen in liquid nitrogen.

Generation of the knockout *Cerkl*-/- mouse model

The strategy, the generation of targeting constructs, initial ES cell screening, breeding, house keeping and molecular genotyping of all the mice after the G0 generation as well as the crosses to obtain the knockout animal model has been performed in our lab. ES transfection, handling and the generation of chimeric embryos for the obtention of the founder mouse *Cerkl*+/- were performed by GenOway (Lyon, France). A diagram of the targeted locus is depicted in Figure 1A. In brief, the genomic sequences corresponding to the 5' and 3' flanking regions of the *Cerkl* promoter and exon 1 were amplified from 129/SvPas genomic DNA. These sequences were referred as long (region before exon 1) and short (intron 1) arms of homology (LA and SA). Several sub-cloning steps were performed to obtain the final targeting vector using pPCR-Script SK (+) vector (Stratagene). The first step consisted in the addition of a loxP site into LA. A synthetic exon 1 construct with new restriction sites (GeneArt) was used to clone the amplified SA fragment. A Neomycin gene flanked by two FRT and one loxP sites were also introduced into SA. Finally, both homology arms were cloned together and the negative selection cassete, DTA (Diphteria Toxin A), was added. The resulting targeting vector stretched 15384 bp, was fully validated by sequencing, and was electroporated into 129Sv ES cells. Positive selection was performed 24 hours

after electroporation by adding geneticin (200 µg/ml), and more than 1000 geneticin-resistant clones were isolated and amplified. After PCR screenings for recombination at the 5' and 3' flanking regions, a total of 14 clones were obtained. Those were characterized by Southern Blot using two different probes, 5' probe and 3' probe (Fig. 1B). Only 5 clones had recombined at the correct sites. ES positive cells were used for c57BL/6J blastocyst injections and led to the generation of 9 male chimeras displaying a chimerism rate ranging from 50 to 80%. Highly chimeric males (80% chimerism) were mated with C57BL/6J Flp-deleter females to allow the excision of the neomycin selection cassette. Pups were genotyped, and those that presented the excision of the cassette were breeded with wild-type C57BL/6J. The first generation of floxed mice was obtained by mating 2 heterozygous floxed males with C57BL/6J Cre-deleter females to allow the germline excission of the floxed region. Mice were breeded subsequently with C57BL/6J mice for a total of 5 generations and pups were genotyped by PCR from tail or ear samples.

Genotyping by Southern Blot and PCR

Genomic DNA from ES cells growing after double positive-negative selection was obtained by standard protocols, after a mild lysis, overnight proteinase K digestion and nucleic acid precipitation with ethanol. Ten micrograms of DNA were digested with informative restriction enzymes, separated by agarose electrophoresis and transferred to Nylon membranes. Standard protocols for pre-hybridization, hybridization with ^{32}P-labelled probes (whose position is indicated in Fig. 1A) were used. Autoradiographic exposition and image acquisition was performed with BioRad Molecular Imager FX Pro Plus (Bio-Rad, Hercules, CA). Three PCR genotyping primers (Fw, Rv1 and Rv2, sequences in Table 1) were used at the same time to allow genotyping of the WT and the floxed alleles in a single reaction (Fig. 1C). The PCR reaction included a first denaturing step of 120 s at 94 ºC, followed by 35 cycles of 94 ºC for 20 s, 59 ºC for 30 s, 72 ºC for 60 s.

TABLE 1 - Sequences of *Cerkl* primers used in the PCR reactions.

Name	Forward primer sequence (5' → 3')	Name	Reverse primer sequence (5' → 3')
Tissue expression			
*Gapdh*_F	TGAAGGTCGGAGTCAACGGATTTGG	*Gapdh*_R	CATGTAGGCCATGAGGTCCACCAC
mRT_For	CTGACTGTGGTGGTCACTGG	mRT_Rev	GAACCTCTGATGCAGCTTCC
NeuroD1_F	TCAATTTTCCCTTTGTGGAGAC		
UTR_F	TGTAGCCACACTTCCTTCCCA		
3a_F	GTTTTGCTGCGTGGCATCTTC		
3b_F	GACGCATCCAGCCCGAGC		
Riboprobes			
Rho_F	GCCCTTCTCCAACGTCACAG	Rho_R	GCAGCTTCTTGTGCTGTACGG
mRT_For	CTGACTGTGGTGGTCACTGG	mRT_Rev	GAACCTCTGATGCAGCTTCC
Genotyping			
F	ACACATTAGAAGCCCTGAAGGA	R1	TCTTTGTGCTGTAGCAGTGACC
		R2	TTGCTGTTTAATCCAGTTGTCCT

RNA extraction and RT-PCR

Twenty-five miligrams of each frozen mouse tissue were homogenized using a Polytron PT 1200 E homogenizer (Kinematica AG, Lucerne, Switzerland). For total RNA extraction, High Pure RNA Tissue Kit (Roche Diagnostics, Indianapolis, IN) was used, following the manufacturer's instructions. Total RNA was quantified using the nanoquant plate in an Infinite 200 microplate reader (Tecan, Männedorf, Switzerland).

The RT-PCR assay was carried out with the Transcriptor High Fidelity cDNA Synthesis Kit (Roche Diagnostics, Indianapolis, IN) performed following the manufacturer's protocol, using 200 ng of mouse total RNA. For tissue expression analysis all reaction mixtures (50 µl) contained 10 µM of each primer pair, 2 µM of dNTPs, 1.5 mM $MgCl_2$ and 1 U of Go*Taq* polymerase (Promega, Madison, WI). A pair of primers was used to amplify mouse *Gapdh* (Table 1) to compare and normalize the samples. Two-step PCR conditions were as follows: 120 s at 94 ºC and 30 cycles of 94 ºC for 20 s and 63 ºC for 120 s. Mouse *Cerkl* expression was detected with primers mRT_F and mRT_R (a first denaturing step of 120 s at 94 ºC, followed by 35 cycles of 94 ºC for 20 s, 60 ºC for 30 s, and a final extension step at 72 ºC for 20 s).

The characterization of the different alternative promoters was performed on cDNAs using a forward primer located in each promoter (NeuroD1_F, UTR_F, 3a_F and 3b_F) and the same reverse primer in exon 12 mRT_R (Table 1). Primers were designed to share the melting temperatures and optimized for the same amplification conditions: 120 s at 94 ºC followed by 40 cycles of 94 ºC for 20 s, 58 ºC for 30 s and 72 ºC for 90 s. Oligonucleotides sequences are listed in Table 1 and their localization is depicted in Supplementary Fig. 2.

In situ hybridization and immunohistochemistry on mouse retina cryosections

Eyecups from 2 to 12 months-old WT and KO mice were fixed in 4% paraformaldehyde (PFA) for 2 h at room temperature (RT), washed, and cryoprotected in sucrose at 4°C (succesive incubations at 20% for 30 min, 30% for 30 min and 40% sucrose for 12 h). Eyecups were then embedded in O.C.T (Tissue-Tek, Sakura Finetech, Torrance, CA) and sectioned at -17°C.

For in situ hybridization, 20 µm sections were recovered on poly-lysine covered slides, dried at RT (30 min), rinsed twice with phosphate-buffered saline (PBS) (10 min), treated with 2 µg/ml proteinase K for 15 min at 37ºC, washed twice

for 5 min with PBS, and postfixed with 4% PFA. The hybridization was performed as described previously[6] with some modifications: Two steps of acetylation with 0.1 M triethanolamine-HCl (pH 8.0) containing 0.25% acetic anhydride and 0.5% were performed (5 min each). The BM Purple AP Substrate (Roche Diagnostics, Indianapolis, IN) reagents were used. Sections were cover-slipped with Fluoprep (Biomérieux, France) and photographed using a Leica DFC Camera connected to a Leica DM IL optic microscope (Leica microsystems, Germany).

For immunohistochemistry, 14 µm sections were recovered on gelatin covered slides, dried for 1 h, washed in PBS (3 x 10 min), and blocked in blocking solution (PBS containing 2% Donkey Serum, 0.2% Triton X-100) at RT (60 min). Incubation with primary antibodies was performed overnight at RT in blocking solution. Sections were rinsed three times in PBS again, followed by incubation with the corresponding secondary antibodies conjugated to either Cy2 or Cy3 (Jackson ImmunoResearch Laboratories, Inc, West Grove, PA) (1:200) at RT (90 min) in blocking solution too. After 3 washes, sections were incubated with DAPI (Sigma-Aldrich, Sant Louis, MO) for 10 min and washed in PBS (3 x 10 min). Sections were cover-slipped with antifading reagent and photographed with a confocal microscope (LEICA TCS-SP5, Wetzlar, Germany). Primary antibodies and dilutions used were: 1:50 for Goat anti-Brn3a (Santa Cruz Biotechnology, Inc., Santa Cruz, CA); 1:200 for mouse anti-Rhodopsin (BIOTREND Chemikalien GmbH, Cologne, Germany); 1:200 for rabbit anti-PAX6 (Covance, Princeton, NJ) and rabbit anti-blue Opsin, 1:400 for rabbit anti-red/green opsin (Millipore, Billerica, MA). GFAP immunostaining was performed as described elsewhere[19] on P60 and P280 WT and KO retina cryosections.

Protein level analysis

Retinas from P60 and P365 WT and KO mice were homogenized in RIPA buffer (50 mM Tris pH 7.5, 1 mM EDTA, 150 mM NaCl, 0.25% Na-Deoxycolate, 1% NP40 plus protease inhibitors). Thirty micrograms of protein were loaded onto 12,5% acrylamide gels. Western blots were performed as described previously[16]. Primary antibodies were used at the following dilutions: 1:8000 mouse anti-α-tubulin (Sigma-Aldrich, Sant Louis, MO); 1:2500 mouse anti-Rhodopsin and 1:2000 mouse anti-GAPDH (Abcam, Cambridge, UK); 1:2000 mouse anti- α-PKC, 1:500 goat anti-RDS, 1:1000 goat anti-Brn3a (Santa Cruz Biotechnology, Inc., Santa Cruz, CA); 1:2000 rabbit anti-PAX6 (Covance, Princeton, NJ); 1:2500 mouse anti-GFAP, 1:2000 rabbit anti-green Opsin and anti-blue Opsin (Millipore, Billerica, MA). Alpha-Tubulin and GAPDH levels were used as normalization controls. Semi-quantification of the bands was carried out using the Quantity One Software (Bio-Rad, Hercules, CA). Statistical significance was analyzed by the Mann-Whitney and t-Student tests.

Electroretinography

Prior to ERG recording, mice were adapted to the dark overnight. Then, mice were anesthetized under dim red light by i.p. injecting a solution of ketamine (95 mg/kg) and xylazine (5 mg/kg) and maintained on a heated pad at 37 °C. Pupils were dilated by topical application of 1% tropicamide (Alcon, Spain) and flash-induced ERG responses were recorded from both eyes in response to light stimuli produced with a Ganzfeld stimulator. The recording protocol consisted of dark-adaptation for 20 min, after which scotopic ERG, maximum ERG, and dark-adapted oscillatory potentials (OPs) were recorded. After the dark-adapted ERGs, the eyes were light-adapted for 10 min, and the photopic ERG and 30-Hz flicker ERG were recorded. The outcome measures were the response amplitudes and implicit time of each ERG component. The ERG complied with International Society for Clinical Electrophysiology of Vision (ISCEV) standards[20]. Kruskal-Wallis and Mann-Whitney *U* tests were used to estimate the level of significance for the difference in the ERG parameters among the study groups as appropriate. The ERG signals were amplified and band filtered between 0.3 and 1000 Hz with a Grass amplifier (CP511 AC amplifier, Grass Instruments, Quincy, MA, USA). Electrical signals were digitized at 10 kHz with a Power Laboratory data acquisition board (ADI Instruments, CA, USA). Bipolar recordings were obtained using an Ag:AgCl mouse electrode fixed on a corneal lens (Burian-Allen electrode, Hansen Ophthalmic Lab, IA, USA), a reference electrode located in the mouth, and with a ground electrode located on the tail. The electrode was mounted on a coarse micromanipulator for easy positioning over the mouse eye. Impedance of active and reference electrodes were less than 20 kΩ.

RESULTS

Cerkl deletion of exon 1 and upstream sequences

The gene targeting strategy resulted in the cre-mediated excision of a genomic region of 2.334 kb encompassing the first *Cerkl* exon and the beginning of the first intron, plus 1.2 kb of upstream sequences that stretched the reported promoter (Fig. 1A). Our strategy included a first step of FLP-mediated excision of the neo^R selection gene in the 129/Sv ES cultured cells. All the homologous recombination events performed in the ES cells were assessed by Southern blot analysis (Fig. 1B) using informative restriction enzyme sites and probes specific for the 5' and 3' events, depicted in Fig. 1A. Positive clones for the two recombinant events were further confirmed by specific PCR and sequencing, and subsequently used to colonize C57BL/6 blastocysts. Two chimaeric males were obtained and bred to obtain the first heterozygous animals, which after successive matings produced the homozygous null *Cerkl-/-* offspring at the expected mendelian ratio (1:4). Genotyping of tail or ear samples from pups was performed by a single PCR assay (primers indicated in Fig. 1A and Table 1) that allowed the

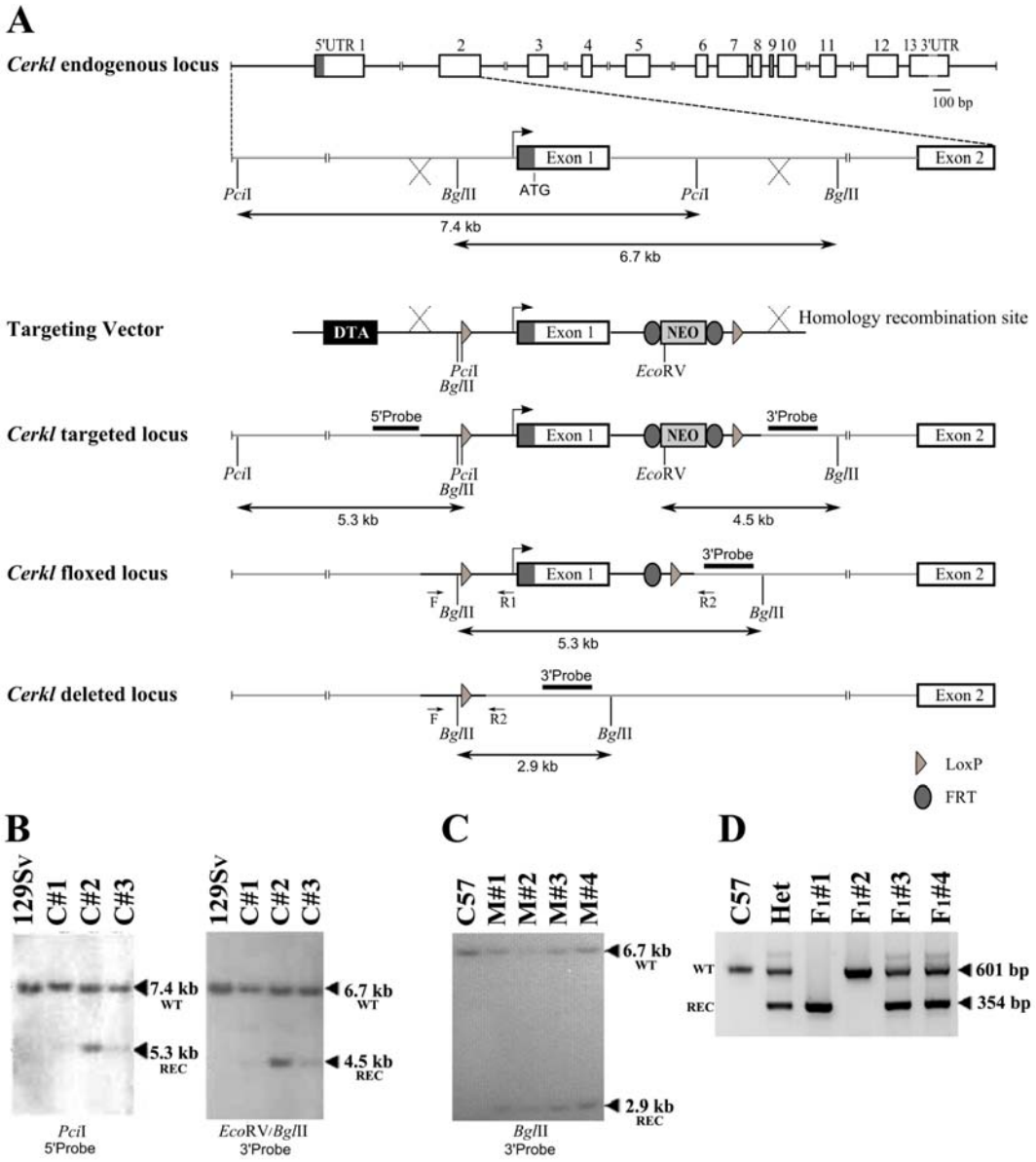

FIGURE 1 - Targeting of the *Cerkl* locus. (**A**) Schematic representation of the *Cerkl* locus (drawn to scale), the region of interest encompassing the proximal promoter and first exon, the targeting vector and the targeted, floxed and deleted loci. *Cerkl* exons, Southern blot probes, restriction sites, oligonucleotides for genotyping are depicted. The targeting vector contained the diphteria toxin A (DTA) and neomycin resistance (NEO) genes, the latter flanked by two direct FRT target sites (dark grey ellipses). Two direct loxP sites (light grey triangles) are at the boundaries of the proximal promoter, exon 1 and the NEO cassette. Mice carrying the *Cerkl*^{neo} allele were crossed to a transgenic CMV-Flp recombinase strain to generate the *Cerkl*^{flox} heterozygotes, which were subsequently crossed with a CMV-Cre strain to obtain the *Cerkl-/-* chromosome. (**B**) Southern blot analysis of targeted ES cells. External probes at 5' and 3' were used to verify homologous recombination. Digestion with *Pci*I hybridized with the 5' probe showed the wild-type (7.4 kb) and recombinant (5.3 kb) alleles, whereas digestion with *Eco*RV and *Bgl*II with the 3' probe produced 6.7 kb (wt) and 4.5 kb (recombinant) bands in clones C#1,2,3. (**C**) Southern blot of the *Cerkl+/-* mice after the *Bgl*II digestion. The bands observed correspond to wt (6.7 kb) and KO recombinant (2.9) alleles of 4 different heterozygous mice (M#1,2,3,5). (**D**) PCR analysis of the first generation mice obtained after breeding two *Cerkl+/-*. Primers F, R1 and R2 were used in the same PCR reaction. The wt allele produced a band of 601 bp (amplified by F and R1), while the recombinant knockout allele generated a 354 bp band (amplified by F and R2). PCR conditions did not allow the amplification of the band corresponding to the wt allele using the F and R2 primers (2,6 kb).

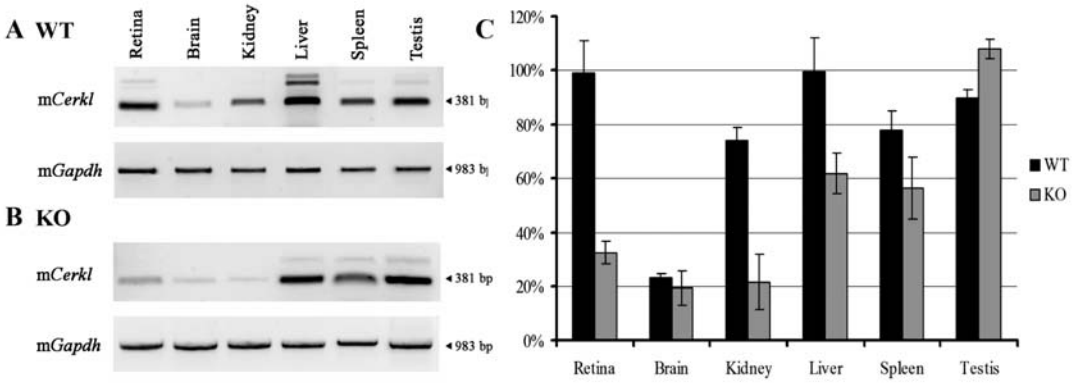

FIGURE 2 - Semi-quantitative expression analysis of *Cerkl* in wild-type and knockout mice. RT-PCR expression in several tissues of *Cerkl*+/+ (A) and *Cerkl*-/- (B) mice, using primers mRT_F and mRT_R, located in exons 9 and 12, respectively, and contained in all isoforms. Primer sequences are provided in Table 1. The amplicon size is indicated for each case. (C) Semi-quantitative analysis of *Cerkl* expression in *Cerkl*+/+ and *Cerkl*-/- mice. Maximum wild-type *Cerkl* levels were arbitrarily set as 100% (liver). At least three independent replicates were performed. *Gapdh* expression was used for normalization. Significant decreased expression is observed in all KO tissues except brain.

simultaneous amplification of the wild-type and floxed knockout alleles (Fig. 1C) (see Material and methods for details).

Assessement of *Cerkl* expression in knockout animals

To assess the abolishment of *Cerkl* expression in the knockout mice, we performed an RT-PCR assay using primers located at the 3' end of the cDNA, a region common to all the *Cerkl* isoforms reported so far. Contrary to our expectations, the deletion of reported the promoter did not completely abrogate *Cerkl* expression, as a faint band could be observed in retina. These surprising results prompted us to assess the levels of expression in several tissues of the knockout versus the wild-type counterparts (Fig. 2A and B).

A semi-quantitative analysis of these results revealed a 65% decrease of *Cerkl* levels in the KO retinas supporting a knockdown model more than a complete knockout (Fig. 2C). Notably, this decrease in *Cerkl* mRNA levels was not homogenous for all tissues, indicating that other promoters, showing tissue specificity, contribute to the final *Cerkl* levels, which is in agreement with recent results showing that at least 3 additional promoters drive *Cerkl* expression in mouse and human[17].

Moreover, a multiple band pattern was observed in some tissues, such as retina, liver, spleen and testis. These bands were excised and sequenced, and correspond to alternatively spliced transcript isoforms, also in agreement with previous data[17].

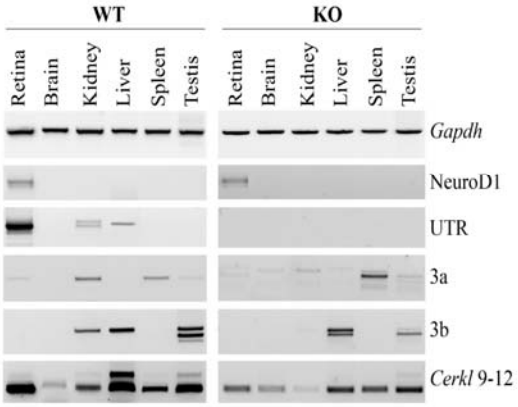

FIGURE 3 - Remnant *Cerkl* expression in the KO mouse is attained by the use of tissue-specific alternate promoters. RT-PCRs were performed on wild-type and KO murine samples to determine the activity of alternate *Cerkl* promoters in different tissues. Different specific forward primers located at each of the transcription start sites previously identified (*NeuroD1* UTR, *Cerkl* UTR, 3a and 3b) were used in combination with the same reverse oligonucleotide in exon 12. Overall *Cerkl* expression was assessed by amplification of a common region to all isoforms (*Cerkl* 9-12). *Gapdh* was used for normalization Primer sequences are provided in Table 1.

Once the different *Cerkl* promoters had been identified, we aimed to assess the contribution of each one to the levels of *Cerkl* expression in the different tissues of the knockout mice compared to the wild-type controls. Indeed, as expected by the design of the targeting and the genotyping of the KO mice, no transcripts from the reported *Cerkl* promoter were observed in any tissue (Fig. 3, UTR).

Concerning the expression of *Cerkl* in the KO retina, residual *Cerkl* transcription from the NeuroD1 and internal 3a promoters can be detected, at similar levels than the WT retinas (Fig. 3), accounting for the 30-35% of the *Cerkl* expression products shown in Fig. 2 and last lane (*Cerkl*) in this figure. The major isoforms in *Cerkl-/-* retinas are two transcripts starting at NeuroD1 and one from the internal 3a promoter, indicated with a symbol (#) in the Supplementary Fig. 2.

Although no compensatory transcriptional activation from the alternative promoters in the KO tissues was detected, moderate transcriptional differences were observed, such as decreased expression in kidney and testis from 3a and 3b, increased expression in spleen, and specific isoform patterns in liver, testis and spleen (Fig. 3).

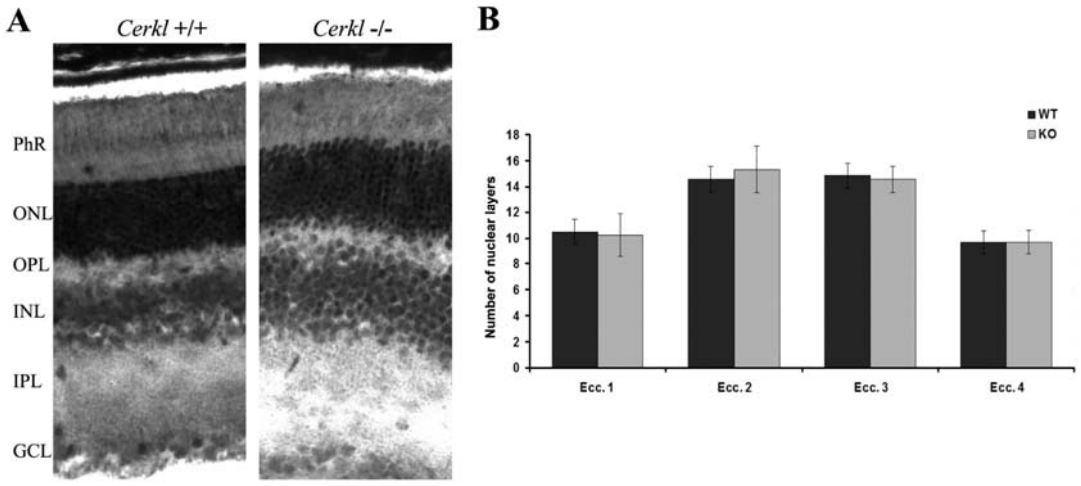

FIGURE 4 - Morphological analysis of the WT and KO mouse retinas. (A) Low magnification of semithin cryosections of retinas stained with hematoxilin-eosin viewed at the light microscope. (**B**) Nuclei counting performed in at least three independent replicates of each type at 4 different eccentricities (Ecc), after DAPI-staining viewed in the fluorescent microscope. Eccentricities 1 and 4 correspond to peripheral retina, whereas 2 and 3 are areas of central retina. PhR- photoreceptor cell layer; ONL- outer nuclear layer; OPL- outer plexiform layer; INL- inner nuclear layer; IPL- inner plexiform layer; GCL- ganglion cell layer.

Morphological analysis of the KO retina

Retinal sections of KO mouse obtained at 2, 4 and 12 months stained with hematoxilin/eosin did not show any gross morphological differences neither in the cell layer organization, nuclei density or photoreceptor outer segment length, when compared to WT animals of the same age (Fig. 4A). Nuclear counts after staining with DAPI visualized in the confocal microscopy did not reveal any significant difference in the density and distribution through all the layers at four different retina eccentricities (Fig. 4B).

The localization of *Cerkl* expression products was then addressed to assess possible differences in intensity/distribution throughout the retinal cell layers. To this aim, in situ mRNA hybridization was performed with a riboprobe against the shared RNA region of all isoforms (stretching exons 8 to 12), using *Rhodopsin* antisense and *Cerkl* sense riboprobes as positive and negative controls, respectively. In agreement with previous findings, wild-type endogenous *Cerkl* is mainly detected in the ganglion cell layer (GCL), and moderate expression at the inner segment of photoreceptors (PhR) and the inner nuclear cell layer (INL) (Fig. 5). As expected, *Cerkl* mRNA levels is decreased in the retina of the KO mouse, as shown by a considerable decrease in hybridization intensity compared to the WT controls, treated and stained under the same conditions and time (Fig. 5). Notably, the more prominent decrease is observed in the GCL, followed by the INL and much less in the PhR (black arrowheads), indicating that there is not an homogeneous decrease in *Cerkl* expression.

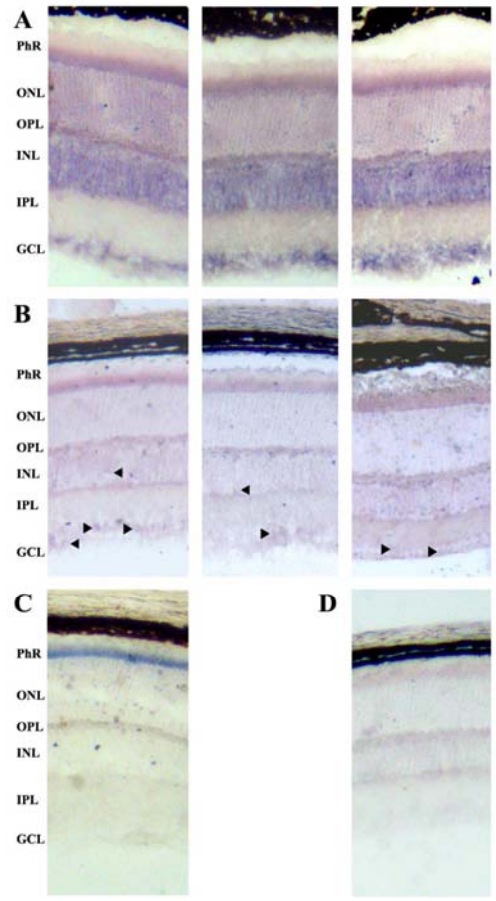

FIGURE 5 - *Cerkl in situ* Hybridization on WT and KO mouse retinas. (A) Three independent replicates of WT retinas with the antisense *Cerkl* probe, staining the GCL, INL and more moderately, the inner photoreceptor segment. **(B)** Three independent replicates of KO retinas with the antisense *Cerkl* probe. Note the much fainter staining in the GCL, INL and the inner photoreceptor segment. Black arrowheads point positive staining. **(C)** Positive control with the antisense Rhodopsin probe, which strongly labels the inner photoreceptor segment. **(D)** Negative control with the sense *Cerkl* probe. A, B and D *in situs* have been allowed to develop for exactly the same time. PhR- Photoreceptor cell layer; ONL- outer nuclear layer; OPL- outer plexiform layer; INL- inner nuclear layer; IPL- Inner plexiform layer; GCL- ganglion cell layer.

Immunolocalization of CERKL

Immunodetection of adult mouse retinas with an in-house anti-CERKL polyclonal antibody (raised against a peptide encoded in mouse *Cerkl* exon 2) indicated that CERKL localized in the Ganglion Cell Layer (GCL), Inner Nuclear Layer (INL), and Photoreceptor layer (PhR) (Fig. 6). In photoreceptors and inner nuclear layer cells, CERKL was shown to be exclusively located in the cytoplasm and nuclear staining was not been observed in these cell types, as it has been described before[21]. A fainter staining in the GCL, INL and the inner photoreceptor segment with our CERKL polyclonal antibody was observed in the KO retinas. Immunohistochemical stainings using antibodies against Brn3a and Calbindin, specific retinal cell markers, showed cytoplasmic colocalization of CERKL with a population of ganglion and amacrine cells but no apparent change in the number and/or distribution of stained cells (Fig. 6). A similar analysis with the retinal cell marker PAX6 did not show any expression pattern alteration either (Supplementary Fig. 3).

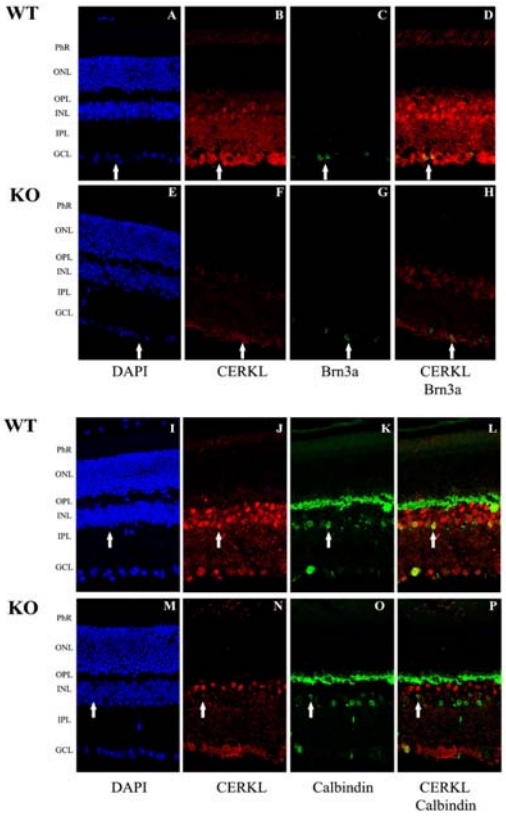

FIGURE 6 - CERKL, Brn3a and Calbindin immunohistochemistry of WT and KO retinas. Fluorescent immunodetection of CERKL, Brn3a (ganglion cell layer marker), Calbindin (amacrine cell marker) and DAPI (nuclear staining) on 14-μm sections from C57BL/6J and *Cerkl* -/- retinas. Photographs were taken in the central retina for comparison. A-D and I-L) WT retinas. E-H and M-P) KO retinas. The CERKL polyclonal antibody (B,F,J and N) reveals a fainter staining in the GCL, INL and the inner photoreceptor segment in the KO vs the WT retinas. The ganglion cell marker Brn3a (C and G) and amacrine cell marker Calbindin (K and O) were used. White arrows indicate colocalization of Brn3a and CERKL in the GCL layer (D and H), and Calbindin and CERKL (L and P) in amacrine cells of INL and GCL. Abbreviations: INL, inner nuclear layer; ONL, outer nuclear layer; GCL, ganglion cell layer.

Cerkl-/- mouse retinas did not show any sign of rod and cone degeneration after rhodopsin/opsin immunostaining, even at 12 months of age (data not shown). Besides, the photoreceptor outer segment length (average ~22 μm), diameter and density were preserved, consistent with neither photoreceptor degeneration nor apoptosis (data not shown).

Given that no clear signals of apoptosis were detected in the *Cerkl-/-* retinas, and that previous results from our group showed that over-expression of CERKL protected cells against oxidative stress injuries[16], we searched for other signals of retinal stress. Glial fibrillary acid protein (GFAP) expression is usually restricted to Müller cell endfeet in the inner limiter membrane[19], but its expression is increased and may extend to other retinal cell layers upon aging and retinal stress. Immunohistochemistry analysis on P60 and P280 WT and KO retinas was performed. Differences in GFAP distribution and expression between WT and KO retinas were very slight, although the expected increase of GFAP with age was clearly detectable in both WT and KO retinas (Supplementary Fig. 1).

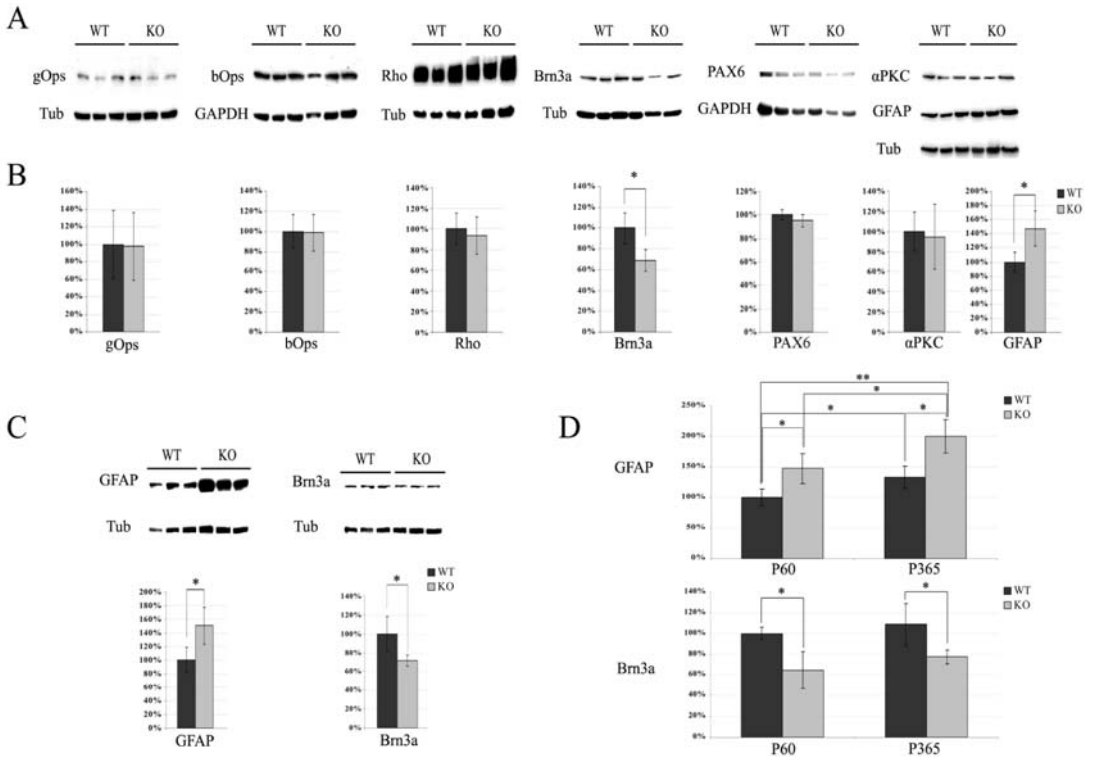

FIGURE 7 – Semi-quantification by Western blot of retinal proteins in WT and KO mice. (A) Thirty micrograms of P60 protein lysates of WT and KO mice retinas were immunodetected with antibodies against the green and blue opsins, rhodopsin, GFAP, Brn3a, PAX6 and α-PKC proteins. Tubulin and GAPDH were used as controls for normalization. **(B)** Semi-quantified proteins are depicted in the histograms. Only GFAP and Brn3a showed significant differences (* $p<0.05$ t-Student). **(C)** Immunodetection and quantification of GFAP and Brn3a markers in lysates of P365 WT and KO mice retinas. **(D)** Expression of GFAP at P60 (100%) and P365 between WT and KO. GFAP levels were increased in aged animals, although the ratio WT/KO appears to be maintained (45-50%) (* $p<0.05$; ** $p<0,01$ t-Student). No differences were observed in Brn3a expression between P60 and P365 animals (data not shown).

Retinal protein markers expression in KO retinas

To assess the effects of the diminished *Cerkl* expression on several retinal markers, indicative of structural/functional alterations in retinal cell layers, we performed a semi-quantitative immunodetection on Western blots in P60 WT and KO retinal lysates. Markers of the functional status of: cones and rods (green opsin, blue opsin and rhodopsin), ganglion (Brn3a), amacrine/ganglion (PAX6) and bipolar (α-PKC) cells, and retinal

stress (GFAP) were immunodetected and analyzed (Fig. 7A). Notably, a statistically significant decrease of Brn3a, but not of PAX6 was detected (Fig. 7B), which indicates a perturbed structural/functional status of the ganglion cells, rather than amacrine cells. Moreover, the GFAP expression is clearly increased, revealing higher levels of retinal stress in the *Cerkl-/-* animals. These results prompted us to analyze the evolution of these altered expression levels with age (Fig. 7C). In one-year (P365) aged animals, the decrease of Brn3a expression remains consistent and at comparable levels than those of P60 mice. Concerning GFAP, relative differences between WT and KO retinas are also maintained at the same level (around 50% increase), and indeed, GFAP levels increase proportionally in the two groups due to aging (Fig. 7D).

The fact that no differences were observed in the other markers analyzed highlight that the effect on Brn3a and GFAP expression is specific and reflect the altered status of the KO retinas.

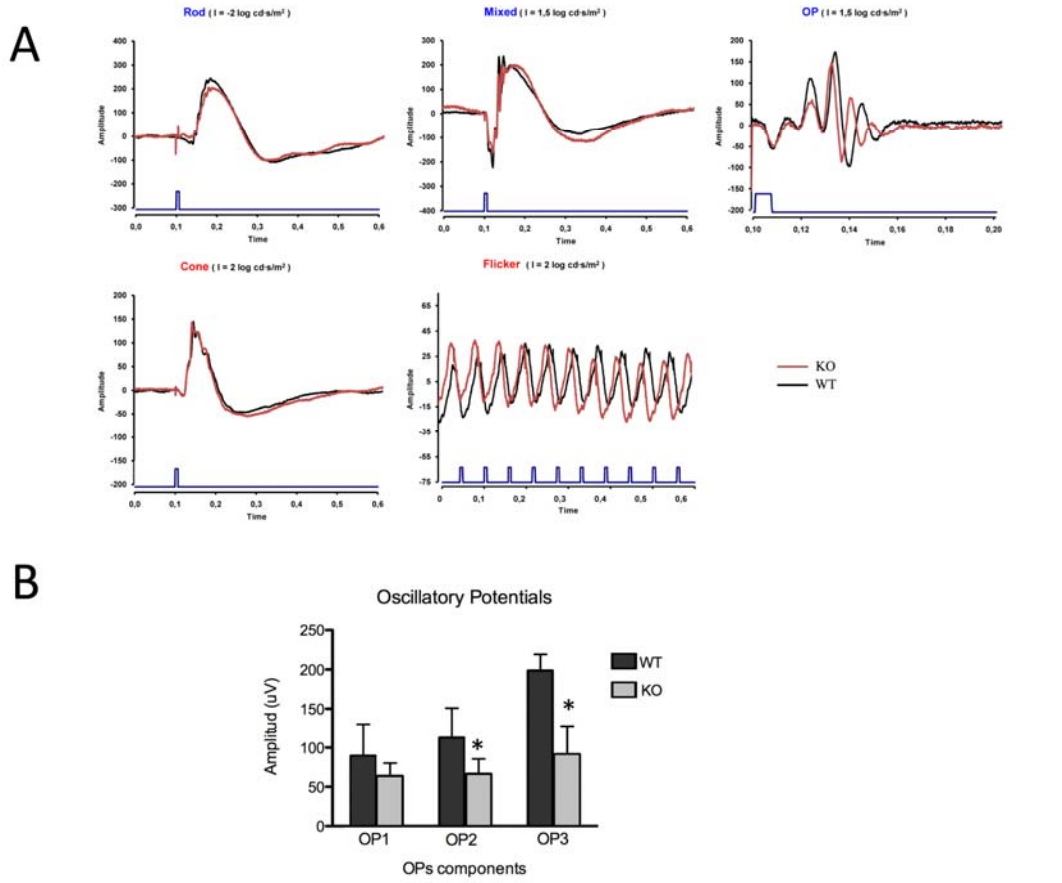

FIGURE 8 - Electroretinographic responses from control C57BL/6J (black) and *Cerkl-/-* mice (red) at P120. (A) Superimposed response waveforms of various ERG components from one control (black traces) and one *Cerkl-/-* mouse (red traces): Rod responses to light flashes of -2.09 log cd·s·m^{-2} and mixed responses (rod and cone) to light flashes of 1.57 log cd·s·m^{-2} were recorded under dark adaptation. Cone responses (photopic ERG, ocillatory potentials and 30 Hz) Flicker) were recorded under light adaptation to light flashes of 1.57 log cd·s·m^{-2}. Horizontal calibration: 100 ms; vertical calibration: 50 uV. **(B)** Histogram representation of the power spectral density (PSD) (mean and SD) of Oscillatory Potentials measured from a group of C57BL/6J (n=8), *Cerkl* +/+ (n=8), and *Cerkl* -/- animals (n=8) (* P <0.05, Mann-Whitney test).

Electroretinographic characterization of the KO retinas

The ERG experiments were performed in 10 C57BL/6J and 12 *Cerkl-/-* mice, and were measured four times at 2–3 months of age and until the animals reached 12 months at 3 month intervals. The ERG data showed that there were not statistically significant differences between the *Cerkl-/-* and normal control mice in neither

scotopic ERG response amplitudes and implicit times, maximum ERG a- and b-wave implicit time, nor in implicit times for photopic single-flash a-wave and 30-Hz flicker ERG. These ERG components did not change significantly between the 3 and 12-month examination point. However, we did observe a significant decrease in the amplitudes of oscillatory potentials in the *Cerkl-/-* mice (Fig. 8). The OPs are four wavelets in the ERG that are present on the rising phase of the b-wave. Most OP components (OP2–OP4) were significantly reduced in amplitude and increased in implicit time in the KO compared with WT animals (P <0.05, Mann-Whitney test). These changes were first seen at P60 and remained consistent at P180 and P360, but showed no progression (data not shown). OPs have been shown to arise in the inner plexiform layer but to have different retinal depth profiles for individual peaks. The OP/a and OP/b ratios in the KO animals did differ significantly compared to amplitudes measured in age-matched C57BL/6J mice (P <0.05, Mann-Whitney test). Together with the same b/a ratio values in both strains, it could be suggested that the neuronal circuitries of the inner retina are somehow affected in this *Cerkl-/-*.

DISCUSSION

Mutations in human *CERKL* cause progressive retinal degeneration leading to CRD or RP[1-8]. Despite its close structural similarity with CERK, all the previous attempts to characterize its putative lipid kinase enzymatic activity have failed so far[14-16]. Taking into consideration: 1) the high transcriptional complexity of *CERKL*, probably leading to a large range of protein isoforms displaying different domains; 2) its wide retinal expression pattern, not restricted to photoreceptors; and 3) its highly dynamic nuclear-cytoplasmic localization, all support that the dissection of the CERKL functional roles and contribution to the retinal pathology is going to be a daunting task.

Following the conventional approach for functional analysis of human genes associated to hereditary diseases, we aimed to generate a knockout mouse model, *Cerkl-/-*. A previous model attempted to reproduce the most common mutation allele (R257X) by deleting exon 5. However, no retinal phenotype or alteration in the ceramide/ceramide-1-P levels could be shown[18]. With the knowledge at that time, the lack of ocular phenotype could have been explained by the fact that this exon is alternatively spliced, therefore other transcript isoforms could still be produced and perform some of the *Cerkl* roles[17]. In this context, we attempted the generation of a total knockout model with a more severe phenotype, and designed the loxP/cre-based deletion of the *Cerkl* first reported exon plus the 1.6 kb upstream region encompassing the transcriptional initiation site and proximal promoter.

Unfortunately, although the targeting was successful, residual *Cerkl* expression (around 30-35%) was still detectable in the KO mouse, driven by previously unreported alternative promoters, among them that of *NeuroD1* gene. The *NeuroD1* promoter is located upstream the *Cerkl* gene, transcribes the same DNA strand, is highly active in the Central Nervous System (CNS) and accounts for most of the remaining *Cerkl* expression in the KO mice retina. Detailed analysis of this transcriptional product revealed that it starts at the first exon of the *NeuroD1* gene (which corresponds exclusively of 5'UTR sequences), fuses to a cryptic small 173-bp exon mapping in the intergenic region between the two genes, which is then directly fused to *Cerkl* exon 2. The cryptic exon contains several methionines, the one in frame being a candidate to initiate protein synthesis thus suggesting that some CERKL protein could be also produced in the KO retina. Indeed, the unexpected *Cerkl* isoforms arising from this promoter could explain the mild retinal phenotype, befitting more to a knockdown than to a full knockout model.

The transcripts starting from the internal Transcription Initiation Site (TIS) 3a also bear presumptive initiating in-frame methionines. In this respect, evidences that internal CERKL initiating methionines could be recognized in vivo in other isoforms have already been gathered in human[17], adding to the panoply of proteins that could be produced from the *Cerkl* gene. The alternative *Cerkl* promoters here identified show tissue-specificity[17]. In the KO mice the transcriptional activity of these

additional promoters does not appear to be increased to compensate for the deficiency in *Cerkl* production. However, some differences in the expression could be detected in liver, testis and spleen, which could be explained by deletion or changes in the relative position of regulatory sequences in the floxed allele, where up to 1.6 kb of genomic 5' sequences have been removed.

In our electroretinographic studies, ERG amplitudes and latencies of scotopic a-waves and b-waves, and photopic b-waves in the *Cerkl-/-* mice were not decreased significantly when compared to amplitudes measured in age-matched C57BL/6J mice. These results lead to the assumption that the basic pathways of phototransduction and signal transmission in the outer retina seem to be unaffected in this *Cerkl-/-* model. However, the observed differences in the oscillatory potentials (OPs) suggest that there are functional alterations in the inner plexiform layer, even when the morphology is preserved. The OPs are high frequency (90–160 Hz), low amplitude wavelets found on the rising edge of the electroretinogram (ERG) b-wave. Depth recordings localise OP oscillators to the inner retina in particular the inner plexiform layer[22]. There is evidence that multiple cell types constitute the neural substrates of OPs. Inhibition of metabotropic glutamate receptors (using 2-amino-4-phosphonobutyric acid, APB), which are specific to the ON-pathways, cause a large reduction of the OPs in a number of vertebrate species[23]. Application of tetrodotoxin (TTX) can also block spiking in amacrine cells and affects dark-adapted OPs in rats[24]. Thus, OPs could be generated by amacrine cells and/or ganglion cells that receive signals from ON bipolar cells. In our study, late OP components were significantly reduced in amplitude and increased in implicit time in the KO compared to the WT mice. In this sense, there is evidence that early and late components of OPs can be modulated independently. Of note, patients with congenital stationary night blindness, who have defective ON-pathways, show losses of the first two oscillations on the rising edge of the photopic b-wave[25]. Also, the OPs at higher frequency have been found to be reduced following ganglion cell injury produced by experimental glaucoma[26]. Moreover, the early and late OPs appeared to be more sensitive to inhibition of retina ON (APB) and OFF pathways (PDA), respectively[27]. *Dong et al.* have shown that TTX application in rabbit retina selectively impairs OPs that occur later[28]. Thus, there is evidence that OPs represent at least two distinct groups OPs could be generated by amacrine cells and/or ganglion cells. Further work will be required to determine whether the affected OP components in the *Cerkl-/-* animals correspond to specific subsets of amacrine and/or ganglion cells. However, the results of diminished Brn3a together with unaltered Calbindin and PAX6 expression support the alteration of the ganglion over the amacrine cells.

Indeed, the *Cerkl-/-* retinas show low levels of *Cerkl* mRNA and protein, but of note, this decrease is more apparent in the GCL, in clear contrast to the highest expression of this gene in this layer in WT animals. That the GCL appears to be the most affected target in *Cerkl-/-* mice is further supported on the grounds of the reduced OP waveforms, decreased expression of Brn3a and unperturbed levels of PAX6. Besides, we cannot rule out that other cells might be functionally disturbed, as reflected by the increased expression of the retinal stress marker GFAP.

To sum up, the analysis of the *Cerkl-/-* retinal phenotype showed much less severe consequences in mouse than those associated with the *CERKL* mutations causing human retinal dystrophies. According to our findings, KO mice did not show any progressive histological alterations even after 12 months, as assessed by the studies of histological sections (performed at 2, 4, 6 and 12 months of age). Although many of the isoforms and some protein domains are missing, additional initiating methionines could produce enough CERKL protein and compensate for the predicted diminished expression and functional deficits. Hitherto, human CERKL mutations have been associated with both, conventional RP and CRD, although none of the two CERKL models showed photoreceptor degeneration. In this context, we cannot rule out that the different phenotypes observed in mice and human could partly be explained by the different patterns of expression in the retina. CERKL immunohistochemistry in mouse showed high expression in cones and ganglion

cells versus moderate expression in rods and other retinal INL cell types[17, 21] (and also in the results presented in this work). No data on human CERKL expression in the retina has been reported so far. Other explanations for this mild ocular phenotype in our *Cerkl-/-* mouse as well as the reported absence of affectation in the homozygous exon 5-deleted *Cerkl* model (where long-term phenotypic characterization is missing) may rely on *Cerkl* being partially redundant in mouse so that other genes compensate for its deletion or changes on the expression pattern at the retinal level, so that the phenotype caused by mutations in mouse does not have to abide to the severity observed in humans. Indeed, the same type of arguments have also been proposed for knockout models of other RD-causative genes with no phenotypic visual alterations, such as the *Rdh12*, *Gcap2* and *Gcap1/2* KO mice[29-32]. On the bright side, the model shows consistent perturbance of the ganglion cell layer, as reflected by the weaker expression of *Cerkl,* correlating with lower levels of Brn3a –a POU-homeobox transcription factor (expressed in ganglion cells) that regulates genes involved in synaptogenesis and axonogenesis[33, 34]–, which adds to the observed oscillatory potential waveforms changes. These results together with the detection of increased retinal stress associated to the reduction of *Cerkl* expression further underscores the role of this retinal dystrophy causing-gene in the homeostasis and preservation of retinal neurons.

Acknowledgments

We would like to acknowledge the technical contribution of Laura Ramírez. A.G and M.R were in receipt of the fellowships FPI BES-2007-15414 and FPU AP2007-00805.

References

1. Ali M, Ramprasad VL, Soumittra N, et al. A missense mutation in the nuclear localization signal sequence of CERKL (p.R106S) causes autosomal recessive retinal degeneration. *Mol Vis* 2008;14:1960-1964.
2. Auslender N, Sharon D, Abbasi AH, Garzozi HJ, Banin E, Ben-Yosef T. A common founder mutation of CERKL underlies autosomal recessive retinal degeneration with early macular involvement among Yemenite Jews. *Invest Ophthalmol Vis Sci* 2007;48:5431-5438.
3. Avila-Fernandez A, Riveiro-Alvarez R, Vallespin E, et al. CERKL mutations and associated phenotypes in seven Spanish families with autosomal recessive retinitis pigmentosa. *Invest Ophthalmol Vis Sci* 2008;49:2709-2713.
4. Pomares E, Marfany G, Brion MJ, Carracedo A, Gonzalez-Duarte R. Novel high-throughput SNP genotyping cosegregation analysis for genetic diagnosis of autosomal recessive retinitis pigmentosa and Leber congenital amaurosis. *Hum Mutat* 2007;28:511-516.
5. Tang Z, Wang Z, Wang Z, Ke T, Wang QK, Liu M. Novel compound heterozygous mutations in CERKL cause autosomal recessive retinitis pigmentosa in a nonconsanguineous Chinese family. *Arch Ophthalmol* 2009;127:1077-1078.
6. Tuson M, Marfany G, Gonzalez-Duarte R. Mutation of CERKL, a novel human ceramide kinase gene, causes autosomal recessive retinitis pigmentosa (RP26). *Am J Hum Genet* 2004;74:128-138.
7. Aleman TS, Soumittra N, Cideciyan AV, et al. CERKL mutations cause an autosomal recessive cone-rod dystrophy with inner retinopathy. *Invest Ophthalmol Vis Sci* 2009;50:5944-5954.
8. Littink KW, Koenekoop RK, van den Born LI, et al. Homozygosity mapping in patients with cone-rod dystrophy: novel mutations and clinical characterizations. *Invest Ophthalmol Vis Sci* 2010;51:5943-5951.
9. Sugiura M, Kono K, Liu H, et al. Ceramide kinase, a novel lipid kinase. Molecular cloning and functional characterization. *J Biol Chem* 2002;277:23294-23300.
10. Bajjalieh SM, Martin TF, Floor E. Synaptic vesicle ceramide kinase. A calcium-stimulated lipid kinase that co-purifies with brain synaptic vesicles. *J Biol Chem* 1989;264:14354-14360.
11. Hannun YA, Obeid LM. Principles of bioactive lipid signalling: lessons from sphingolipids. *Nat Rev Mol Cell Biol* 2008;9:139-150.
12. Miranda GE, Abrahan CE, Politi LE, Rotstein NP. Sphingosine-1-phosphate is a key regulator of proliferation and differentiation in retina photoreceptors. *Invest Ophthalmol Vis Sci* 2009;50:4416-4428.
13. German OL, Miranda GE, Abrahan CE, Rotstein NP. Ceramide is a mediator of apoptosis in retina photoreceptors. *Invest Ophthalmol Vis Sci* 2006;47:1658-1668.
14. Bornancin F, Mechtcheriakova D, Stora S, et al. Characterization of a ceramide kinase-like protein. *Biochim Biophys Acta* 2005;1687:31-43.
15. Inagaki Y, Mitsutake S, Igarashi Y. Identification of a nuclear localization signal in the retinitis pigmentosa-mutated RP26 protein, ceramide kinase-like protein. *Biochem Biophys Res Commun* 2006;343:982-987.
16. Tuson M, Garanto A, Gonzalez-Duarte R, Marfany G. Overexpression of CERKL, a gene responsible for retinitis pigmentosa in humans, protects cells from apoptosis induced by oxidative stress. *Mol Vis* 2009;15:168-180.
17. Garanto A, Riera M, Pomares E, et al. High transcriptional complexity of the retinitis pigmentosaCERKL gene in human and mouse. *Invest Ophthalmol Vis Sci* 2011.
18. Graf C, Niwa S, Muller M, Kinzel B, Bornancin F. Wild-type levels of ceramide and ceramide-1-phosphate in the retina of ceramide kinase-like-deficient mice. *Biochem Biophys Res Commun* 2008;373:159-163.
19. Chakraborty D, Conley SM, Stuck MW, Naash MI. Differences in RDS trafficking, assembly and function in cones versus rods: insights from studies of C150S-RDS. *Hum Mol Genet* 2010;19:4799-4812.
20. Marmor MF, Holder GE, Seeliger MW, Yamamoto S. Standard for clinical electroretinography (2004 update). *Doc Ophthalmol* 2004;108:107-114.
21. Vekslin S, Ben-Yosef T. Spatiotemporal expression pattern of ceramide kinase-like in the mouse retina. *Mol Vis* 2011;16:2539-2549.
22. Wachtmeister L. Oscillatory potentials in the retina: what do they reveal. *Prog Retin Eye Res* 1998;17:485-521.
23. Fortune B, Bui BV, Morrison JC, et al. Selective ganglion cell functional loss in rats with experimental glaucoma. *Invest Ophthalmol Vis Sci* 2004;45:1854-1862.
24. Bui BV, Fortune B. Ganglion cell contributions to the rat full-field electroretinogram. *J Physiol* 2004;555:153-173.
25. Lachapelle P, Little JM, Polomeno RC. The photopic electroretinogram in congenital stationary night blindness with myopia. *Invest Ophthalmol Vis Sci* 1983;24:442-450.

26. Rangaswamy NV, Zhou W, Harwerth RS, Frishman LJ. Effect of experimental glaucoma in primates on oscillatory potentials of the slow-sequence mfERG. *Invest Ophthalmol Vis Sci* 2006;47:753-767.
27. Zhou W, Rangaswamy N, Ktonas P, Frishman LJ. Oscillatory potentials of the slow-sequence multifocal ERG in primates extracted using the Matching Pursuit method. *Vision Res* 2007;47:2021-2036.
28. Dong CJ, Agey P, Hare WA. Origins of the electroretinogram oscillatory potentials in the rabbit retina. *Vis Neurosci* 2004;21:533-543.
29. Kurth I, Thompson DA, Ruther K, et al. Targeted disruption of the murine retinal dehydrogenase gene Rdh12 does not limit visual cycle function. *Mol Cell Biol* 2007;27:1370-1379.
30. Makino CL, Peshenko IV, Wen XH, Olshevskaya EV, Barrett R, Dizhoor AM. A role for GCAP2 in regulating the photoresponse. Guanylyl cyclase activation and rod electrophysiology in GUCA1B knock-out mice. *J Biol Chem* 2008;283:29135-29143.
31. Howes KA, Pennesi ME, Sokal I, et al. GCAP1 rescues rod photoreceptor response in GCAP1/GCAP2 knockout mice. *Embo J* 2002;21:1545-1554.
32. Mendez A, Burns ME, Sokal I, et al. Role of guanylate cyclase-activating proteins (GCAPs) in setting the flash sensitivity of rod photoreceptors. *Proc Natl Acad Sci U S A* 2001;98:9948-9953.
33. Collum RG, Fisher PE, Datta M, et al. A novel POU homeodomain gene specifically expressed in cells of the developing mammalian nervous system. *Nucleic Acids Res* 1992;20:4919-4925.
34. Xiang M, Zhou L, Macke JP, et al. The Brn-3 family of POU-domain factors: primary structure, binding specificity, and expression in subsets of retinal ganglion cells and somatosensory neurons. *J Neurosci* 1995;15:4762-4785.

Construcció d'un model murí *knockout* per C*erkl*

CONSTRUCCIÓ D'UN MODEL MURÍ *KNOCKOUT* PER *CERKL*

ANTECEDENTS

La construcció d'un model murí deficient pel gen *Cerkl* era totalment necessària per tal de poder elucidar la funció d'aquest gen, la qual continua essent tot un misteri. La generació del *knockout* es va realitzar, en part, a l'empresa Genoway (Lió, França) i la major part de la caracterització molecular al nostre laboratori, seguint els passos descrits a la PUBLICACIÓ 3.

Els models animals resulten atractius i molt informatius per realitzar aquest tipus d'estudis funcionals, ja que permeten l'estudi del desenvolupament i progressió de la malaltia, la qual, en alguns casos, mimetitza en quant a simptomatologia i progressió, la patologia humana [129]. Endemés, la majoria de models són fàcilment manipulables i es poden realitzar estudis amb un alt poder estadístic ja que es pot treballar en grans grups degut a la seva fàcil obtenció. En el camp de les distròfies de retina, a més a més, el model més emprat és el murí, el qual té una retina estructuralment similar a la humana, i conserva les mateixes interaccions entre cons-bastons i l'RPE [130].

La generació del *knockout* i la seva caracterització inicial es troba a la PUBLICACIÓ 3. En aquesta part del treball, volem posar de manifest les dificultats que van aparèixer durant els 4 anys que es va trigar en obtenir el primer individu quimèric fundador.

MATERIAL I MÈTODES

Extracció de genòmic de cèl·lules ES

En cada pou s'afegeixen 50 µl de tampó de lisi (10 mM Tris-HCl pH 7.5, 10 mM EDTA, 10 mM NaCl, 1 mg/ml proteïnasa K i 0.5% SDS) i s'incuba a 55 °C durant 12-16 h. Passat aquest temps, s'afegeixen 100 µl de NaCl/EtOH (15 µl de NaCl 5 M per cada 1 ml d'etanol fred) i es deixa precipitar el DNA durant 2 h. Mitjançant la inversió de la placa, s'elimina el sobrenedant, i es fan 2 rentats amb 200 µl d'etanol 70% en un tub d'1.5 ml. Finalment, es resuspen en 40 µl de TE (10 mM Tris-HCl pH 8 i 1 mM EDTA). Per les plaques de 12 pous, es va realitzar exactament el mateix protocol multiplicant els volums per 8, i amb la diferència que el DNA formava una medusa visible que es va "pescar", en comptes de decantar el sobrenedant invertint la placa.

Anàlisi dels clons per PCR

Les PCRs per l'anàlisi de les cèl·lules ES es van posar a punt amb 10 ng genòmic de ratolí 129Sv barrejat amb dilucions seriades del vector MAG1-C+. La reacció es va preparar a un volum final de 50 µl, afegint 5 µl de DNA de les cèl·lules ES, 10 pmol de *primer forward* (PCR a 3': CCA TCT GCA CGA GAC TAG TGA GAC G, PCR a 5': TAA GAA TAG TGT TTT CAG GAG GCT CC), 10 pmol de *primer reverse* (PCR a 3': CTC CAG CGG ACT TAC TAC CAG TTC C, PCR a 5': AAG AGA CAC AAA GGA GTT TCA GTG C), 0.2 mM dNTPs, 1.5 U *Taq* DNA polimerasa, 10 µl de tampó i 1.5 mM

de $MgCl_2$. Les condicions van ser per la PCR a 3': 5 min a 94 °C, seguits de 35 cicles 30 seg a 94 °C, 30 seg a 65 °C i 3 min a 68 °C i un últim pas de 5 min a 68 °C. La PCR a 5' es va realitzar sota les mateixes condicions, amb la diferència que el pas d'elongació va ser de 5 min.

Extracció de genòmic de ratolí

S'incuba durant tota la nit a 55 °C un tros de cua d'uns 3 mm amb 700 µl de *Tail buffer* (20 mM Tris-HCl pH 8, 5 mM EDTA, 0.5% SDS, 200 mM NaCl i 50 µg/ml de proteïnasa K). L'endemà, el tub es centrifuga 10 min a màxima velocitat en una microcentrífuga i es recupera el sobrenedant en un nou tub. S'afegeixen 500 µl d'isopropanol i es barreja bé per inversió. S'agafa la medusa de DNA i es submergeix en etanol 70%. Per últim, es resuspen en 150 µl de TE.

Reacció de PCR per genotipar

La reacció de 20 µl estava formada per 10 µl de *GreenMaster mix*, 2 µl d'una barreja amb els 3 oligonucleòtids (10 mM de cadascun), 1-2 µl de DNA i H_2O fins a 20 µl. Les condicions de la reacció són 94 °C durant 2 min, 35 cicles: 20 seg a 94 °C, 30 seg a 58 °C i 30 seg a 72 °C. Les seqüències dels oligonucleòtids són les següents: For: ACA CAT TAG AAG CCC TGA AGG A, Rev1: TCT TTG TGC TGT AGC AGT GAC C i Rev2: TTG CTG TTT AAT CCA GTT GTC CT.

RESULTATS

Obtenció del vector de direccionament

Per la construcció del vector de direccionament gènic (MAG1-HR), es van realitzar clonatges successius, generant nous vectors tal i com es representa esquemàticament en la FIGURA 38. Els passos que es van seguir per generar aquest vector de 15348 pb, van començar a partir d'un pPCR-Script que contenia el promotor i l'exó sintetitzats químicament, en el qual es van afegir noves dianes de restricció (MAG1-Script Linker). El següent pas va consistir en la inserció d'un braç curt d'homologia (SA) de 2444 pb situat a 3' de l'exó 1 i que havia estat prèviament amplificat per PCR, a partir d'una soca de ratolí 129Sv (MAG1-SA). En aquest mateix vector es va clonar el gen de resistència a la neomicina (NEO) flanquejat per 2 senyals FRT i un lloc LoxP, donant lloc al vector amb el nom MAG1-C+, el qual es va digerir per *Bst*EII per eliminar 1 kb. Aquest nou vector es va anomenar MAG1-SA/Neo. En paral·lel es va amplificar un fragment de la regió genòmica a 5' de l'exó 1, a partir també de DNA genòmic de ratolins 129Sv, com a braç llarg d'homologia (LA). A més a més se li va afegir una seqüència LoxP en la mateixa direcció que l'anterior. Aquest braç amb el LoxP es va inserir en el MAG1-SA/Neo, obtenint un vector MAG1-LSA de 11945 pb. Finalment, es va afegir a 5' de l'exó 1 el gen responsable de la selecció negativa DTA que codifica per la toxina diftèrica A. Tot el vector va ser validat per combinacions de digestions, així com per seqüenciació.

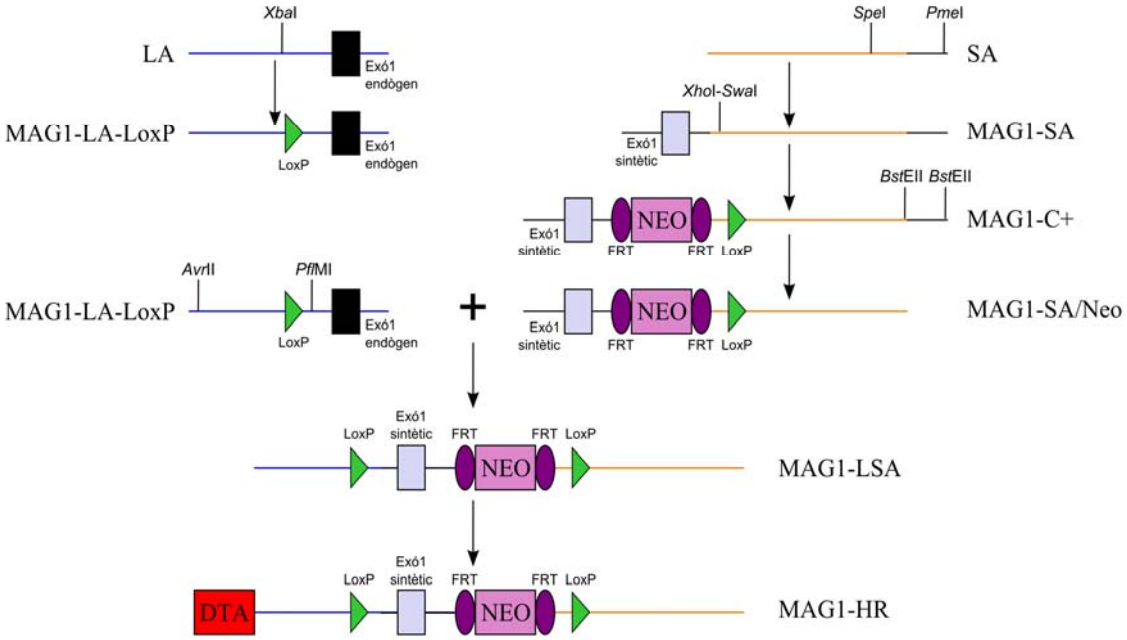

FIGURA 38 - Esquema de la construcció del vector MAG1-HR.

***Screening* de les cèl·lules ES**

El vector resultant, es va transfectar en cèl·lules ES de ratolí 129Sv i es va procedir a la doble selecció negativa/positiva. Tots aquells clons que no haguessin recombinat correctament per cap, o només un dels dos braços d'homologia provocarien la inserció del *cassette* de DTA, el qual produiria la mort de la cèl·lula (selecció negativa), d'altra banda, les cèl·lules es van incubar en presència de geneticina de manera que, només aquelles cèl·lules amb el *cassette* de NEO van sobreviure (selecció positiva).

La part d'electroporació i selecció de cèl·lules es va realitzar a França i, consecutivament, un cop crescudes les cèl·lules, ens van enviar plaques de 96 pous per realitzar l'extracció de gènomic i posterior anàlisi per PCR dels clons obtinguts. L'estudi per PCR dels clons ens va permetre diferenciar entre aquells que havien recombinat de manera atzarosa i els que ho havien fet en la regió cromosòmica correcta, utilitzant un oligonucleòtid dins el *cassette* de NEO i un altre en la regió del braç curt. En total es va fer l'escrutini de més de 1000 clons diferents, dels quals 712 van ser caracteritzats al nostre laboratori. La freqüència de recombinació homòloga segons l'experiència de Genoway, hauria de ser del 10%. En el nostre cas, l'eficiència va ser molt més baixa, al voltant d'un 1%, és a dir, es van obtenir un total de 14 clons, dels quals 4 van ser identificats en el nostre laboratori, i els altres 10, en una quarta tongada d'electroporació i anàlisi que van realitzar directament a Genoway. Probablement, aquesta baixa eficiència podria ser deguda que l'exó 1 està en un lloc cromosòmic de difícil accès, la qual cosa impediria una bona recombinació homòloga requerida. Un cop fet l'escrutini a la regió 3' es va realitzar una PCR per tal de confirmar que a la regió 5' també havia recombinat correctament.

Southern blot

Un cop comprovat que havien recombinat en la regió d'interès, es van créixer les cèl·lules ES seleccionades en plaques de 12 pous (Genoway) i es va procedir a l'extracció del DNA genòmic dels clons positius seguint el mateix protocol que en l'*screening*. Aquests DNAs van ser digerits pels enzims *Eco*RV i *Bgl*II per una banda, i amb *Pci*I per l'altra (vegeu PUBLICACIÓ 3 pels detalls del *Southern blot*). Sorprenentment, es va observar que dels 3 clons analitzats en el nostre laboratori, 2 d'ells havien recombinat entre l'exó 1 i el senyal LoxP, ja que les bandes que s'obtenien eren idèntiques a les del WT (FIGURA 39). Posteriorment, al seqüenciar el fragment obtingut per PCR a 5' es va poder demostrar que el LoxP no hi era. El clon 4, no es va analitzar degut a la poca quantitat de DNA que es va obtenir de l'extracció, que va impossibilitar que es pogués veure quelcom mitjançant aquesta tècnica.

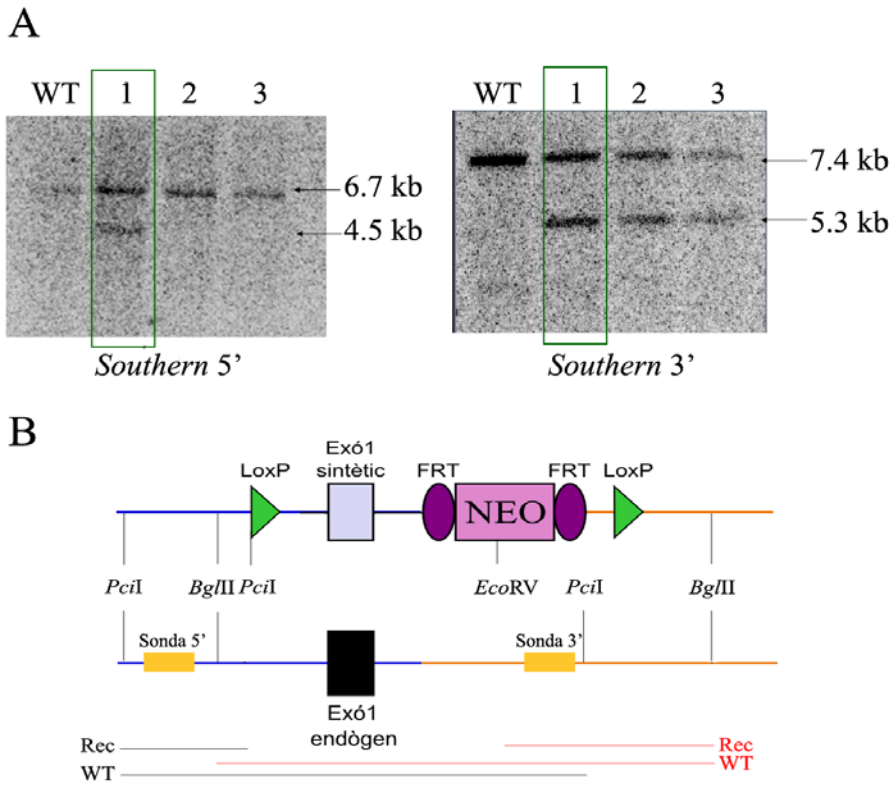

FIGURA 39 - Comprovació de la recombinació homòloga per *Southern blot*. Resultat de les hibridacions a les regions 5' i a 3' (**A**). Només el clon 1 va recombinar correctament. Representació de les dianes de restricció i la posició de les sondes (**B**). Les línies de color vermell indiquen els dos fragments que es generen en la hibridació a 3', mentre que les negres il·lustren les de la hibridació amb la sonda 5'.

Obtenció del primer KO

El disseny del model animal va començar a principis de l'any 2005 i durant aquell any es van començar a amplificar els dos braços d'homologia. Coincidint amb l'inici d'aquest treball, es van abordar els clonatges per generar el vector de direccionament, amb els escrutinis corresponents durant els anys 2006 i 2007. A finals d'aquest últim any, es començaren a implantar les cèl·lules ES en blastocists de femelles de la soca C57BL/6J. Atès que els ratolins C57 són de color agutí i els 129Sv de color negre, els grau de quimerisme de la descendència podia ésser calculat. Durant els primers intents, els nivells de quimerisme van resultar ser inferiors al 30%, i per tant, segons el consell de Genoway, no suficients com per assegurar que el clon s'hagués implantat en la línia germinal. Finalment, es van aconseguir 4 mascles

amb un bon nivell de quimerisme, que oscil·lava entre el 50-80%. L'escissió del *cassette* de NEO en els embrions, va ser fruit del creuament entre aquests quimeres amb ratolins femelles C57BL/6J que expressen la recombinasa FLP, encarregada de reconèixer els llocs FRT. Finalment, l'any 2009, es van obtenir els primers heterozigots després de creuar femelles C57BL/6J que expressen la recombinasa CRE, amb els mascles que tenien l'exó 1 de *Cerkl* flanquejat per les seqüències LoxP i, a més, no eren portadors del *cassette* de resistència a geneticina. Al setembre de 2009, i després d'una gran inversió de diners, temps, esforç i una llarga espera van arribar els primers heterozigots deficients per *Cerkl* (2 mascles i 2 femelles).

Un cop a Barcelona, els ratolins heterozigots van ser creuats entre ells per tal d'ampliar la colònia. La primera generació obtinguda va ser de 8 ratolins, que van ser marcats amb un codi de forats a les orelles, i genotipats a partir d'un tros de cua. Per genotipar els animals, es va dissenyar una reacció de PCR amb 3 oligonucleòtids a la vegada: un *forward* comú tant al al·lel WT com al KO (For), i 2 *reverse*, el primer situat a una regió comuna (Rev1) i l'altre localitzat dins l'exó 1 (Rev2). D'aquesta manera s'amplifica amb la parella For i Rev1 l'al·lel KO (amplicó de 354 pb) i amb For i Rev2 l'al·lel WT (601 pb). La parella For i Rev1 al cromosoma WT amplifica una fragment de 2625 pb que no es veu afavorit per les condicions de PCR que s'utilitzen (FIGURA 40). En la primera ventrada, nascuda a finals del mes d'octubre del 2009, es va obtenir la primera femella KO (FIGURA 40).

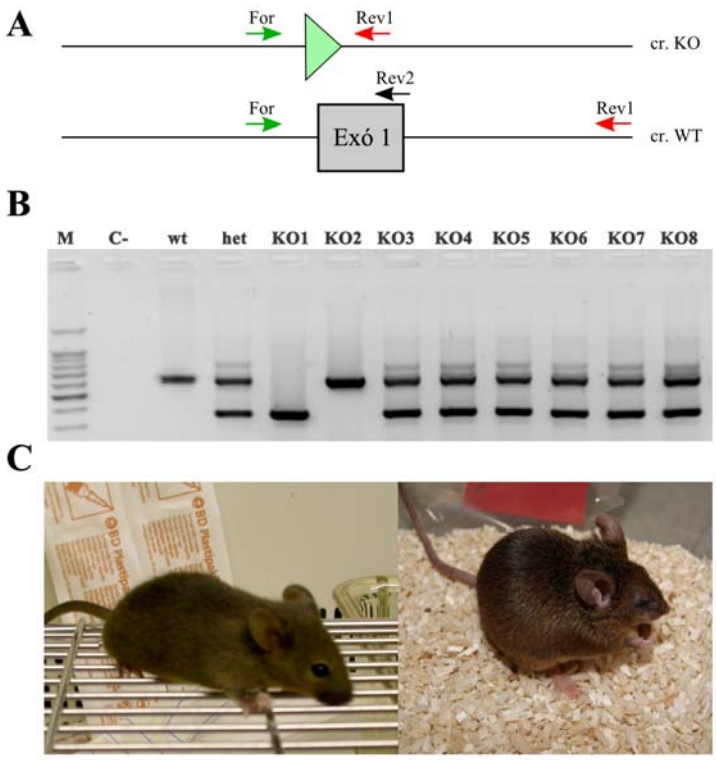

FIGURA 40 - Genotipat i obtenció del primer ratolí *knockout*. Localització dels oligonucleòtids emprats per la PCR de genotipat (**A**). Resultat d'una PCR de genotipat de la ventrada d'un creuament *Cerkl* +/- x *Cerkl* +/-, en la qual es pot observar que KO1 es homozigot KO, KO2 homozigot WT i KO3 fins KO8 són heterozigots (**B**). Primer organisme KO obtingut (**C**). A la esquerra la femella KO1 a P20, a la dreta als 16 mesos.

Caracterització funcional del ratolí C*erkl -/-*

CARACTERITZACIÓ FUNCIONAL DEL RATOLÍ *CERKL -/-*. ANÀLISIS DE LIPIDÒMICA

ANTECEDENTS

Actualment, s'han generat dos models animals deficients per *Cerkl*. El primer va ser obtingut per Graf i col·laboradors l'any 2008 (vegeu INTRODUCCIÓ), i consistia en una deleció de l'exó 5, quedant afectades només aquelles isoformes que, per *splicing* alternatiu, inclouen aquest exó. Aquests ratolins, com ja hem esmentat anteriorment, no van presentar cap canvi significatiu en les concentracions de ceramides i C1P a retina [162].

L'altre model, ha estat generat pel nostre grup, com a part fonamental d'aquesta Tesi. El ratolí KO per *Cerkl* es va generar mitjançant l'escissió de l'exó 1 i el promotor (vegeu PUBLICACIÓ 3). Aquests animals, a l'igual que els descrits al 2008, són viables i fèrtils, i no presentaven cap fenotip aparent a nivell histològic. Endemés, l'estudi en detall de *Cerkl* en ratolins, va revelar una gran multiplicitat de transcrits produïts per l'ús de múltiples exons en diferents combinacions, gràcies a l'*splicing* alternatiu, i a l'activitat de més d'un TIS, fins ara desconeguts (vegeu PUBLICACIÓ 2). Aquest fet es va traduir en la detecció d'un 30-35% d'expressió de *Cerkl* residual a la retina, teixit en el qual centrarem tota la feina que es presenta en aquest apartat.

Diversos grups, entre ells el nostre (vegeu PUBLICACIÓ 1), hem estat buscant el substrat de CERKL, sense gaire èxit, basant-nos sempre en la idea de que la proteïna havia de fer un paper similar a la seva homòloga més propera CERK. En tots els casos, s'ha pogut observar que la ceramida no sembla ser el substrat de CERKL i que no hi ha variacions en els nivells de C1P [39, 41, 162].

D'altra banda, la localització de CERKL sembla ser dinàmica (vegeu PUBLICACIÓ 1) i pot entrar activament a nucli, fet que suggereix que la proteïna podria jugar algun paper modulant l'activitat transcripcional d'alguns gens.

Així doncs, en base a totes les dades que teníem i atès que, disposàvem un model animal deficient pel gen, vam decidir estudiar la lipidòmica de les retines WT i KO i, contrastar-la amb estudis previs que havíem realitzat sobreexpressant CERKL en cèl·lules en cultiu, dels quals no s'havien obtingut resultats concloents. Endemés, vam voler estudiar l'expressió d'alguns gens implicats en el metabolisme dels esfingolípids.

MATERIAL I MÈTODES

Obtenció i preparació de retines per lipidòmica:

Es van fer servir 6 animals C57BL/6J WT i 6 KO de 2 mesos d'edat sacrificats per dislocació cervical. Tot el procediment es va realitzar seguint els suggeriments del comitè ètic de la Universitat de Barcelona i seguint la declaració d'ARVO per la utilització d'animals d'experimentació en el camp de la

visió. Les dues retines van ser disseccionades i congelades immediatament en nitrogen líquid. Es van homogeneïtzar en 150 µl de tampó d'homogeneïtzació (25 mM KCl, 50 mM Tris-HCl pH 7.5, 0.5 mM EDTA i 0.25 M sucrosa) amb 20 cops de Dounce. D'aquest volum, 100 µl van ser utilitzats per l'extracció de lípids i la resta per fer la quantificació de proteïna per BCA.

Obtenció i preparació de les cèl·lules per lipidòmica:

Es van transfectar cèl·lules COS7 i HEK293 amb les diferents construccions de *CERKL*, així com el vector buit i *CERK* com a control negatiu i positiu, respectivament. A 44 h post-transfecció es van tractar amb 10 µg/ml de Brefeldina A (BFA - inhibidor del tràfic vesicular ER-Golgi) i 100 µM de N-butildesoxinojirimicina (NB-DNJ, un inhibidor de la glucosilceramida sintasa) durant 4 h. Posteriorment, es van tripsinitzar les cèl·lules, comptar i rentar en PBS. Els pellets es van congelar a -80 °C fins el moment de l'extracció.

Lipidòmica:

L'extracció d'esfingolípids es va dur a terme a partir de 100 µl de teixit o 300000 cèl·lules, seguint un mètode adaptat a partir del descrit per Merril i col·laboradors [210]. En cada tub es van afegir 500 µl de metanol (grau HPLC) i 250 µl de cloroform. En el cas de les cèl·lules també es va afegir 100 µl d'H_2O. Endemés, en aquest punt es van addicionar els estàndards interns (espècies exògenes de 12 carbonis de Cer, SM, GlcCer). La solució es va incubar durant 16 h a 48 °C. El següent pas va consistir en la incubació de la solució durant 2 h a 37 °C després d'addicionar 75 µl de KOH 1 M. Finalment, es va aturar la reacció afegint 75 µl d'àcid acètic 1 M i es va procedir a l'evaporació sota N_2. Els lípids extrets es van solubilitzar en 150 µl de metanol. L'aparell de cromatografia líquida / espectrometria de masses consisteix en un sistema d'UPLC connectat a un espectròmetre de masses (Waters), operat en mode de ionització positiu. Es va adquirir l'espectre complet entre 50 i 1500 Da i l'individual i van ser sumats per obtenir resultats cada 0.2 segons. Es van utilitzar 2 fases mòbils, metanol, 1 mM format d'amoni (fase A) i H_2O, 2mM format d'amoni (fase B) totes dues amb 0.05 mM d'àcid fòrmic. El gradient programat va ser: 0 min, 80% B; 3min, 90% B; 6 min 90% B; 15 min, 99% B; 18 min, 99% B; 20 min, 80% B i un flux de 0.3 ml/min. La columna es va mantenir a 30 °C. La quantificació es va dur a terme mitjançant l'ús del cromatograma de l'extracció iònica de cada compost, utilitzant una finestra de 50 mDa. El rang lineal dinàmic es va determinar per la injecció d'una barreja d'estàndards. La identificació dels compostos es va basar en una mesura acurada de la massa amb un error <5 ppm i el temps de retenció es va comparar amb el dels estàndards (±2%). Els valors obtinguts per cada mostra es van estandarditzar pel número de cèl·lules (en el cas de les mostres de cultius cel·lulars) o per mg de proteïna (en els experiments amb teixits animals).

Extracció d'RNA i RT-PCRs:

L'extracció d'RNA es va realitzar a partir de dues retines de ratolí mitjançant l'ús del producte *High Pure RNA Tissue Isolation Kit* (Roche). La generació del cDNA es va dur a terme utilitzant el *Transcriptor High Fidelity cDNA Synthesis Kit* (Roche). En ambdós casos es va seguir el protocol

recomanat pel fabricant. Un cop obtingut el cDNA es va realitzar una PCR específica per cadascun dels gens escollits incloent-hi el gen *Gapdh* (per normalitzar les mostres) i *Cerkl*. Les condicions de PCR van ésser: 2 min a 94 °C seguit de 35 cicles, 20 seg a 94 °C, 55, 58 o 60 °C durant 30 seg (1 min en el cas del *Gapdh*) i 30 seg a 72 °C. Els fragments amplificats eren d'entre 450 a 500 pb, a excepció del *Gapdh* que era de 983 pb. La seqüència dels oligonucleòtids utilitzats, així com els gens sobre els quals s'ha realitzat l'estudi, es resumeixen en la taula següent.

Gens i seqüències dels oligonucleòtids			
Gen	***Forward***	***Reverse***	**Tm °C**
Gapdh	TGAAGGTCGGAGTCAACGGATTTGG	CATGTAGGCCATGAGGTCCACCAC	58
Cerkl	CTGACTGTGGTGGTCACTGG	GAACCTCTGATGCAGCTTCC	58
Cert	CGTAGACATGGCTCAATGGTG	ACTCTTCCTCATTAATCAGACTG	58
Fapp2	TGGATTGCAGCATCTCCAGTG	AGACCTCTCTTCAGCCACAAG	58
Cerk	GCTTCCATCACTACGGAGATC	CTGAGAAATCATACCGGACGAG	58
Sphk1	GCATAATGGGAACGGCCAFACTG	GTTCTGGTACCACAGTCCAATG	58
Sphk2	GGCAGCGCTGTATGGACCAC	GCACTGCACCCAGTGTGAATC	58
Uggt1	TGATGAAGGACATTAGTCAGAAC	TCTCGGCGATGCTAATCAACTC	55
Uggt2	CATCGTATACTCACTGTGGATG	CAGCAATAATCCACAGAGTGAC	55
Cgt	GAGCTGGTGTCAAGTATCTGTC	GGGCTCCGTCATGGCGAAG	52/55/58
Sgms1	CACGCTGTACCTGTATCGGTG	ATGGTAAGATCGAGGTACAATTC	58
Sgms2	GGAACTTTATACCTGTATCGCTG	GCAAGGAATTGAGCCTTGCAC	52/55/58
Lass3	GAAAATGGTTCTGGTCGGAG	CTCCCAGAGGTCATATGCCC	52/55/58
Degs1	GCGTGTCCCGAGAGGAGTTC	GCAGAAGAACCAGCCCTCG	
Degs2	AATGGTACTGGTTCAGGTGCTG	GCTGCTGCCTAGAAGGTAGAC	55

TAULA 11 - Gens, seqüència dels oligonucleòtids i temperatura d'anellament (Tm) de la PCR. El gen *Gapdh* es va utilitzar per normalitzar les mostres entre WT i KO. La resta de gens s'agrupen en quinases (*Cerk*, *Sphk1* i *Sphk2*), transportadors (*Cert* i *Fapp2*), sintases de esfingolípids complexos (*Uggt1*, *Uggt2*, *Cgt*, *Sgms1* i *Sgms2*), sintases de ceramida (*Lass3*) i desaturases (*Degs*1 i *Degs2*), així com el gen d'estudi *Cerkl*. Tres dels gens (*Cgt*, *Sgms2* i *Lass3*) no van amplificar cap fragment en les Tm provades, indicant que, o el gen s'expressa poc a retina, o bé degut als elevats nivells d'*splicing* a la retina, els primers escollits localitzen en un exó que pot ser saltat pels mecanismes d'empalmament i maduració del mRNA.

RESULTATS

Lipidòmica

L'estudi dels lípids de les retines de 6 animals WT i 6 KO de 2 mesos d'edat va consistir en l'anàlisi per UPLC de diferents compostos pertanyents a la família dels esfingolípids: dihidroceramida (DHCer), dihidroesfingomielina (DHSM), ceramida (Cer), esfingomielina (SM), glucosil- i galactosilceramida (GlcCer/GalCer), lactosilceramida (LacCer) i el gangliòsid GM3. També, es van mesurar les espècies insaturades de Cer i SM, així com els àcids grassos lliures.

Per dur a terme l'estudi, primer es van calcular les concentracions (pmol/mg de proteïna) de cadascun d'aquests lípids segons la longitud de la cadena del seu àcid gras (en número de carbonis) i de les insaturacions que aquest presenta. Aquest càlcul es va basar en la conversió a picomols de l'àrea del pic detectat en el cromatograma, utilitzant com a referència l'àrea del pic de la barreja d'estàndards de 12 carbonis equivalent a 200 pmols. Posteriorment, es va utilitzar la concentració de proteïna obtinguda per cada lisat per normalitzar els valors entre mostres.

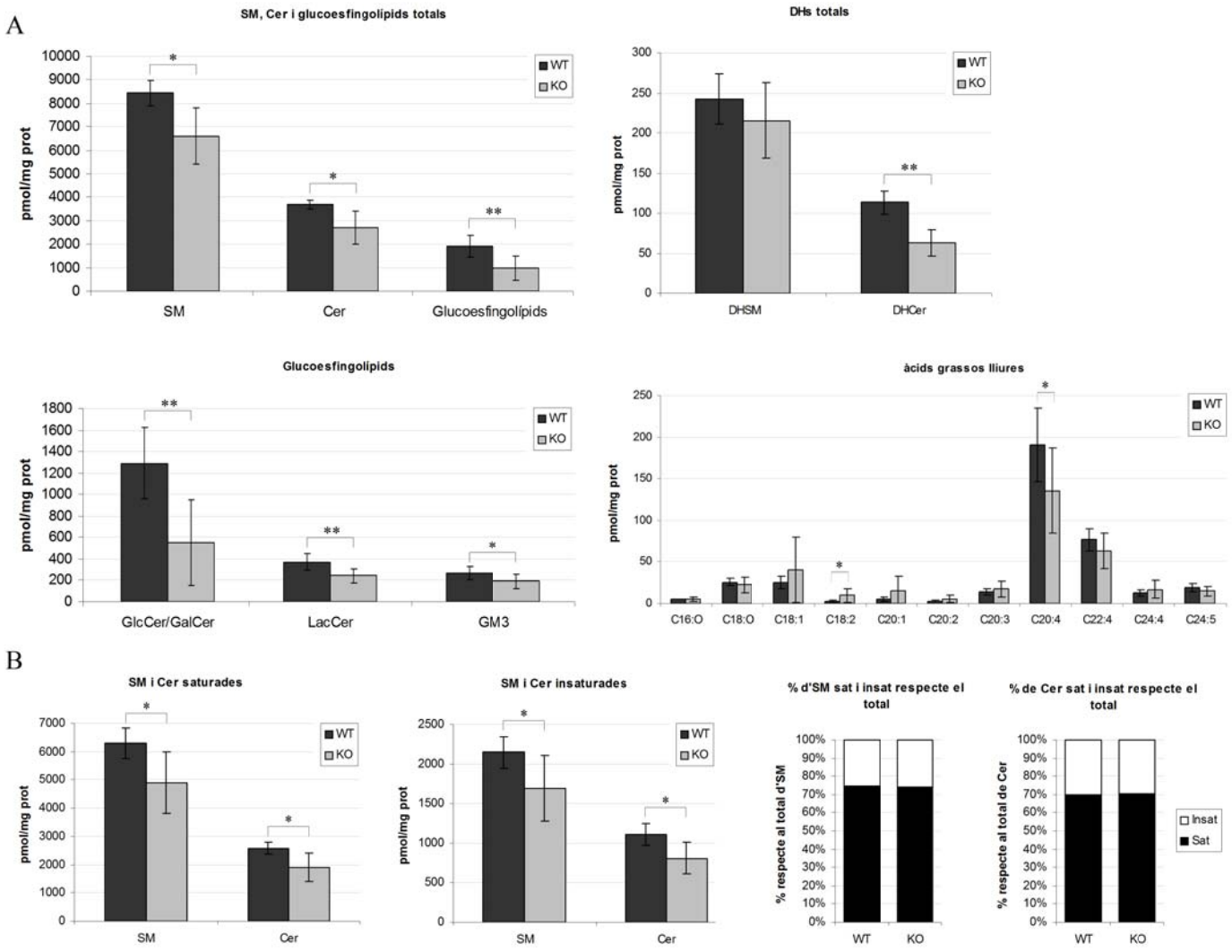

FIGURA 41 - Representació gràfica de la concentració total de diversos esfingolípids i àcids grassos entre retines d'animals WT i KO. D'una banda es mostren els resultats obtinguts pel total de totes les espècies de cada esfingolípid, també la quantitat d'SM i Cer saturada i insaturada, així com la proporció en la que es troben. D'altra banda, es representen les dades dels àcids grassos que van poder ser observats. * indica un $p<0.05$ i ** $p<0.01$ pel test estadístic t-Student.

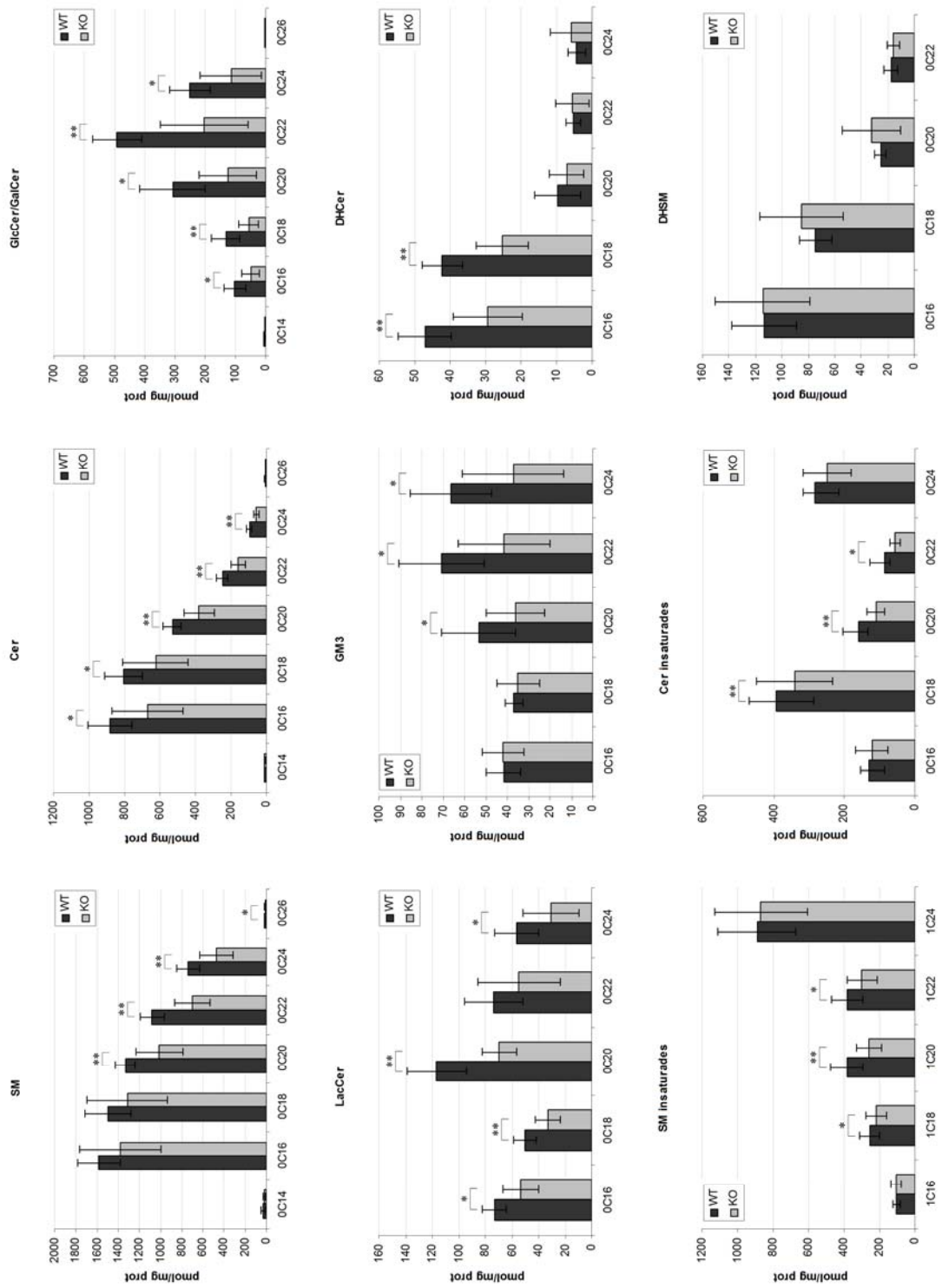

FIGURA 42 - Representació gràfica de la composició per espècies de diversos esfingolípids entre retines d'animals WT i KO Es mostren les concentracions obtingudes per les espècies d'SM, Cer, GlcCer/GalCer, LacCer, GM3, DHSM i DHCer, així com les formes insaturades de Cer i SM. * indica un $p<0.05$ i ** $p<0.01$ pel test estadístic t-Student.

A la FIGURA 41 es mostren els resultats del total de cadascun dels esfingolípids, així com la quantificació de les formes insaturades de ceramida i SM i per últim, els àcids grassos lliures. L'anàlisi en detall va mostrar una clara davallada de tots els lípids, molt especialment en el grup de la glucosil- i galactosilceramida (la massa de tots dos lípids és la mateixa, i per tant es veuen en un mateix pic). En canvi, no va haver-hi diferències en la proporció entre ceramides i esfingomielines saturades i insaturades (FIGURA 41). Endemés, l'estudi per separat de les diferents espècies de cada esfingolípid va mostrar que els nivells de gairebé totes les espècies de Cer eren menors en les retines dels KO, el mateix cas es donava en els de GlcCer/GalCer. Excepte la DHSM, la resta d'esfingolípids van mostrar davallades significatives en alguna de les espècies. En especial, les més afectades semblen ser, sobretot, les espècies de 18, 20 i 22 carbonis (FIGURA 42).

Tot i la baixada en els nivells de la majoria d'esfingolípids estudiats, no es van trobar diferències significatives en quant a la distribució de les espècies de carbonis d'aquests (vegeu figures de l'ANNEX).

D'altra banda, estudis previs realitzats a l'inici d'aquest treball, utilitzant cèl·lules HEK293 i COS7 transfectades amb CERKL, CERK i el vector buit, mostraven una certa tendència a tenir un lleuger augment, no significatiu, en la quantitat de GlcCer, justament el contrari del que s'observa en el KO. Per tant, la GlcCer, després de diversos assaigs, sembla ser un bon candidat per ser el substrat de CERKL, tot i que els resultats obtinguts fins ara no ens permeten discernir sobre si CERKL actua directa- o indirectament sobre la GlcCer.

RT-PCRs

Les diferències observades entre els ratolins WT i KO a les anàlisis de lipidòmica ens van suggerir que potser la disminució de producció d'esfingolípids al KO, com ara l'SM o la GlcCer, era causada per un efecte sobre la transcripció dels gens implicats en la biosíntesi d'aquests lípids. El resultat dels estudis d'expressió dels diversos gens del metabolisme dels esfingolípids, entre ratolins WT i KO va mostrar que no hi havia diferències entre ells. D'una banda es va utilitzar el gen *Gapdh* per tal de normalitzar les mostres. Els gens estudiats es van escollir en base als resultats de lipidòmica que vam observar. Així doncs, d'una banda es va voler veure si hi havia canvis en la transcripció dels gens que codifiquen per proteïnes transportadores (*Cert* i *Fapp2*). També, vam voler veure que passava a nivell de *Cerk*, el gen que codifica per la proteïna més propera a CERKL, així com les altres dues quinases d'esfingolípids importants (*Sphk1* i *Sphk2*). En cap d'aquests casos vam observar diferències en els nivells d'expressió. D'altra banda, van voler estudiar alguns dels enzims de la síntesi *de novo* de la ceramida, com són el gen *Lass3* (també anomenat *CerS3* -ceramida sintasa 3-) i el de les desaturases *Degs1* i *Degs2*. Per últim es va estudiar l'expressió dels gens implicats en la síntesi d'esfingolípids complexos com ara les esfingomielina sintases (*Sgms1* i *Sgms2*) i de les glucosil- (*Uggt1* i *Uggt2*) i galacotsilceramida sintases (*Cgt*). Novament, no es van observar diferències significatives entre WT i KO en l'anàlisi transcripcional (FIGURA 43).

Són molts els gens implicats, i resten, per tant, nombrosos gens per estudiar, com els de la ruta de degradació d'esfingolípids complexos, les fosfatases i altres ceramida sintases (*Lass1*, *Lass2*, *Lass4*, *Lass5* i *Lass6*). Endemés, en 3 dels gens, no vam poder obtenir producte en cap de les condicions provades. Es tracta dels gens *Cgt*, *Lass3* i *Sgms2*. Aquest fet podria indicar dues coses: i) aquests gens s'expressen molt poc o gens a la retina o ii) degut a l'elevada taxa d'*splicing* alternatiu de la retina (Abstract #2560 ARVO 2011) els *primers* estan en exons que podrien no formar part del transcrit principal. La discussió d'aquests resultats es presenta a la seqüent secció.

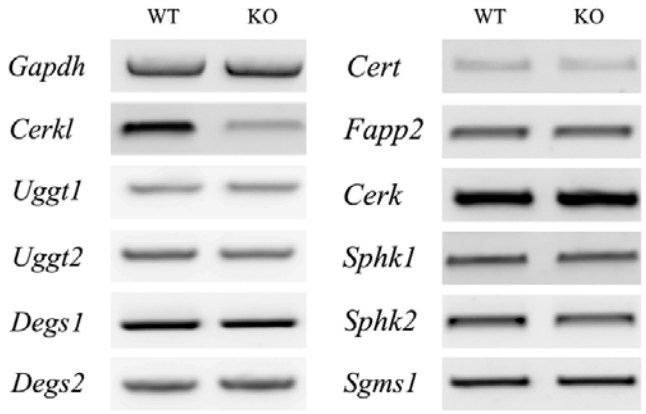

FIGURA 43 - Anàlisi transcripcional dels gens implicats en el metabolisme dels esfingolípids. No es va observar cap diferència en els nivells d'expressió entre retines d'animals WT i KO.